Observability and Determinability of Discrete Time Switched Linear Singular Systems

Sutrisno, Sutrisno; Trenn, Stephan

Observability and Determinability of Discrete Time Switched Linear Singular Systems: Multiple Switches Case

Sutrisno, Sutrisno; Trenn, Stephan

Published in:
2021 Benelux Workshop on Systems and Control

Benelux Workshop

on

Systems and Control

June 29, 2021

Rotterdam, The Netherlands

Book of Abstracts

The Benelux Workshop on Systems and Control is sponsored by

dutch institute of systems and control

Erjen Lefeber and Julien Hendrickx (Eds.)
Book of Abstracts — Benelux Workshop on Systems and Control

Delft University of Technology
Mekelweg 2
2628 CD Delft
The Netherlands

ISBN: 978-94-6384-233-4

Part 1

Organizational Comments

Welcome

The Organizing Committee has the pleasure of welcoming you to the *Benelux Workshop on Systems and Control*, at De Doelen in Rotterdam, The Netherlands.

Due to COVID-restrictions we had to cancel the Benelux Meeting on Systems and Control last March, but fortunately we are able to organize an in-person meeting now. We still have to adhere to all kinds of restrictions, as explained below, but at least we can meet in person.

Aim

The aim of the Benelux Meeting is to promote research activities and to enhance cooperation between researchers in Systems and Control.

Scientific Program Overview

Only contributed short lectures. See the list of sessions for the titles and authors of these lectures. One of the restrictions is that at most 50 people are allowed in one room (in particular also during the breaks), and the number of contacts should be minimized. This makes that we have more or less two programs in parallel, where each program consists of two rooms in parallel. Each participant is assigned to one room, namely the room in which his/her presentation is scheduled.

Directions for speakers

For a contributed lecture, the available time is 20 minutes. Please leave a few minutes for discussion, and adhere to the indicated schedule. In each room LCD projectors are available, as well an HDMI cable, so no VGA cable. If you do not have an HDMI connector port on your notebook, make sure to bring your own connector. *You have to provide a notebook yourself.*

Registration

On-site registration is *not* possible.

The registration fee includes:

- Admission to your session room.
- An online copy of the Book of Abstracts.
- Coffee and tea before the start of the workshop
- Lunch-bag (sandwich, wrap, bun, juice, fruit, candybar)
- Bottled water during the break.

Organization

The meeting has been organized by Erjen Lefeber (Eindhoven University of Technology) and Julien Hendrickx (UCLouvain) with the support of Henk Nijmeijer (Eindhoven University of Technology) and Martha Otte (Delft University of Technology)

Sponsor

The meeting is supported by the following organizations:

- Dutch Institute for Systems and Control (DISC).

Conference location

The lecture rooms of De Doelen are situated on the third floor. Consult the map at the end of this part of the booklet to locate rooms. Upon start of the lunch break, lunch bags will be handed out at the doors of the meeting rooms. You can have your lunch in the foyer or at the rooftop terrace. Pick your spot for having lunch and stay there for the entire break to minimize movement.

The address of De Doelen is

De Doelen — Willem Burger Zaal
Kruisplein 40
3012 CC Rotterdam
The Netherlands

Best junior presentation award

There will be no junior presentation award.

Website

An *electronic version* of the Book of Abstracts can be downloaded from the Benelux Meeting web site.

COVID-restrictions

Within the current Dutch measures against the coronavirus we can organise a safe and responsible meeting. This workshop, however, will be slightly different from other workshops and conferences. We have four rooms for parallel sessions, and each PhD student will be assigned to one the rooms of his/her presentation. To reduce the number of contacts, you have to stay in your assigned room for the entire meeting, so session hopping is not allowed. Furthermore, as becomes clear from the program, the rooms will have their start and ending

times and their breaks in two separated groups to reduce the number of contacts. The rooms are large enough to guarantee that 1.5-meter distance can be kept easily. We also have to comply with the business protocol of De Doelen:

General measures

- Wash your hands with water and soap frequently, or us a disinfectant.
- When coughing or sneezing, cover your mouth and nose with the inside of your elbow or use a tissue.
- Greet each other with a smile; do not shake hands.
- Give each other some space: keep a 1.5-meter distance.
- If you are showing symptoms of the Coronavirus, please stay home.

Measures at De Doelen

General

- Use a face mask inside. Please do not take it off until seated, at a 1.5-meter distance from the next person
- Restrooms are located on the ground floor, on the third floor of the Willem Burger Area. They will be accessible at all times.
- Avoid crowding at the restrooms.
- Always keep a 1.5-meter distance from each other. De Doelen will be reminding visitors of this rule in various ways.
- Wherever possible, please use the stairs. If you must use the elevators, please keep a 4-step distance.
- The ventilation system brings in fresh air from outside, and dispenses the air from the auditoriums.

Cleaning

- An extra cleaner will be present during any event.
- Disinfection columns are placed throughout the building for visitors to disinfect their hands.

Catering

- We offer a special range of Corona-proof food items, including only sealed items.
- Food and drinks will be available through self-service. All drinks come in biodegradable disposables or bottles.
- All buffets have one-way walking routes.
- Bars will not be cleaned until visitors have left the room.
- Tables will be cleaned throughout the day, wherever possible.

Arrival, organisation

- Upon arrival, one of the Corona coordinators (*Martha Otte*, *Erjen Lefeber*) is required to carry out a health check before entering the building.
- Follow the walking routes marked throughout the building. Be mindful that narrow corridors are one-way routes.
- Please refrain from using a restroom unless necessary; there is limited restroom space.
- All equipment must be clean and disinfected on arrival.
- Everyone is to wear a face mask when entering the stage and/or setting up on stage.
- After the workshop, visitors are requested to leave as quickly as possible.

Halls and foyers

- Our calculations for the maximum capacity of each space assume 5 square meters per person. The addition of catering facilities or exhibition spaces requires a recalculation, still assuming 5 square meters per person.
- Please adhere to the one-way routes in the auditoriums as much as possible.
- The larger auditoriums have separate entrances and exits.
- Seating will be marked for availability, in keeping with the 1.5 meter rule.
- Participants must come to an agreement on how to leave the auditorium.

Willem Burger Kwartier
Begane Grond

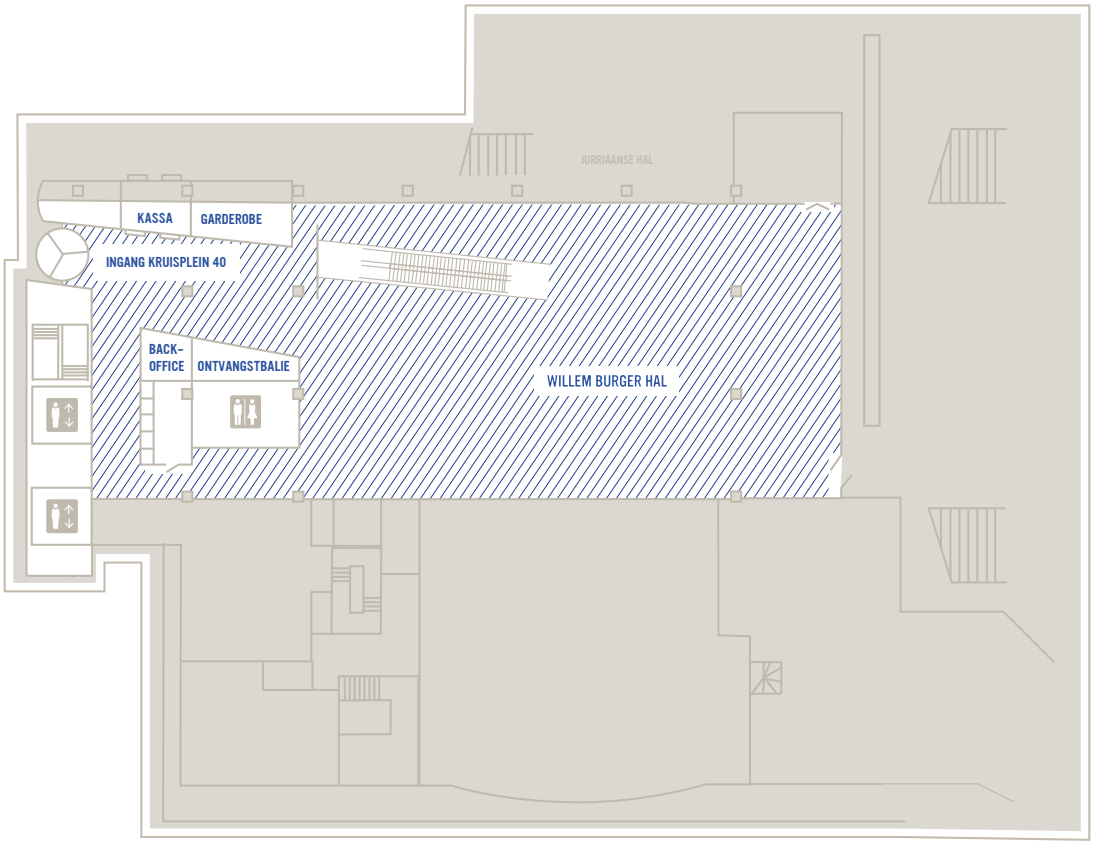

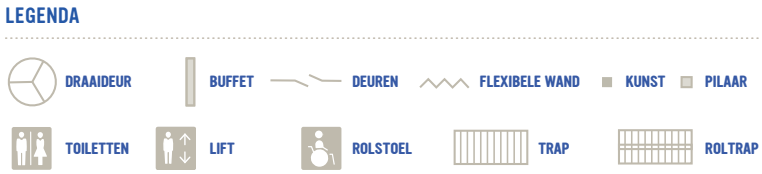

Willem Burger Kwartier
Derde Verdieping

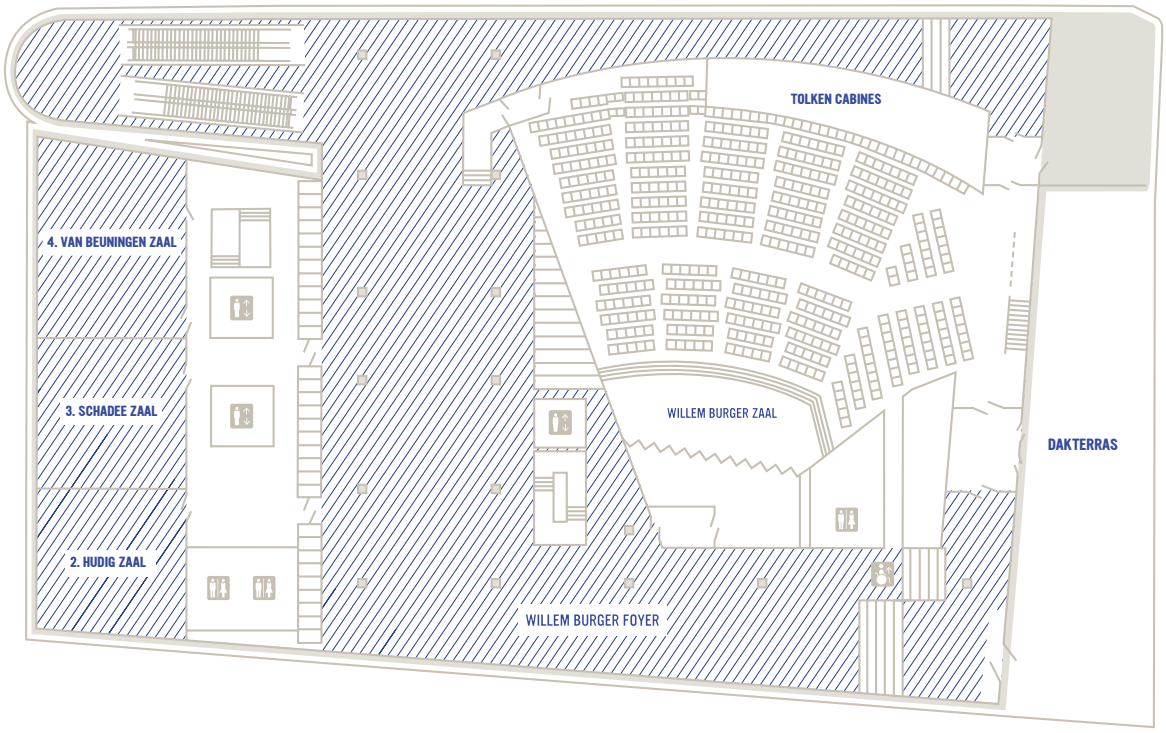

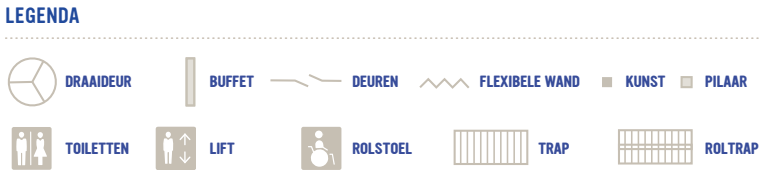

Part 2

Programmatic Table of Contents

Willem Burger Zaal: 10.00-17.20

Willem Burger Zaal
Opening
Chair: Henk Nijmeijer 10.00-10.10

TuM01 Willem Burger Zaal
Mechanical and Electromechanical engineering
Chair: Henk Nijmeijer 10.10-12.10

TuA01 Willem Burger Zaal
Aerospace Engineering
Chair: Erjen Lefeber 12.40-15.00

TuE01 **Willem Burger Zaal**
Robotics
Chair: Erjen Lefeber **15.20-17.20**

Van Beuningen Zaal: 10.00-17.20

Van Beuningen Zaal
Opening
Chair: Erjen Lefeber 10.00-10.10

TuM02 Van Beuningen Zaal
System Identification
Chair: Congcong Sun 10.10-12.10

TuA02 Van Beuningen Zaal
Model Based Control
Chair: Congcong Sun 12.40-15.00

TuE02 Van Beuningen Zaal
System Identification and Observers
Chair: Congcong Sun 15.20-17.20

Schadee Zaal: 11.00-17.55

Schadee Zaal
Opening
Chair: Julien Hendrickx 11.00-11.10

TuM03 Schadee Zaal
Systems Biology and Medical Applications
Chair: Julien Hendrickx 11.10-13.10

TuA03 Schadee Zaal
Distributed and Networked Systems
Chair: Julien Hendrickx 13.40-15.40

TuE03 **Schadee Zaal**

Optimization

Chair: Julien Hendrickx **15.55-17.55**

Hudig Zaal: 11.00-17.55

Hudig Zaal
Opening
Chair: Erjen Lefeber 11.00-11.10

TuM04 Hudig Zaal
Mechanical and Electromechanical engineering
Chair: Carlos Murguia 11.10-13.10

TuA04 Hudig Zaal
Model Reduction
Chair: Carlos Murguia 13.40-15.40

TuE04 Hudig Zaal
System identification & System Theory
Chair: Carlos Murguia 15.55-17.55

Part 3

Contributed Lectures

Improved commutation methods for moving-magnet planar actuators

Yorick Broens[1], Hans Butler[1,2] and Roland Tóth[1,3]
[1] Control Systems Group, Eindhoven University of Technology, 5600 MB Eindhoven, The Netherlands
[2] ASML, Veldhoven 5504 DR, The Netherlands
[3] Systems and Control Laboratory, Institute for Computer Science and Control, Kende u. 13-17, H-1111 Budapest, Hungary
Email: Y.L.C.Broens@tue.nl

1 Introduction

Using a high precision lithographic process, integrated circuits are produced by projecting extreme ultraviolet light on a silicon wafer using projection optics. The growing demands in the semiconductor industry require enhanced throughput, while maintaining high reliability. To meet the challenging requirements, an advanced design of a moving-magnet planar actuator is considered with a single stroke only for sub-nanometer accurate positioning of the wafer under aggressive reference trajectories. The moving-magnet planar motor configuration exhibits advantages over the currently employed moving-coil configuration, such as complete environmental decoupling of the mover and a reduction of the mover's mass, see [1]. However, these advantages come at the cost of introducing highly complex dynamic behaviour to be tamed by motion control.

2 Problem description

A moving-magnet planar motor is a MIMO system, which exhibits position dependency in both actuation and sensing. Figure 1 illustrates the control architecture of a moving-magnet planar actuator, where the planar motor is rigid body decoupled using the commutation $\hat{\Gamma}^{-1}(\rho) \in \mathbb{R}^{40\times 6}$ and the position reconstruction matrix $\Psi(\rho) \in \mathbb{R}^{6\times 9}$, see [2]. Since the commutation matrix $\hat{\Gamma}^{-1}(\rho)$ is constructed using first-principle modelling strategies, the control design is sensitive to model inaccuracies and therefore limits the position tracking performance of the mover. In order to improve position tracking performance, an improved commutation must be employed, which accurately represents the physical relation between the currents in the coils and the physical forces acting on the mover.

3 Methodology

The currently employed model based commutation is constructed using Lorentz's force principle. The law of conservation of energy allows for reformulation of the current-to-force relation into an equivalent velocity-to-voltage relation:

$$U = \Gamma(\rho)v. \tag{1}$$

The velocity-to-voltage relation allows for experimental identification of the effect of commutation by measuring the back-EMF of passive coils during motion of the mover.

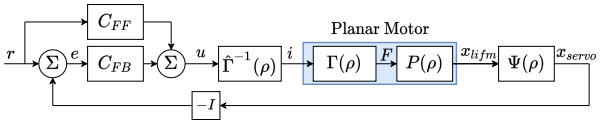

Figure 1: Control architecture of a moving-magnet planar actuator, where $\hat{\Gamma}^{-1}(\rho)$ denotes the commutation matrix and $\Psi(\rho)$ denotes the position reconstruction matrix.

This experimental concept is illustrated in Figure 2, where the passive coils are depicted in blue.

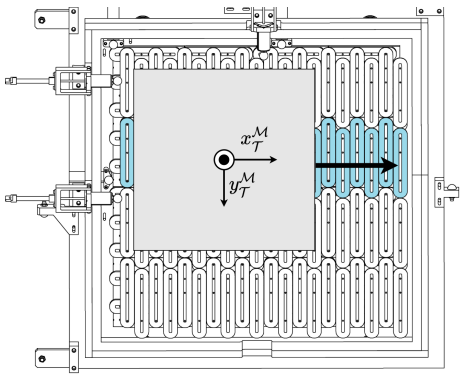

Figure 2: Schematic representation of the experimental concept, which allows for gathering data with respect to construction of a data based commutation algorithm.

The general challenge of this method is to systematically construct a data-based commutation algorithm, which accurately represents the physical relation between the currents in the coils and the physical forces acting on the mover, such that rigid body decoupling is ensured and hence position tracking performance is maximized. A possible direction is to investigate machine learning algorithms in order to obtain an accurate estimator of the commutation, based on the data gathered using the proposed experimental setting.

References

[1] I. Proimadis, *Nanometer-accurate motion control of moving-magnet planar motors*. PhD thesis, Department of Electrical Engineering, 2020.

[2] H. Butler, "Position control in lithographic equipment," *IEEE Control Systems Magazine*, vol. 31, no. 5, pp. 28–47, 2011.

Optimal power dispatching in offshore wind farms ensuring power reserve for frequency control and load mitigation

Michel KINNAERT, Younes OUDICH
Université Libre de Bruxelles
Department of Control Engineering and System Analysis
CP 165/55, 50 Av.F.D. Roosevelt, B-1050 Bruxelles, Belgium
Emails: michel.kinnaert@ulb.ac.be, younes.oudich@ulb.ac.be

1 Introduction

In the last two decades, increasing interest is brought to control the output active power of wind farms in order to meet power set-points sent to the wind turbines and fulfill the power demand. However, the ability to participate in the frequency regulation and provide ancillary services to the TSO (Transmission System Operator) is one of the present offshore wind farm challenges. The goal of this research project is to further investigate how wind farms can achieve this goal at best by taking into account wake effects, load mitigation and active power reserve in the dispatching of the active power set points to the individual turbines. The control strategy will be based on three modules. A module estimating the total power available in the immediate future, a module deducing the plant wide power reserve needed to ensure proper frequency regulation, and a module performing the optimal power dispatching including load mitigation. The developed control strategy will be implemented and validated in simulation using software like FAST.Farm and SOWFA.

2 The control strategy

The present control strategy in the Belgian offshore wind farms is based only on controlling the output power in order to dispatch the demand from ELIA (the Belgian TSO) as displayed in **Figure.1** by following the blue dots. Indeed, thanks to measurements and historical data inputs, the available power of the wind farm is predicted one day ahead. On this basis, ELIA decides on a power reference that goes through a power controller dispatching the power needed for the demand. Finally, the wind farm gives back new SCADA measurements as input to the power prediction algorithm. Our contribution is to assess the opportunity for offshore wind farms to participate in the utility grid. Indeed, by following the orange dots **Figure.1**, the wind farm power is predicted in the immediate future then converted to know the immediate future power reserve at hand. If a fault is detected, a frequency controller overcomes this disturbance by appropriate action on the wind farm power set-points.

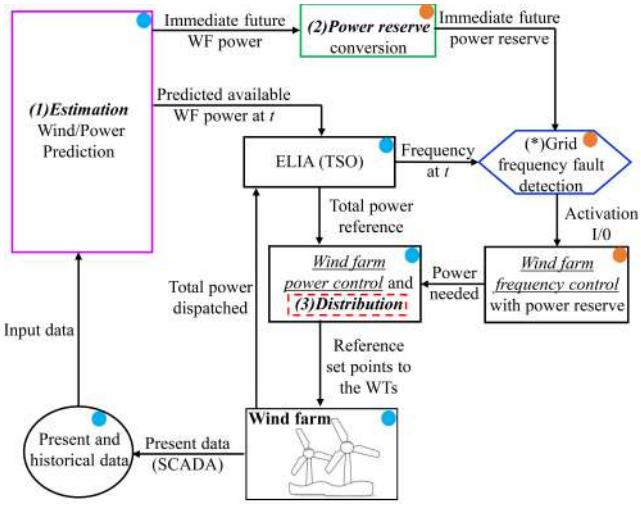

Figure 1: The control strategy of the belgian offshore wind farms (blue dots in the top right corners), and our contribution (orange dots in the top right corners

3 Future work

The research project will focus on the three following modules that are also displayed in **Figure.1**:

1. Estimation: predict the total power available now and in the immediate future.
2. Power reserve: determine the plant-wide power reserve level needed to provide frequency regulation.
3. Distribution (Control): Determine the optimal power set points to distribute to the wind turbines.

4 Acknowledgement

This research is part of the Belgian PhairywinD project, which aims to develop the current and the future offshore wind farms in a multi-disciplinary framework. It is funded by the Belgian Energy Transition Fund (FPS Economy).

References

[1] Jan-Willem van Wingerden, Lucy Pao, Jacob Aho, Paul Fleming, "Active Power Control of Waked Wind Farms" IFAC-PapersOnLine,Volume 50, Issue 1, 2017.

Intermittent Sampling in Repetitive Control: Exploiting Time-Varying Measurements

Johan Kon[1,*], Nard Strijbosch[1], Sjirk Koekebakker[2], Tom Oomen[1]
[1]Control Systems Technology, Eindhoven University of Technology, P.O. Box 513, 5600MB Eindhoven, The Netherlands
[2]Canon Production Printing, P.O. Box 101, 5900MA Venlo, The Netherlands
[*]Email: j.j.kon@tue.nl

1 Background

Repetitive control (RC) is a feedback control method that significantly reduces periodic errors, which result from periodic disturbances or references, by learning from past executions of the same task [1]. Both RC and iterative learning control (ILC) are based on the internal model principle (IMP) [2]. However, in RC, the initial condition of the current task carries over from the previous task, as opposed to ILC, in which the initial condition is the same for each task. An extensive RC framework has been developed for equidistant error data resulting from a discrete time, linear time-invariant (LTI) system [3], with frequency domain stability tests and design procedures using non-parametric models, i.e., identified frequency response functions (FRF).

2 Problem Formulation

In many industrial applications, a measurement of the error is often not available at each time step, but the time instance of the measurement, i.e. its timestamp, is available, resulting in non-equidistant (intermittent) but exact measurement data. Relevant examples include optical encoders that output the exact position at line transitions [4], and networked control systems subject to packet loss or cyberattacks.

The aim of this work is to develop a new repetitive control framework for this intermittent sampling setting, combining the traditional RC setup and a timestamping operator to model the availability of data at each timestep.

3 Results

The developed RC framework guarantees stability of the repetitive controller in the intermittent sampling setting for any realization of the measurements. The stability test can be verified in the frequency domain using a non-parametric model in the form of an identified FRF. This results in an intuitive design framework based on loopshaping techniques, allowing to explicitly address uncertainty in the non-parametric model.

The RC framework is validated on an industrial printbelt system at Canon Production Printing, in which optical sensors are used in combination with a perforated belt to measure the position of the belt. Fig. 1 shows the converged RC error in this intermittent sampling setting, compared to the initial error without RC. The developed RC framework is able to reduce the repetitive error of the printbelt significantly: from ± 370 μm to ± 60 μm, a reduction of a factor 6.

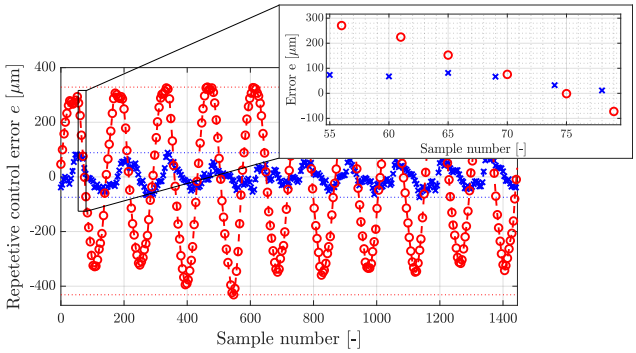

Fig. 1: Converged error of the intermittent sampling RC design at timestamps (×), as compared to the error without RC at timestamps (○). It can be observed that the available error is non-equidistant in time. Furthermore, the time instances of the available data vary over different executions of the same task. The linear interpolation of the error is shown in (- -) in the respective color.

4 Acknowledgements

This work is part of the research programme VIDI with project number 15698, which is (partly) financed by the Netherlands Organisation for Scientific Research (NWO).

References

[1] R. W. Longman, "On the theory and design of linear repetitive control systems," *European Journal of Control*, vol. 16, no. 5, pp. 447 – 496, 2010.

[2] B. Francis and W. Wonham, "The internal model principle of control theory," *Automatica*, vol. 12, no. 5, pp. 457 – 465, 1976.

[3] R. W. Longman, "Iterative learning control and repetitive control for engineering practice," *International Journal of Control*, vol. 73, no. 10, pp. 930–954, 2000.

[4] N. Strijbosch and T. Oomen, "Beyond quantization in iterative learning control: Exploiting time-varying timestamps," in *Proc. of the 2019 American Control Conference (ACC)*, Jun. 2019, pp. 2984–2989.

Efficient Model-Free Iterative Learning Control for Massive MIMO Systems using Stochastic Approximation

Leontine Aarnoudse[1,*], Tom Oomen[1]
[1]Control Systems Technology, Eindhoven University of Technology, P.O. Box 513, 5600MB Eindhoven, The Netherlands
[*]Email: l.i.m.aarnoudse@tue.nl

1 Background

Iterative learning control (ILC) aims to achieve high performance while providing robustness against model errors. Typical optimization-based ILC approaches use models combined with experimental data [1], and existing data-based methods such as [2] are experimentally expensive. This research aims to develop an efficient model-free ILC approach for massive MIMO systems using an unbiased gradient estimate that is obtained from a single experiment.

2 Problem formulation

Consider a MIMO system $J \in \mathbb{R}^{n_o N \times n_i N}$ with n_i inputs and n_o outputs, given in lifted form by

$$e = r - Jf \tag{1}$$

with input $f \in \mathbb{R}^{n_i N \times 1}$, error $e \in \mathbb{R}^{n_o N \times 1}$ and unknown exogenous disturbance $r \in \mathbb{R}^{n_o N \times 1}$. The criterion

$$\mathcal{J}(f) = \|e\|^2_{W_e} + \|f\|^2_{W_f} \tag{2}$$

with $\|x\|_W = \sqrt{x^\mathsf{T} W x}$ is minimized iteratively using a gradient descent algorithm with parameter update

$$f_{j+1} = f_j - \varepsilon_j g(f_j) \tag{3}$$

with step size ε_j and gradient

$$g(f_j) = -2J^\mathsf{T} W_e e_j + 2W_f f_j. \tag{4}$$

The gradient can be obtained using a model, or through $n_i \times n_o$ dedicated experiments on the adjoint of the system J [2, 3]. This research aims instead to use an approximation $\hat{g}(f_j)$ obtained from a single experiment.

3 Approach

A stochastic approximation adjoint ILC (SAAILC) approach is proposed, in which an unbiased approximation of the gradient is obtained from a single experiment as

$$\hat{g}(f_j) = -2\mathcal{T}^{n_i} A_j J A_j \mathcal{T}^{n_o} W_e e_j + 2W_f f_j. \tag{5}$$

The entries of matrix A_j are samples from a symmetric Bernoulli ± 1 distribution, and $\mathcal{T}$ is a time-reversal operator, for which it holds that $\mathcal{T} J^{11} \mathcal{T} = (J^{11})^\mathsf{T}$ for a SISO system J^{11}. Estimate (5) replaces $g(f_j)$ in (3), and since $\mathbb{E}(\hat{g}(f_j)) = g(f_j)$, the resulting algorithm can be interpreted as a Robbins-Monro type stochastic gradient descent algorithm, for which convergence can be shown.

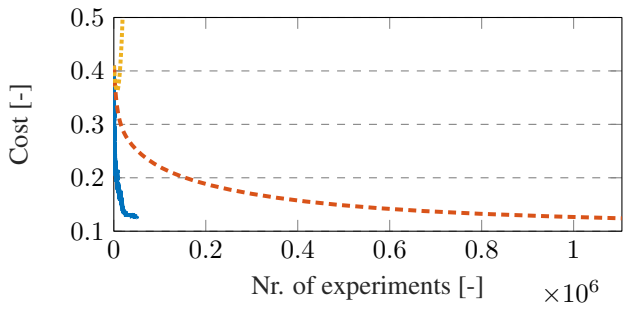

Figure 1: The cost as a function of the number of experiments in adjoint ILC for a non-symmetric 21×21 MIMO system. SAAILC (—) requires far fewer experiments to reach the same cost as non-symmetric deterministic adjoint ILC (- -), while symmetric deterministic adjoint ILC (·····) results in a diverging cost.

The proposed SAAILC approach is experimentally advantageous compared to the deterministic approach in [2], which essentially applies the method by [3] to each subsystem of J subsequently, thus requiring $n_i \times n_o$ dedicated experiments to obtain the gradient for a non-symmetric n_i by n_o system.

4 Results

In Figure 1, SAAILC is illustrated using a random non-symmetric 21×21 MIMO system. It is shown that SAAILC achieves the same cost as the deterministic MIMO adjoint ILC algorithm, while reducing the number of required experiments significantly. In addition, it is shown that assuming that the system is symmetric in order to reduce the number of experiments results in a diverging cost.

References

[1] S. Gunnarsson and M. Norrlöf, "On the design of ILC algorithms using optimization," *Automatica*, vol. 37, no. 12, pp. 2011–2016, 2001.

[2] J. Bolder, S. Kleinendorst, and T. Oomen, "Data-driven multivariable ILC: Enhanced performance by eliminating L and Q filters," *Int. J. Robust Nonlinear Control*, vol. 28, no. 12, pp. 3728–3751, 2018.

[3] B. Wahlberg, M. B. Syberg, and H. Hjalmarsson, "Non-parametric methods for L2-gain estimation using iterative experiments," *Automatica*, vol. 46, no. 8, pp. 1376–1381, 2010.

Non-smooth dynamics modeling of drill-string systems in interbedded formations

Arviandy G. Aribowo[1], Roeland Wildemans[1], Emmanuel Detournay[2], Nathan van de Wouw[1,2]
[1]Department of Mechanical Engineering, Eindhoven University of Technology, The Netherlands
[2]Department of Civil, Environmental and Geo-Engineering, University of Minnesota, U.S.A.
Email: a.g.aribowo@tue.nl

1 Introduction

The loads acting on Polycrystalline-Diamond-Compact (PDC) bits in rotary drilling systems (see Figure 1-left) change abruptly when drilling into interbedded rock formations consisting of hard and soft layers. Such fast load changes due to formation heterogeneity can significantly affect the dynamic response of the system and therewith the vibrational signature at the bit, which in turn may influence the durability of the bit and drilling efficiency. Therefore in this abstract we develop a dynamic model for drill-string systems for such drilling scenarios.

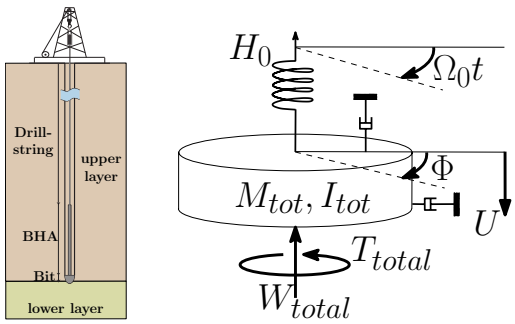

Figure 1: The schematic of drilling system (left); model of drill-string system (right).

2 Dynamic model of drill-string systems in interbedded formations

The drill-string system model in [1] (see Figure 1-right) is extended for drilling scenarios in interbedded formations, particularly for the transitional phase of the bit motion in two heterogeneous layers. This extension involves updated bit/rock interface laws that take into account that the bit can be partially engaged in more than one rock layer. As the pivotal element in the model, the bit-rock interaction couples the axial and torsional dynamics of the drill-string and has two main components (cutting and wearflat contact), that are extended to account for the heterogeneity effect of two distinct layers. The resulting dynamic model is given by

$$\mathbf{M}\ddot{\mathbf{q}} - \mathbf{h}\left(t, \mathbf{q}, \dot{\mathbf{q}}, \mathbf{q}_{t_n}\right) = \mathbf{W}\boldsymbol{\lambda}. \tag{1}$$

Herein, $\mathbf{q} = [U, \Phi]^\top$ are the generalized coordinates, where U is the axial position of the bit and Φ is the angular position, and all are functions of time t. The single and double dot symbols denote the time derivatives of $\mathbf{q}$. Furthermore, $\mathbf{q}_{t_n}$ represents the delayed coordinates of $\mathbf{q}$, where t_n is the (state-dependent) time-delay appearing in the rock cutting process due to the regenerative effect. The mass matrix is denoted by $\mathbf{M}$, while vector $\mathbf{h}$ consists of the generalized forces and torques, including those from the cutting process. Vector λ represents the wear-flat contact force (λ_a^{tot}) and the associated frictional torque (λ_t^{tot}) acting on the bit wear-flat, and their generalized force directions are contained in matrix $\mathbf{W}$. The contact-related force and torque obey set-valued force laws [1].

3 Preliminary simulation results

Figure 2 shows the simulation result of the heterogeneous model (1), particularly the rate-of-penetration ($\dot{U}$). This response illustrates that the system exhibits axial stick-slip limit cycles with a periodicity reflecting the spatial periodicity of the formation layering. This indicates that in the case of interbedded formations the response is essentially different from that in homogeneous rock formations and hence, the heterogeneous model (1) is indeed required to describe the drill-string dynamics.

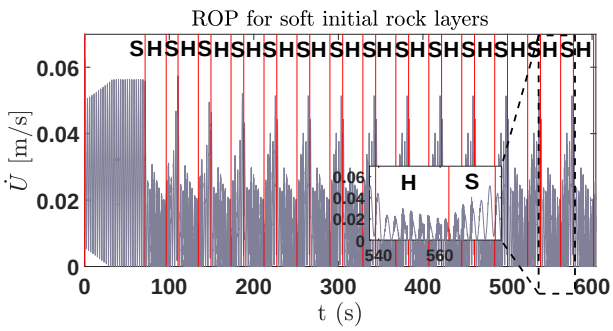

Figure 2: ROP ($\dot{U}$) in drilling interbedded formations. Red lines show the layer boundaries (S = soft, H = hard).

References

[1] R. Wildemans, A.G. Aribowo, E. Detournay, N. van de Wouw (2019) Modelling and dynamic analysis of an anti-stall tool in a drilling system including spatial friction. *Nonlinear Dynamics, Volume 98, Issue 4, pp 2631–2650.*

Design and Control of an Innovative Experimental Setup for Control Engineering Education: the Centrifugal Ring Positioner

Xavier Jordens
SAAS, Université libre de Bruxelles
50, av. F.D. Roosevelt, CP 165/55
1050 Bruxelles
Belgium
Email: xavier.jordens@ulb.be

Michel Kinnaert, Laurent Catoire
SAAS, Université libre de Bruxelles
50, av. F.D. Roosevelt, CP 165/55
1050 Bruxelles
Belgium
Email: michel.kinnaert@ulb.be

Within the years, control engineering has constantly evolved and has become present in multiple areas. The evolution of control theory is closely linked to the ability for control engineering students and researchers to perform practical experiments. This work contributes to control engineering and mechatronics teaching through the design, the construction and the control of a new experimental set-up, called the Centrifugal Ring Positioner (CRP). Detailed design process is presented with the aim of providing the required information to reproduce such device. This was the object of a master thesis project and resulted in a new teaching device used for the first time in an advanced control engineering course this year.

The device consists of a ring sliding on a rod able to move thanks to the balance between the gravity and the centrifugal force induced by the rotation of the system. This rotation is achieved by a DC gearmotor driven by a motor driver receiving analog voltage from an Arduino DUE microcontroller. Such actuator was chosen based on preliminary simulations of the system dynamics. The motor angular velocity is derived from an incremental encoder. Among potential candidates for ring position sensor, a specific optical infrared sensor was chosen based on features such as measuring range, output signal, short measuring cycle...Most pieces of the CRP are 3D-printed using Poly-Lactic Acid (PLA) as printing material. The development of such benchmark shows that 3D-printing can be used to design small mechanical devices that are easy to reproduce, low-cost and stimulating students work thanks to the presence of moving parts that are usually attractive.

The main control requirement of the CRP is defined as ring position setpoint tracking. In the present work, a cascade control strategy is implemented. The inner loop, consisting of the control of the motor angular velocity, is controlled by a P controller. Two different controllers, a PID and a PD, are designed to control the outer loop which output consists of the ring position. The PD controller is considered to obtain a closed-loop system with a higher phase margin. Both controllers fulfill the requirement in simulation as well as on the real device. The PID actually shows better control results than the PD controller since its integrating action allows to strongly reduce the offset with respect to the position setpoint. The remaining offset is mainly due to friction phenomena.

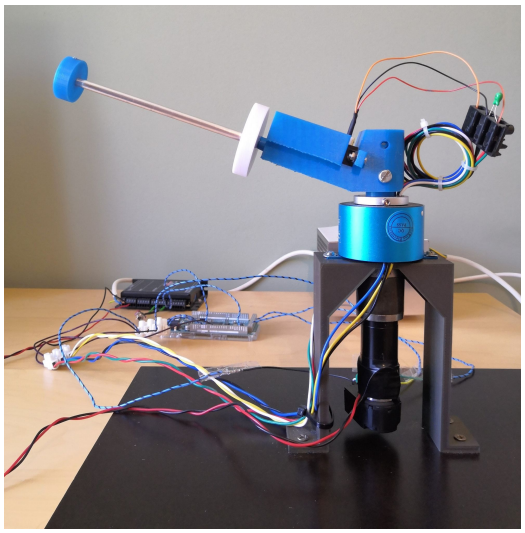

Figure 1: Centrifugal Ring Positioner.

This CRP is meant to be used as an experimental device for control engineering students. In terms of learning content, it is an unstable and non-linear system that allows to illustrate several control system concepts such as system identification, model validation, PID control, state-feedback control, LQG control...In addition to control theory, classical mechanics, instrumentation and signal processing concepts are required to achieve satisfying control performances (determination of a precise model, digital implementation of the controllers, signal noise management...). This makes the CRP a highly multidisciplinary device.

Control of Evasive Maneuvers in Automated Driving

Leila Gharavi, Bart De Schutter
Delft Center for Systems and Control
Email: L.Gharavi@tudelft.nl

Simone Baldi
Southeast University
Email: S.Baldi@tudelft.nl

1 Introduction

Autonomous driving is a potential solution to reduce traffic congestion, increase road safety, and enhance mobility for the disabled and elderly. Driving automation levels have been defined by the Society of Automotive Engineering (SAE), starting from level 0 with no automation up to level 5 involving full driving automation with an unlimited operational design domain [1]. One of the primary objectives in the driving task is collision avoidance, where performing an evasive maneuver is crucial when braking proves insufficient, especially in high-speed scenarios. In spite of the substantial research on self-driving cars, the implementation of evasive maneuvers in high levels of automation is still years away. The next section introduces some key challenges in control of evasive maneuvers and some methods for overcoming these issues.

2 Vehicle Control in Evasive Maneuvers

At least five factors contribute to challenges in controlling evasive maneuvers; each should be properly addressed if an effective solution is to be reached.

First, since experimental *data in hazardous driving scenarios are neither sufficient nor reliable*, maneuvers in such applications cannot be controlled using model-free control approaches. Second, the *vehicle's dynamics move beyond the linear range* during evasive maneuvers. As the vehicle is more likely to become unstable in such motions, more accurate dynamics must be incorporated when modeling the vehicle for reliable stability analysis. Third, the *ambient conditions* such as the road curvature, presence of other vehicles, or friction *change constantly during driving tasks*. Therefore, proposed controllers should be adaptive to the environment. Fourth, the *system is subject to uncertainties* through sensor measurements and unmodeled dynamics. Hence, control design should be accompanied by a comprehensive robustness analysis. Finally, a *fast response is essential* in avoiding collision effectively. With the necessity of complex nonlinear modeling for evasive maneuvers, the computation time and accuracy should be carefully balanced so that the proposed solution remains computationally efficient.

Tires play the major role in a vehicle's interactions with its environment by providing necessary longitudinal and lateral forces. In [2], Pacejka developed a nonlinear vehicle model through the use of the "Magic Formula", which is used to describe the longitudinal force F_x as a function of the longitudinal slip s, and both the lateral force F_y and the aligning torque M_z as a functions of the lateral slip α as follows:

$$F_x(s) = D_1 \sin\left(C_1 \tan^{-1}\left[B_1 s - E_1\left\{B_1 s - \tan^{-1}(B_1 s)\right\}\right]\right)$$
$$F_y(\alpha) = D_2 \sin\left(C_2 \tan^{-1}\left[B_2 \alpha - E_2\left\{B_2 \alpha - \tan^{-1}(B_2 \alpha)\right\}\right]\right)$$
$$M_z(\alpha) = D_3 \sin\left(C_3 \tan^{-1}\left[B_3 \alpha - E_3\left\{B_3 \alpha - \tan^{-1}(B_3 \alpha)\right\}\right]\right)$$

where B_i, C_i, D_i, and E_i with $i \in \{1,2,3\}$ are constants dependent on the friction coefficient and the normal force between tire and road. As the friction is prone to change during vehicle motion and this affects the tire forces, the control action should be adaptive to such changes.

Model Predictive Control (MPC) is an optimization strategy where the control signal is obtained by utilizing a model of the system while minimizing an objective function over a finite-time horizon. In controlling the evasive maneuvers, the objective function corresponds to path tracking error and energy consumption, and the optimization problem is solved at each step considering collision avoidance, vehicle stability, and trajectory constraints.

3 Future Research

Pacejka vehicle models and MPC-based controllers have been widely used in autonomous driving; nevertheless, they have been mostly limited to cases where linear models are applicable, such as lane-keeping during autonomous braking or safe lane-change during takeovers. Thereby, our future research with focus on using a nonlinear form of the Pacejka model while optimizing the accuracy/time tradeoff for evasive maneuvers. In addition, our MPC-based motion controller will be accompanied by an assessment of its robustness to parameter and model uncertainties.

The research is supported by the Dutch Science Foundation NWO-TTW within the EVOLVE project (nr. 18484).

References

[1] SAE International Surface Vehicle Recommended Practice. Taxonomy and Definitions for Terms Related to Driving Automation Systems for On-Road Motor Vehicles. SAE Standard J3016, Rev. Jun. 2018.

[2] H. Pacejka. *Tire and Vehicle Dynamics*. 2005.

Structured Singular Value Analysis of Incremental Dynamic Inversion

Tijmen Pollack
Faculty of Aerospace Engineering
Delft University of Technology
Kluyverweg 1
2629 HS Delft
The Netherlands
Email: T.S.C.Pollack@tudelft.nl

Erik-Jan van Kampen
Faculty of Aerospace Engineering
Delft University of Technology
Kluyverweg 1
2629 HS Delft
The Netherlands
Email: E.vanKampen@tudelft.nl

1 Introduction

Incremental Nonlinear Dynamic Inversion (INDI) is a control design methodology that forms a derivative of the widely known Nonlinear Dynamic Inversion design strategy, which is also known as feedback linearization. The incremental counterpart of NDI circumvents the need for an accurate model of the plant dynamics for system linearization by adopting direct measurement of the output derivative instead, which makes it a sensor-based control method. Previous research has shown that INDI features excellent robust performance properties in the face of regular perturbations or real uncertainties in case certain conditions are met, such as high sampling rates [1]. It is this beneficial property that has sparked substantial interest in the flight control research community in this incremental control technique, which has led to a multitude of simulation studies and in-flight demonstrations on various experimental platforms ranging from Unmanned Aerial Vehicles (UAVs) [2] to a CS-25 certified Cessna Citation II research aircraft [3].

These appealing properties notwithstanding, there are legitimate concerns about the robust stability of INDI when subjected to singular perturbations such as (uncertain) time delays, sensor dynamics, and other types of high-frequency uncertain dynamics acting in various locations of the control system. To this end, the robustness of INDI when subjected to both singular and regular perturbations is investigated using the structured singular value (μ) framework.

2 General Dynamics F-16 short-period design

The analysis is centered around a case study of a linear INDI-based (IDI) pitch rate control law design for the General Dynamics F-16, for which an open-access model is available [4]. The aircraft dynamics are linearized around a single flight condition and center of gravity location for which the vehicle is statically unstable around the pitch axis. To simplify the analysis, the resulting model is reduced to the short-period mode only. Two types of uncertainty are added to this model: 1) real uncertainty corresponding to the angle of attack stability derivative M_α and control effectiveness M_{δ_e}, and 2) complex multiplicative uncertainties at the actuator and bare airframe input channels, which are scaled to exceed 100% uncertainty at high frequencies. The overall control law consists of an incremental pitch rate inversion loop and a two degree-of-freedom outer linear control structure to achieve accurate tracking of pilot stick commands, which consists of a proportional-integrator (PI) pitch rate compensator and a reference model describing the desired dynamics. The control objectives are captured by weighting functions describing the tracking error and the disturbance profile.

3 Results

Analyzing μ and comparing IDI with its more conventional non-incremental counterpart shows that IDI enjoys more favourable robust performance properties, but also faces more severe limitations in terms of robust stability when subjected to large-scale singular perturbations. The latter stability robustness property appears to be a relative strongpoint of model-based dynamic inversion.

References

[1] X. Wang, E. van Kampen, Q. Chu and P. Lu, "Stability Analysis for Incremental Nonlinear Dynamic Inversion Control," *Journal of Guidance, Control, and Dynamics*, 42:5, 1116-1129, 2019, DOI: 10.2514/1.G003791

[2] V. Akkinapalli and F. Holzapfel, "Incremental Dynamic Inversion based Velocity Tracking Controller for a Multicopter System," AIAA 2018-1345, *2018 AIAA Guidance, Navigation, and Control Conference*, 2018, DOI: 10.2514/6.2018-1345

[3] F. Grondman, G. Looye, R. Kuchar, Q. Chu and E. van Kampen, "Design and Flight Testing of Incremental Nonlinear Dynamic Inversion-based Control Laws for a Passenger Aircraft," AIAA 2018-0385, *2018 AIAA Guidance, Navigation, and Control Conference*, 2018, DOI: 10.2514/6.2018-0385

[4] R. Russel, "Non-linear F-16 Simulation using Simulink and Matlab," University of Minnesota, 2003.

Data-Based Control Structure Selection for RCCI Engine with Electrically Assisted Turbocharger

Maarten Vlaswinkel
Einhoven University of Technology
m.g.vlaswinkel@tue.nl

Bram de Jager
Einhoven University of Technology
a.g.de.jager@tue.nl

Frank Willems
Einhoven University of Technology
f.p.t.willems@tue.nl

1 Abstract

The ever tightening worldwide emission regulations enforce major innovations in Internal Combustion Engines (ICEs) to comply with challenging real-world targets for nitrogen oxides (NO_x) and soot. Reactivity Controlled Compression Ignition (RCCI) engines promise to meet these regulations [1]. RCCI engines are a class of highly efficient engine using a high reactivity and a low reactivity fuel. The combustion in this type of engine relies on auto-ignition of the air-fuel mixture. Over the years, several RCCI control approaches have been presented (see, e.g., [2] for an overview). They are typically based on a linear diagonal controller and a static decoupling. The problem of selecting a suitable Input-Output (IO) scaling and pairing is not straight forward and not addressed in great detail in the available literature.

In this presentation, we will focus on selecting a suitable IO scaling and pairing for a decentralized feedback controller with linear parallel filters. Our method consist of three steps and are given by:

1. estimating the impulse response of the system using the Wiener filter [3];
2. IO scaling to equalize the importance of the IO signals using the Sinkhorn-Knopp (SK) algorithm [4] and, the $\mathscr{H}_2$-norm of the impulse response of step 1; and
3. IO pairing creating the basis for the diagonal structure of the controller using a Gramian-based Interaction Measure (IM) [5], IO scaling of step 2 and, the $\mathscr{H}_2$-norm of the impulse response of step 1.

The RCCI engine used in this presentation is shown in Fig. 1. It uses two fuels: natural gas for Port Fuel Injection (PFI) and Diesel for Direct Injection (DI). We are able to control the masses of fuel injected per cycle and the Start of Ignition (SOI) of the DI fuel. Furthermore, the engine is equipped with a controllable Variable Turbine Geometry (VTG), Exhaust Gas Recirculation (EGR) and E-assisted turbo.

Fig. 2 shows the magnitude of response of the scaled linearized system where the selected IO pairs are shown in red. This is not the fully decoupled system preferred when designing parallel controllers. However, these IO pairs have the least amount of interaction without losing the physical interpretation of the IO signals often the case with a static decoupling.

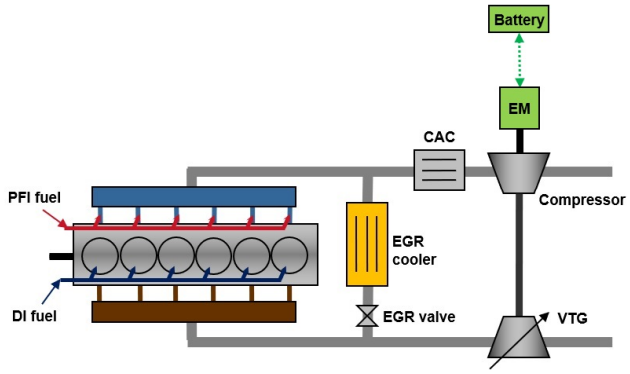

Figure 1: Schematic representation of the RCCI engine with electrically assisted turbo

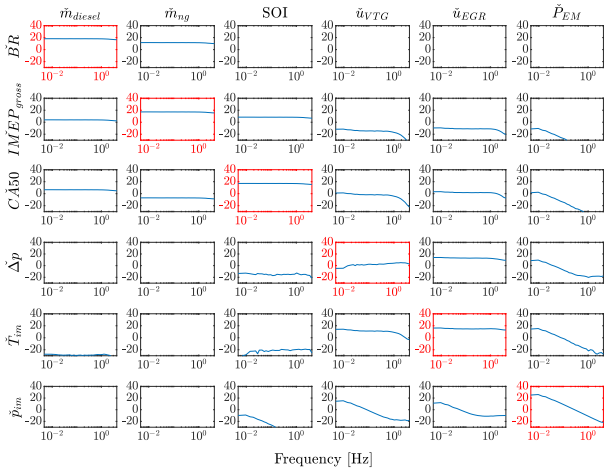

Figure 2: Magnitude of the frequency response of the scaled system with E-turbo $\check{G}(s)$, where the IO pairing is shown in red

References

[1] R. D. Reitz and G. Duraisamy, "Review of high efficiency and clean reactivity controlled compression ignition (RCCI) combustion in internal combustion engines," *Progress in Energy and Combustion Science*, vol. 46, pp. 12–71, Feb. 2015.

[2] F. Willems, "Is Cylinder Pressure-Based Control Required to Meet Future HD Legislation?" *IFAC-PapersOnLine*, vol. 51, no. 31, pp. 111–118, Jan. 2018.

[3] R. G. Brown and P. Y. C. Hwang, *Introduction to Random Signals and Applied Kalman Filtering: With MATLAB Exercises and Solutions*, 3rd ed. New York: Wiley, 1997.

[4] P. A. Knight, "The Sinkhorn–Knopp Algorithm: Convergence and Applications," *SIAM Journal on Matrix Analysis and Applications*, vol. 30, no. 1, pp. 261–275, Jan. 2008.

[5] B. Halvarsson, "Interaction Analysis in Multivariable Control Systems : Applications to Bioreactors for Nitrogen Removal," 2010.

MPC policies in Imitation Learning for Human-like Autonomous Driving

Flavia Sofia Acerbo[1,2,3], Jan Swevers[1], Tinne Tuytelaars[2] and Tong Duy Son[3]
[1] MECO Research Team, Dept. Mechanical Engineering, KU Leuven
[2] PSI Research Team, Dept. Electrical Engineering, KU Leuven
[3] Siemens Digital Industries Software, Leuven
Email: flaviasofia.acerbo@kuleuven.be

1 Introduction

To ensure user acceptance of Autonomous Vehicles (AVs), it is desired that they provide comfortable human-like driving styles, which can be learned from demonstrations of human driving itself. Imitation learning algorithms can address this problem, but usually neglect safety and sample efficiency issues, when working with deep learning policies for the AV controller. This work suggests the use of Model Predictive Control (MPC) as policy class for imitation learning in AVs, as it can provide safe model-based control, while being adaptable for different comfort perceptions.

2 Behavioral Cloning with MPC policy

Behavioral cloning seeks to find the parameters θ of a generic policy $u = \pi(x, \theta)$ to minimize the imitation loss with respect to an expert policy, characterized by $\hat{\theta}$ unknown parameters, i.e. $\mathscr{L} = ||u_{t=1:T}(x, \theta) - u_{t=1:T}(x, \hat{\theta})||_2^2$. In this setting, we can treat MPC as a policy class π.

Behavioral cloning is usually solved by gradient-based optimization algorithms, considering: $\nabla_\theta \mathscr{L} = \left[\frac{\partial u}{\partial \theta}\right]^T \nabla_u \mathscr{L}$. When u is the solution of an Optimal Control Problem (OCP), as in the case of MPC, this product can be seen as an *adjoint sensitivity* for the seed vector $\nabla_u \mathscr{L}$. This term can be accurately and efficiently computed by applying the implicit function theorem to the Karush–Kuhn–Tucker conditions of the OCP and reverse mode algorithmic differentiation [1]. From these considerations, it is possible to formulate the behavioral cloning algorithm with MPC policy as in Figure 1.

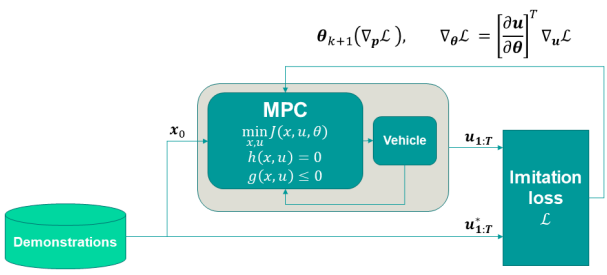

Figure 1: MPC - Behavioral Cloning Algorithm

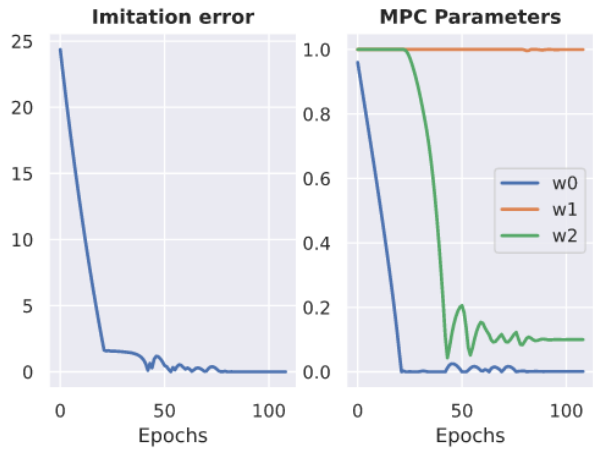

Figure 2: Evolution of the imitation error (MSE on the state trajectories) and of the learning parameters across training epochs (110 epochs)

3 Example: car moving on a linear track

As an example, we present the problem of learning the cost function objective weights for a car moving longitudinally on a linear track of length d. The adjustable cost function is in the form:

$$J(x,u) = w_0||u(t)||^2 + w_1||x(t=T) - d||^2 + w_2||v(t) - \frac{v_{max}}{2}||^2 \quad (1)$$

i.e. defining the desired balance between the control action amplitude, the total distance traveled and the vehicle speed with respect to half of the maximum speed available.

Demonstrations of the task are generated by an MPC with predefined weights ($w = [0.001, 1, 0.1]$) and imitated with Adam optimizer ($l_r = 0.01$). The learning curve of the Mean Squared Error with respect to the demonstrations, on the state trajectories, is shown in Figure 2, together with the parameter values. Their final value is $w = [0.00096, 0.998, 0.1]$.

References

[1] J. A.E. Andersson and J. B. Rawlings, "Sensitivity Analysis for Nonlinear Programming in CasADi," 2018.

Wheel Slip Estimation for Omnidirectional Vehicles

Bastiaan Vandewal Joris Gillis Jan Swevers
MECO Research Team, Department of Mechanical Engineering, KU Leuven, Belgium
Core Lab DMMS-M, Flanders Make, Leuven, Belgium
Email: bastiaan.vandewal@kuleuven.be

1 Introduction

Accurate modeling and prediction of the amount of wheel slip can strongly improve the driving behaviour and position estimates of autonomous vehicles. We present a model-based approach to improve motion planning for omnidirectional vehicles by defining a simplified traction force model for the road-tire interactions.

2 Background

The amount of longitudinal wheel slip v_{slip}, is typically defined as the difference between the surface speed of the wheel with radius r and rotational velocity ω and the translational velocity of the wheel center v:

$$v_{slip} = r\omega - v. \tag{1}$$

The longitudinal slip ratio of a wheel, also known as the slip coefficient τ, is defined as follows:

$$\tau = \begin{cases} \dfrac{v_{slip}}{r\omega}, & \text{if } r\omega \geq v \quad \text{(acceleration)} \\ \dfrac{v_{slip}}{v}, & \text{if } r\omega < v \quad \text{(braking)} \end{cases} \tag{2}$$

Tire friction models describe a normalized tire friction μ defined as the ratio of friction force to normal force. Usually, this is done by a non-linear relationship between the friction and the longitudinal slip ratio, e.g. the Magic Formula, as can be seen in Figure 1a for different road surface conditions [1]. These models are characterized by some dimensionless coefficients. A main drawback of these models is the fact that they only describe steady-state wheel slip-force relations (found under constant but not matching translational and rotational velocities). These conditions are never met during driving conditions as both velocities cannot be controlled individually.

3 Methodology

Another difficulty with road-tire friction modelling based on the slip ratio, is the varying definition of the longitudinal slip ratio to distinguish the cases of acceleration and braking. A third issue entails an undefined slip ratio if either the vehicle or a wheel is standing still. We propose to use a formulation, which is suited to be implemented in an optimal control problem by introducing a simplified differentiable friction model, expressed as function of the wheel's relative velocity v_{slip} as defined above. This directly solves all described difficulties and, by proper model choice, uses only two model parameters w_1 and w_2, related to the maximum friction coefficient and the slope of the coefficient in the low slip velocity region.

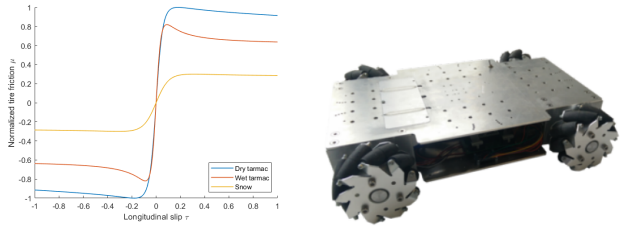

(a) Variation of tire/road friction profiles for different road surface conditions.

(b) Ourbot.

Figure 1

$$\tau = w_1 \tanh(w_2 v_{slip}) \tag{3}$$

This slip model is implemented on an in-house developed omnidirectional vehicle, the Ourbot, with four separately driven DC motors with Mecanum wheels. This vehicle, as can be seen in Figure 1b, encounters a lot of slip due to its configuration with freely rotating rollers. We only consider slip in the direction longitudinal to the axis of the rollers and assume that there will be no sliding velocity in the direction perpendicular to the roller axis as the rollers will take all movement in this rolling direction.

Firstly, a parameter estimation will be executed to find both parameters in the model. Secondly, a motion planning algorithm will incorporate this slip model to compute the wheel velocities that produce the requested movement. In this way, slip can be seen as a working tool in order to increase the mobility of the vehicle.

Acknowledgement This work has been carried out within the framework of Flanders Make's SBO project MultiSysLeCo (Multi-System Learning Control). Flanders Make is the Flemish strategic research centre for the manufacturing.

References

[1] C. Canudas-de-Wit, P. Tsiotras, E. Velenis. "Dynamic Friction Models for Road/Tire Longitudinal Interaction." in Vehicle System Dynamics 39, 3 (2003), 189–226.

Analytical Redundancy based Fault Detection for a Primary Flight Electromechanical Actuator

Benjamin Wauthion, Michel Kinnaert
SAAS, Université Libre de Bruxelles
50, av. Roosevelt, 1050 Bruxelles, Belgique
Email: bewauthi@ulb.ac.be

Paul Alexandre
SociétéAnonyme Belge deConstruction Aéronautique
Chaussée de Haecht 1470, 1130 Bruxelles, Belgium
Email: paul.alexandre@sabca.be

1 Introduction

It is within the framework of the 'more electrical aircraft' trend, in the nineties, that the development of electrically powered actuators for flight controls has started. A notable step of this evolution is the design of the Electro-Hydrostatic Actuators (EHAs) which grant the suppression of one of the three independent hydraulic systems present on a conventional aircraft [1]. As an alternative to EHAs, the Electromechanical Actuator (EMA) provides a simpler solution that could improve weight, consumption and reliability figures while decreasing maintenance requirements. However, the reliability of EMA technology has not yet been sufficiently demonstrated for its use on critical applications. Indeed, due to the EMA design, i.e. gear teeth, ball bearings and screw, the prediction of its behaviour over a long time horizon is difficult for the primary flight control application. In particular, the occurrence of mechanical jamming has to be excluded for safety reason. This is why health monitoring is used to quantify the degradation of EMA components, and this before a failure appears. Such an approach will ensure the enhancement of the safety margins [2].

This abstract introduces a model-based fault detection algorithm for friction change detection of an EMA and this using the usual pre flight check up position triangle performed by the pilot. The approach presently relies on the assumption that the detection of any abnormal behaviour is a direct indicator of the initiation of a mechanical fault. The industrial partner, SABCA, provides test benches to test and validates EMA models as well as monitoring approaches.

2 The approach

To construct the fault detection method a model of the EMA is required. This model describes the EMA (constituted of an electric motor, a gear box, a nut/screw mechanism, and a rod) and its environment, namely, the controlled surface (CS) linked to the EMA and the external force applied on the CS. This external part models either an in flight aerodynamic force or the interaction with the test bench. Figure 1 gives an overview of the system. A six parameters Stribeck friction model including stiction and viscous frictions terms and accounting for dependence with respect to the load is considered within the EMA model.

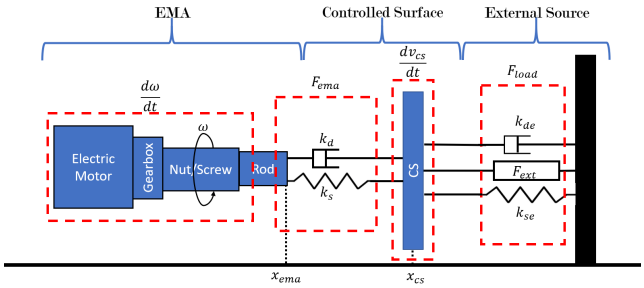

Figure 1: Schematic view of the EMA and its environment

A state space model of the EMA can be written:

$$\dot{X} = f(X, U, \Theta_0) \tag{1}$$

Where X and U are the states and inputs vectors and Θ_0 is the vector of friction parameters associated to healthy EMA operation. Given the available measurements, an analytical redundancy relations can be deduced from Equation (1), and used to obtain a residual, namely a fault indicator. The latter deviates from a zero value as soon as the measurements are associated to a modified friction behaviour characterised by a vector of friction parameters $\Theta_f \neq \Theta_0$. Proper lowpass filtering is introduced to cope with measurement noise and spurious residual values due to transient are eliminated by exploiting the repeatability of the pre-flight EMA position triangle.

3 Acknowledgement

This work is supported by the Brussels-Capital Region (Innoviris) through the project MONISA (Health Monitoring for a Primary Flight Surface Electromechanical

References

[1] D. Van Den Bossche, "The A380 flight control electrohydrostatic actuators, achievements and lessons learnt," 25th International Congress of the Aeronautical Sciences, 2006.

[2] M. Todeschi and L. Baxerres, "Health monitoring for the flight control EMAs," IFAC-Papers,48(21), 2015.

Safe Flight Envelope of Closed-loop Quadcopters

G. Delansnay[1], H. G. Harno[2], Y. Kim[2], A. Vande Wouwer[1]
[1] System, Estimation, Control and Estimation (SECO), University of Mons, Belgium
[2] Department of Aerospace and Software Engineering, Gyeongsang National University, Republic of Korea
Email: gilles.delansnay@umons.ac.be

1 Introduction

In past years, quadcopters have experienced an ever increasing success due to the myriad of possible applications in transportation, photography and filming, structure inspection, farming, etc. Unfortunately, aerial vehicles are subject to perturbations or loss of control which can lead to important material damage or injuries. In order to secure aerial flight, safety tools should be developed. One of them is the Safe Flight Envelope (SFE) which determines the possible safe positions of the vehicle and allows establishing a safe strategy. It is defined as *a region within which the vehicle possesses the ability to leave, and then, return the trim condition in a finite time horizon* [1]. This study proposes an original procedure to compute the SFE by a forward-backward reachability analysis (see figure 1) based on zonotopes [2], and applied to a Parrot Mambo quadcopter.

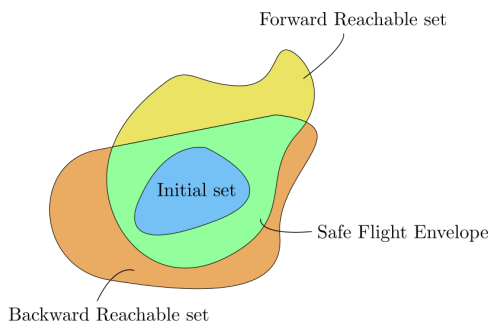

Figure 1: Safe Flight Envelope through Forward and Backward Reachability.

2 Closed-loop model identification

Quadcopters use complex control structures in order to achieve performance and robustness. The closed-loop structure has the decisive advantage of providing a partial linearization of the system, and the underlying idea of our analysis in order to develop an approximate linear state space representation of the system by resorting to input-ouput data sets and subspace identification. This model is at the core of the zonotopic reachability analysis.

3 Zonotopic Forward and Backward Reachability

Consider a set of initial conditions $\mathscr{X}_0$, a reference trajectory $u(.)$ with $\mathscr{X}_f(t_f, x_0, u(.)$ the set of solutions of our identified model and $\mathscr{X}_b(t_f, x_0, u(.))$ the set of solutions from the backward model. The forward and backward reachable set are given by:

$$R_f(t_f) = \{\mathscr{X}_f(t_f, x_0, u(.)) \in \mathbb{R}^n | x_0 \in \mathscr{X}_0, \forall t : u(t) \in \mathscr{U}(t)\}$$
$$R_b(t_f) = \{\mathscr{X}_b(t_f, x_0, u(.)) \in \mathbb{R}^n | x_0 \in \mathscr{X}_0, \forall t : u(t) \in \mathscr{U}(t)\}$$

Both sets are computed using the CORA toolbox [3]. The Safe flight Envelope corresponds to the intersection of the two sets.

4 Results

Figure 2 shows a safe Flight envelope using the approach described above.

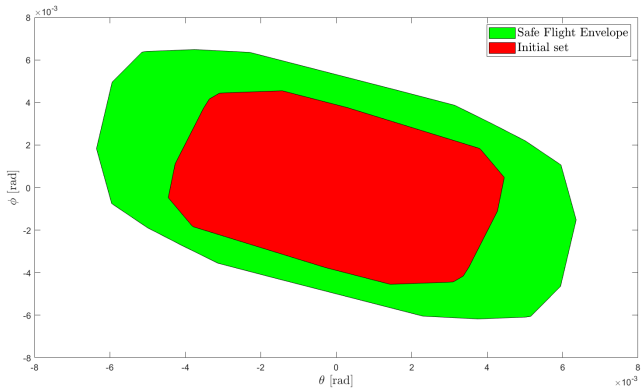

Figure 2: Safe Flight Envelope (green) for pitch and roll angles after 0.005 s from given initial set (red) and under an unitary step altitude reference.

References

[1] S. Sun, C.C. de Vissery, "Quadrotor Safe Flight Envelope Prediction in the High-Speed Regime: A Monte-Carlo Approach", Delft University of Technology, AIAA Scitech 2019 Forum.

[2] H. G. Harno, Y. Kim, "Flight envelope estimation for helicopters under icing conditions via the zonotopic reachability analysis", Gyeongsang National University, Aerospace Science and Technology, volume 102, 105859, July 2020 .

[3] M. Althoff, N Kochdumper, and M. Wetzlinger, "CORA 2020 Manual", Technical University of Munich, 2020.

A Traffic-Rule Compliant Motion Planner for Autonomous Vessels Using Nonlinear Model Predictive Control

A. Tsolakis L. Ferranti V. Reppa R. R. Negenborn
Delft University of Technology
Mekelweg 2, 2628 CD Delft, The Netherlands
{a.tsolakis, l.ferranti, v.reppa, r.r.negenborn} @tudelft.nl

Autonomous vessels will have a crucial role in the near future for both navigation in inland waterways and harbor areas (e.g., Port of Rotterdam) aiming at improving efficiency and safety. However, there are urgent societal concerns we need to address to fully benefit from these technologies. In particular, autonomous vessels need to *safely interact with human-operated vehicles in mixed traffic conditions*. In addition, they must *handle unexpected events*, such as faults, without causing disruptions and jeopardizing human safety. These issues should be overcome to enhance the trust of the ship owners, passengers, and stakeholders, in order to make autonomous vessels a reality in our daily life.

The motion planning module of autonomous vessels plays a fundamental role to address these societal concerns. The motion planner elaborates the information the sensors provide about the environment and generates collision-free paths for the low-level path following controller. The task of the motion planner is complicated by the presence of various sources of uncertainties, even in structured environments (such as seaports or canals). A major source of uncertainty is caused by the unknown human behaviour in mixed-traffic conditions given that it is extremely difficult to predict the actions of human operated vessels. Moreover, the motion planner should consider the International Regulations for Preventing Collisions at Sea (COLREGS). These traffic rules specify the type of maneuvers that should be taken by marine vessels in situations where there is risk of collision.

Recently, extensive research has been conducted to develop collision avoidance strategies that are COLREGS-compliant, leveraging the fact that all marine surface vessels must adhere to these regulations. Some of these strategies follow a reactive approach, such as Artificial Potential Fields (APF) [1] or Velocity Obstacles (VO) [2], while others follow higher level approaches, such as Rapidly-exploring Random Tree (RRT) [3], or optimization-based approaches, such as Model Predictive Control (MPC) [4, 5]. Compliance with COLREGS however is non trivial, as highlighted by the state of the art. Existing methods usually consider a subset of these rules, thus allowing explicit violations in some scenarios (e.g., making minor course alterations that are difficult to detect by other ships or turning to port when a collision risk exists). Moreover, there is still limited research that focuses on decision making for complex multi-vessel scenarios, in which the Autonomous Surface Vessel (ASV) may encounter various situations (i.e., crossing, head-on and/or overtaking) with respect to the other vessels simultaneously. One major source of these limitations is the assumption that all the other vessels maintain their course and speed.

In this work we design a COLREGS compliant motion planner based on MPC. More specifically, we express the most relevant subset of these rules as a combination of both hard and soft constraints of an online optimization problem based on which we can predict the human-operated vessels' trajectories and therefore design a rule-compliant and collision-free trajectory for the ASV. The work proposed here aims to form the foundation of our future work, addressing the problem of motion planning in congested traffic scenarios. In addition, the proposed framework also aims to accommodate cooperation among other autonomous vessels by utilizing information exchange to enhance robustness with respect to mixed traffic uncertainties in challenging multi-vessel traffic scenarios.

References

[1] Hongguang Lyu and Yong Yin. COLREGS-constrained real-time path planning for autonomous ships using modified artificial potential fields. *The Journal of Navigation*, 72(3):588–608, 2019.

[2] Yoshiaki Kuwata, Michael T Wolf, Dimitri Zarzhitsky, and Terrance L Huntsberger. Safe maritime autonomous navigation with COLREGS, using velocity obstacles. *IEEE Journal of Oceanic Engineering*, 39(1):110–119, 2013.

[3] Hao-Tien Lewis Chiang and Lydia Tapia. COLREG-RRT: An RRT-based COLREGS-compliant motion planner for surface vehicle navigation. *IEEE Robotics and Automation Letters*, 3(3):2024–2031, 2018.

[4] Tor Arne Johansen, Tristan Perez, and Andrea Cristofaro. Ship collision avoidance and COLREGS compliance using simulation-based control behavior selection with predictive hazard assessment. *IEEE transactions on intelligent transportation systems*, 17(12):3407–3422, 2016.

[5] Z. Du, V. Reppa, and R.R. Negenborn. MPC-based COLREGS compliant collision avoidance for a multi-vessel ship-towing system. In *European Control Conference (ECC'21)*, June/July 2021.

Putting Back Actuation in Pneumatically Actuated Soft Robots: modeling and backstepping control

Maximilian Stölzle
Cognitive Robotics
Delft University of Technology
Mekelweg 2
2628 CD Delft
The Netherlands
Email: M.W.Stolzle@tudelft.nl

Cosimo Della Santina
Cognitive Robotics
Delft University of Technology
Mekelweg 2
2628 CD Delft
The Netherlands
Email: C.DellaSantina@tudelft.nl

1 Introduction

The control of continuum soft robots is very challenging because of the unlimited degrees of freedom and the considerable nonlinear characteristics such as multi-body dynamics and nonlinear potentials [1]. This complexity can be tamed by combining feedback controllers (which are inherently robust to model uncertainties), and simplified models of the soft robot's dynamics. For what concerns the latter, many approaches investigated the use of the Constant Curvature (CC) assumption and its extensions for static and dynamic control [2] for continuum soft robotic manipulators. While the actuator dynamics are neglectable for tendon-driven robots, the actuator dynamics of pneumatic actuators is slower and more nonlinear [1]. But existing model-based dynamic controllers for soft robots do not consider these actuator dynamics if not through simple heuristics. We propose a general approach based on backstepping to incorporate pneumatic actuator dynamics into model-based control for soft robots independent of the chosen model for the soft system.

2 Dynamic model and backstepping control

We consider a robot with n_S segments each of them with n_D configurations q and actuated with a set of n_C dedicated pneumatic chambers. We model the fluid as an ideal gas in first approximation and consider the process to be isotherm. We require access to a function $V_{C,i}(q)$ which maps the robot configuration $q \in \mathbb{R}^{n_S \times n_D}$ to the volume of fluid stored in the robot chamber i. This function can be derived either analytically for the specific system or off-line from data. We derive the acting forces and equations of motion of the pneumatic actuator using the conversation of energy principle.

We use the backstepping [3] control technique to derive the model-based controller taking into account the full system dynamics including the dynamics of the pneumatic actuator. We assume that we have access to a feedback controller $\gamma(\mathbf{q}, \dot{\mathbf{q}})$ such that the reduced system without actuator dynamics convergences to a desired trajectory $\bar{\mathbf{q}}$ and suppose that convergence can be proven using the Lyapunov function $H(\mathbf{q}, \dot{\mathbf{q}})$. We subsequently prove convergence for the full system using backstepping in two steps first for the velocity of the pistons $\dot{\mu}_p$ and subsequently for the required actuation force on the pistons $\mathbf{f}_p$.

3 Example: Tracking posture under PCC approximation

We show the effectiveness of our approach for the example of a soft continuum manipulator robot modelled using the Piecewise Constant Curvature (PCC) assumption. We use a trajectory tracking controller based on the PCC model [2] and derive the full system controller using backstepping as explained above and evaluate the actuation-aware controller against the same PCC controller unaware of the actuation dynamics. We expect our approach to perform very similarly in quasi-static conditions and much better for highly dynamic movements. [2] shows that for sinusoidal movements with high frequencies the tracking error is still significant especially at the extremas of the movement.
We verify our approach in a FEM simulation with integrated CFD to simulate the behaviour of the pneumatic fluid. We discretize each arm segments into several rigid links connected through a revolute joint.
We additionally perform experiments using a soft planar robotic arm inspired by an elephant trunk analogue to [2].

References

[1] T. George Thuruthel, Y. Ansari, E. Falotico, and C. Laschi, "Control strategies for soft robotic manipulators: A survey," *Soft robotics*, vol. 5, no. 2, pp. 149–163, 2018.

[2] C. Della Santina, R. K. Katzschmann, A. Bicchi, and D. Rus, "Model-based dynamic feedback control of a planar soft robot: trajectory tracking and interaction with the environment," *The International Journal of Robotics Research*, vol. 39, no. 4, pp. 490–513, 2020.

[3] P. V. Kokotovic, "The joy of feedback: nonlinear and adaptive," *IEEE Control Systems Magazine*, vol. 12, no. 3, pp. 7–17, 1992.

Trajectory-Based Motion Prediction for Second-Order Systems

Aykut Isleyen Nathan van de Wouw Ömür Arslan
Department of Mechanical Engineering, Eindhoven University of Technology
P.O. Box 513, 5600 MB Eindhoven, The Netherlands
Email: {a.isleyen,n.v.d.wouw,o.arslan}@tue.nl

1 Introduction

The stability of a second-order dynamical motion can be achieved using several standard methods [1]. However, this does not ensure that the resulting motion trajectory of the system moving among obstacles is free of collisions, because stability does not mean safety, and vice versa. We present two different ways of constructing convex trajectory bounds for use in the motion prediction of overdamped second-order systems that can be used for efficient collision checking, safety assessment, and motion planning.

2 Overdamped Second-Order Systems

Consider a second-order dynamical system (1), with position $\mathrm{x} \in \mathbb{R}^n$ and velocity $\dot{\mathrm{x}} \in \mathbb{R}^n$, that moves toward a goal $\mathrm{x}^* \in \mathbb{R}^n$:

$$\ddot{\mathrm{x}} = -\kappa_p(\mathrm{x} - \mathrm{x}^*) - \kappa_d \dot{\mathrm{x}}, \tag{1}$$

with x^*, a constant position reference, under proportional-derivative control with scalar gains $\kappa_p, \kappa_d > 0$ that ensure the system is overdamped, i.e., $\kappa_d^2 - 4\kappa_p > 0$. The motion trajectory of the system, starting from initial condition $\mathrm{x}(0) = \mathrm{x}_0$ and $\dot{\mathrm{x}}(0) = \dot{\mathrm{x}}_0$, is given by

$$\mathrm{x}(t) = \mathrm{c}_0 + \mathrm{c}_1 e^{-\tau_1 t} + \mathrm{c}_2 e^{-\tau_2 t}, \tag{2}$$

for all $t \geq 0$, where $\tau_{1,2} = \frac{\kappa_d \pm \sqrt{\kappa_d^2 - 4\kappa_p}}{2}$, and

$$\mathrm{c}_0 = \mathrm{x}^*, \quad \mathrm{c}_1 = -\frac{\tau_2(\mathrm{x}_0 - \mathrm{x}^*) + \dot{\mathrm{x}}_0}{\tau_1 - \tau_2} \quad \mathrm{c}_2 = \frac{\tau_1(\mathrm{x}_0 - \mathrm{x}^*) + \dot{\mathrm{x}}_0}{\tau_1 - \tau_2}. \tag{3}$$

3 Total Energy-Based Motion Prediction

Let the total energy $E_{\mathrm{x}^*}(\mathrm{x}, \dot{\mathrm{x}})$ of the system in (1) with respect to the goal x^* be defined as

$$E_{\mathrm{x}^*}(\mathrm{x}, \dot{\mathrm{x}}) = \tfrac{1}{2}\kappa_p \|\mathrm{x} - \mathrm{x}^*\|^2 + \tfrac{1}{2}\|\dot{\mathrm{x}}\|^2, \tag{4}$$

which dissipates according to $\dot{E}_{\mathrm{x}^*}(\mathrm{x}, \dot{\mathrm{x}}) \leq -\kappa_d \|\dot{\mathrm{x}}\|^2$. From LaSalle's invariance principle [1], one has that the state (position and velocity) trajectory of the system lies in the level sets of the total energy. Hence, the motion trajectory $\mathrm{x}(t)$ of the system is contained in the projection of the energy level sets onto the position coordinates [2], which is the ball centered at x^* and with squared radius $\frac{2}{\kappa_p} E_{\mathrm{x}^*}(\mathrm{x}_0, \dot{\mathrm{x}}_0)$, denoted by

$$\mathrm{B}_{\mathrm{x}^*}(\mathrm{x}_0, \dot{\mathrm{x}}_0) = \left\{ y \in \mathbb{R}^n \middle| \|\mathrm{y} - \mathrm{x}^*\|^2 \leq \tfrac{2}{\kappa_p} E_{\mathrm{x}^*}(\mathrm{x}_0, \dot{\mathrm{x}}_0) \right\}, \tag{5}$$

i.e., $\mathrm{x}(t) \in \mathrm{B}_{\mathrm{x}^*}(\mathrm{x}_0, \dot{\mathrm{x}}_0)$ for all $t \geq 0$.

Proposition 1 *The total energy ball in (5) is positively inclusive (meaning that it shrinks forward in time), i.e.,*

$$\mathrm{B}_{\mathrm{x}^*}(\mathrm{x}(t_1), \dot{\mathrm{x}}(t_1)) \supseteq \mathrm{B}_{\mathrm{x}^*}(\mathrm{x}(t_2), \dot{\mathrm{x}}(t_2)) \qquad \forall t_1 \leq t_2. \tag{6}$$

4 Trajectory-Based Motion Prediction

The motion trajectory of the system in (2) can be leveraged to derive a motion prediction that is highly dependent on the initial conditions, x_0, $\dot{\mathrm{x}}_0$, and the control parameters, κ_p, κ_d.

Proposition 2 *The motion trajectory $x(t)$ of an overdamped second-order dynamical system in (1) is bounded as*

$$\mathrm{x}(t) \in \mathrm{T}_{\mathrm{x}^*}(\mathrm{x}_0, \dot{\mathrm{x}}_0) := \mathrm{conv}(\mathrm{x}^*, \mathrm{x}_0, \mathrm{x}_0 + \tfrac{\dot{\mathrm{x}}_0}{\tau_1}) \quad \forall t \geq 0, \tag{7}$$

where conv *denotes the convex hull of its arguments.*

Proposition 3 *The triangular motion prediction in (7) shrinks (i.e., is positively inclusive) for all future times, i.e.,*

$$\mathrm{T}_{\mathrm{x}^*}(\mathrm{x}(t_1), \dot{\mathrm{x}}(t_1)) \supseteq \mathrm{T}_{\mathrm{x}^*}(\mathrm{x}(t_2), \dot{\mathrm{x}}(t_2)) \qquad \forall t_1 \leq t_2. \tag{8}$$

5 Motion Prediction with Goal Updates

In motion planning, one constantly needs to change the goal location x^*, for example, in order to track a complex navigation trajectory. In this part, we present how an existing motion prediction can be updated after the goal is changed.

Suppose a new goal position $\hat{\mathrm{x}}^* \in \mathbb{R}^n$ is selected within $\varepsilon \geq 0$ distance to the original goal x^*, i.e., $\|\hat{\mathrm{x}}^* - \mathrm{x}^*\| \leq \varepsilon$. Let $\mathrm{x}(t)$ and $\hat{\mathrm{x}}(t)$ denote the motion trajectories of the system, starting from the same initial condition $\mathrm{x}(0) = \hat{\mathrm{x}}(0) = \mathrm{x}_0$ and $\dot{\mathrm{x}}(0) = \dot{\hat{\mathrm{x}}}(0) = \dot{\mathrm{x}}_0$ towards x^* and $\hat{\mathrm{x}}^*$, respectively.

Proposition 4 *If $M_{\mathrm{x}^*}(\mathrm{x}_0, \dot{\mathrm{x}}_0)$ is a set containing the motion trajectory $\mathrm{x}(t)$ towards x^* for all $t \geq 0$, then the motion trajectory $\hat{\mathrm{x}}(t)$ of the system towards $\hat{\mathrm{x}}^*$ is contained in $M_{\mathrm{x}^*}(\mathrm{x}_0, \dot{\mathrm{x}}_0) \oplus \mathrm{B}_\varepsilon$ for all $t \geq 0$, where $\oplus$ denotes the Minkowski sum and $\mathrm{B}_\varepsilon := \left\{ \mathrm{y} \in \mathbb{R}^n \middle| \|\mathrm{y}\| \leq \varepsilon \right\}$ is the origin-centered ball of radius ε.*

Proposition 5 *For a goal update from point x^* to $\hat{\mathrm{x}}^*$ with $\|\hat{\mathrm{x}}^* - \mathrm{x}^*\| \leq \varepsilon$, the triangular trajectory bound in (7) satisfies*

$$\mathrm{T}_{\hat{\mathrm{x}}^*}(\mathrm{x}_0, \dot{\mathrm{x}}_0) \subseteq \mathrm{conv}(\mathrm{x}^* \oplus \mathrm{B}_\varepsilon, \mathrm{x}_0, \mathrm{x}_0 + \tfrac{\dot{\mathrm{x}}_0}{\tau_1}) \subseteq \mathrm{T}_{\mathrm{x}^*}(\mathrm{x}_0, \dot{\mathrm{x}}_0) \oplus \mathrm{B}_\varepsilon$$

6 Conclusions

In this paper, we present a novel trajectory-based motion prediction algorithm for overdamped second-order systems that has a stronger dependency on initial conditions and control parameters than the classical energy-based motion prediction approach, while still enjoying a similar positive inclusion property that is critical for recursive safety assessments and motion planning. Our ongoing research focuses on the generalization of these tools to higher-order systems and their applications in reactive safe motion planning [2].

References

[1] H. K. Khalil, *Nonlinear Systems*. Prentice Hall, 2001.

[2] Ö. Arslan and D. E. Koditschek, "Smooth extensions of feedback motion planners via reference governors," in *IEEE Int. Conf. on Robotics and Automation*, 2017, pp. 4414–4421.

Efficient path planning for automated guided vehicles using A* (Astar) algorithm incorporating turning costs in search heuristic

K.J.C. Fransen[1,2] & J.A.W.M. van Eekelen[1,2]
[1]Vanderlande Industries B.V., P.O. Box 18, 5460AA, Veghel, The Netherlands
[2]Eindhoven University of Technology, P.O. Box 513, 5600MB, Eindhoven, The Netherlands
karlijn.fransen@vanderlande.com

1 Introduction

Automated Guided Vehicles (AGVs) are mobile robots that are widely used in flexible manufacturing systems, logistic systems and other industrial environments. The path planned for an AGV is often derived from the lowest-cost path in the corresponding (weighted) geometric graph. A geometric graph is a graph where vertices represent physical locations in a 2D plane and edges represent straight line segments connecting those locations. Several well-known algorithms can be used to find the lowest-cost path; here we focus on the A* algorithm [1].We propose a heuristic for the A* algorithm, in order to efficiently find the lowest-cost path on a geometric graph, taking into account costs for turns that need to be made on the spot. We assume that the weights in the graph represent notions of time. In order to find the lowest-cost, or shortest-time, path, we need an underestimation of the costs from current vertex to destination vertex, i.e. an admissible heuristic needs to be defined. The closer the value of the heuristic to the actual costs, the more efficient the heuristic is (i.e. the lower the number of iterations needed to find the lowest-cost path).

2 Heuristic

Our heuristic $h(v_c, v_d)$ from current vertex v_c to destination vertex v_d, is equal to the sum of a part related to translation, $h_{\text{trans}}(v_c, v_d)$, and a part related to rotation, $h_{\text{rot}}(v_c, v_d)$. The part $h_{\text{trans}}(v_c, v_d)$ is a lower bound estimate of the time needed by the AGV to translate from current vertex v_c to destination vertex v_d over the edges in the graph. It is equal to the Euclidean distance $d(v_c, v_d)$ between v_c and v_d, divided by the maximum AGV speed, s_{max}, i.e.:

$$h_{\text{trans}}(v_c, v_d) = \frac{d(v_c, v_d)}{s_{\text{max}}}. \tag{1}$$

The part related to rotation, $h_{\text{rot}}(v_c, v_d)$, is equal to:

$$h_{\text{rot}}(v_c, v_d) = p_{\text{turn}}\theta_{\text{min}}(v_c, v_d), \tag{2}$$

with p_{turn} the turning costs per radian, which represents the minimum time it takes for an AGV to rotate over one radian, and $\theta_{\text{min}}(v_c, v_d)$ a lower bound estimate of the necessary rotations needed to move from (current orientation at) v_c to (desired end orientation Φ_{end} at) v_d. This lower-bound estimate is equal to the sum of three minimum absolute angles

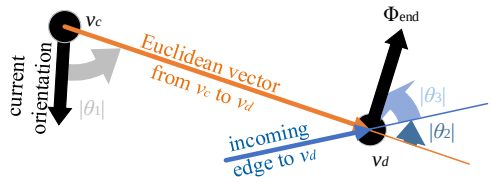

Figure 1: Minimum absolute angles of rotation $|\theta_1|$, $|\theta_2|$ and $|\theta_3|$ for current vertex v_c and destination vertex v_d.

of rotation. These angles of rotation are shown in Figure 1 as $|\theta_1|$, $|\theta_2|$ and $|\theta_3|$. The last two angles of orientation depend on the incoming edge to destination vertex v_d; the lower-bound estimate $\theta_{\text{min}}(v_c, v_d)$ is therefore computed as:

$$\theta_{\text{min}}(v_c, v_d) = |\theta_1(v_c, v_d)| + \min_{(v_i, v_d) \in E}(|\theta_{2,(v_i,v_d)}| + |\theta_{3,(v_i,v_d)}|), \tag{3}$$

with E the set of all edges in the graph.

3 Results

A simulation study has been executed to determine the number of iterations needed to travel from one to another vertex, for different graphs, for all source-destination combinations, for different heuristics. Compared to a modified version of the heuristic defined by [2], and the heuristic defined by a.o. [3], a decrease of up to 68% for the weighted average number of iterations needed to find one vertex in the lowest-cost path was achieved, depending on the selected input parameters. Using information about the graph structure in the heuristic can further decrease the number of iterations.

References

[1] P. E. Hart, N. J. Nilsson, and B. Raphael, "A formal basis for the heuristic determination of minimum cost paths," *IEEE Trans. Syst. Sci., Cybern.*, vol. 4, no. 2, pp. 100–107, 1968.

[2] Y. Cui, D. P. Ma, Y. Fang, and Z. Lei, "Conflict-free path planning of AGV based on improved A-star algorithm," in *ICICE*, 2018, pp. 31–34.

[3] J. Bae and W. Chung, "A heuristic for path planning of multiple heterogeneous automated guided vehicles," *Int. J. Precis. Eng. Man.*, vol. 19, no. 12, pp. 1765–1771, 2018.

Collision-free path planning for robot manipulators using spline approximations of the cartesian motion

Dries Dirckx, Jan Swevers, Wilm Decré, Joris Gillis, Goele Pipeleers
MECO Research Team, Department of Mechanical Engineering, KU Leuven
DMMS-M Core Lab, Flanders Make, Leuven, Belgium
Celestijnenlaan 300, B-3001 Heverlee
Belgium
Email: dries.dirckx@kuleuven.be

1 Introduction

Current research efforts in robotics focus on automatic, optimal, collision-free path planning algorithms in cluttered environments. Industrial application areas of interest include automated bin picking, automated assembly and human-robot collaboration. To enforce near-continuous collision avoidance, several algorithms use the convex hull of the robot's motion within a control interval, which is complex to compute for a general 3D motion. This work introduces a novel motion planning algorithm that establishes a continuous, piecewise polynomial approximation of the robot's trajectory. Path planning is formulated as a time-optimal control problem with joint accelerations $\ddot{q}$ as control input. This abstract's contribution is introducing a continuous-time alternative to classical time-gridding approaches, enforcing constraints efficiently at all times, instead of only on discrete control points.

2 Spline approximation of Cartesian trajectory

The joint dynamics for an acceleration-resolved robot controller are described by the double-integrator system $\dot{x} = [\dot{q}, \ddot{q}]$ using $\mathrm{x} = [q, \dot{q}]^T$ as the robot's control state. Discretisation yields joint trajectories with piecewise quadratic time-dependency. Using the forward kinematics $F[q(t)]$ of the robot, an approximation of the Cartesian trajectory $p(t)$ is constructed per control interval

$$p(t) = \sum_{i=0}^{n} F[q(\frac{i\Delta t}{n})])b_{i,n}(t) \quad t \in [0, \Delta t] \tag{1}$$

where $b_{i,n}(t)$ represent n^{th} degree Bernstein basis polynomials [1]. Near-continuous collision avoidance is imposed using the convex hull property of Bernstein polynomials and the separating hyperplane theorem discussed by Mercy et al. [2] By constraining the polynomial's coefficients, the actual trajectory continuously satisfies constraints up to an approximation error.

3 Numerical validation

Figure 1 shows a robot trajectory avoiding a cube. The obstacle is avoided over the whole trajectory, not only on the control points.

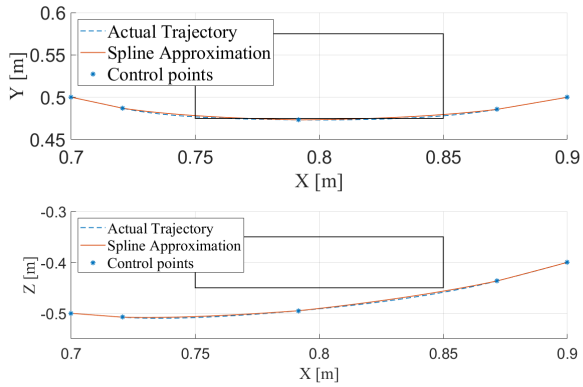

Figure 1: 2D representation of approximation vs actual trajectory for 3D example

The proposed technique avoids calculating the convex hull of the robot arm at each control interval. It will be further analysed in depth in terms of computational costs, (time-) optimality of the final trajectory and accuracy of collision avoidance for several challenging situations. A theoretical bound on the approximation error will be formulated to construct an upper limit on the accuracy.

References

[1] J. De Villiers, "Mathematics of approximation" Paris:Atlantis Press, 2012.

[2] T. Mercy, R. Van Parys, and G. Pipeleers, "Spline-Based Motion Planning for Autonomous Guided Vehicles in a Dynamic Environment" ." IEEE Transactions on Control Systems Technology, vol. 26, no. 6, 2018.

Acknowledgement

This research is supported by Flanders Make ICON FROGS: Flexible and Robust Robotic Gripping Solutions able to deal with product variability. Flanders Make is the Flemish strategic research centre for the manufacturing industry.

Heterogeneous Robotic System for Bricklaying

M. Ambrosino [1], P. Delens[2], and E. Garone[1]

[1]Service d'Automatique et d'Analyse des Systèmes, Université Libre de Bruxelles, Brussels, Belgium.
[2]Entreprises Jacques Delens S.A., Brussels, Belgium.
[1]Email corresponding author: Michele.ambrosino@ulb.be

1 Introduction

Most of the solutions proposed so far for robotic bricklaying are based on rigid arm and did not pass the prototype status. To overcome this problem we propose an innovative bricklaying concept based on two robotic sub-units: a crane, in charge of holding most of the weight of the block, and a rigid robot to achieve the desired precision during the fine placement of the block, Fig.1.

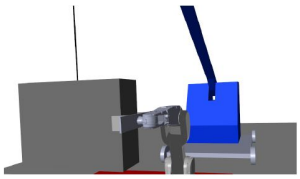

Figure 1: Robotic System

2 Modeling and Control Design

The dynamic model of the system can be obtained using the *Euler-Lagrange method* [1] considering as set of generalized coordinates q_r for the robot and q_c for the crane. The connection between the two systems can be model as *holonomic constraints*. The robot end-effector pose can be expressed as $x_r = k_r(q_r) = k_c(q_c)$, where $k_i(q_i)$ is the direct kinematics. This leads to the following constraints: $h(q) = k_r(q_r) - k_c(q_c) = 0$, where $q = \left[q_r, q_c\right]^T \in \mathbb{R}^n$. The dynamic model of the constrained mechanical system can be compactly rewritten as the following *descriptor system*

$$B(q)\ddot{q} + C(q,\dot{q})\dot{q} + g(q) = u + A(q)^T\lambda \tag{1}$$

$$\text{s.t.} \qquad A(q)\dot{q} = 0, \tag{2}$$

where $A(q) = \partial h(q)/\partial q$ is the Jacobian of the constraints, u the inputs, λ are the *Lagrangian multipliers*, the matrices $B(q)$, $C(q,\dot{q})$, and $g(q)$ represent the inertia, centripetal-Coriolis, and gravity vector, respectively. By imposing m constraints (*i.e.* $h(q) = 0$), on the n generalized coordinates, it is possible to reduce the constrained robot dynamics expressed by (1) to a $n-m$ dimensional configuration space. Let us to define a vector $v \in \mathbb{R}^{n-m}$ that represents the so-called *'pseudo velocities'* expressed by $v = D(q)\dot{q}$, where the matrix D(q) is such that

$$\begin{pmatrix} A(q) \\ D(q) \end{pmatrix} \in \mathbb{R}^{n\times n} \tag{3}$$

is a non singualar matrix. The inverse relationships from 'pseudo' to 'generalized' velocities are $\dot{q} = F(q)v$, where the columns of the matrix $F(q)$ are basis for the null space of $A(q)$. It is possible prove that the *reduced-dynamic model* can be expressed as

$$(F^T BF)\dot{v} = F^T(u - C\dot{q} - g + B\dot{F}v). \tag{4}$$

Performing an *ad hoc* feedback linearization of (4) is possible to ensure that: *i*) the block is positioned correctly, *ii*) the rigid arm is never overloaded. A physical CAD-based simulator of the overall system was developed to demonstrate the feasibility of the proposed control law. As expected, Fig.2 shows that the block reaches the desired position. Fig.2c shows that the torques applied by the robot motors are well within the typical limits of the joint actuators. The simulations prove that the robot is able to manage a block that weights the double of its weight.

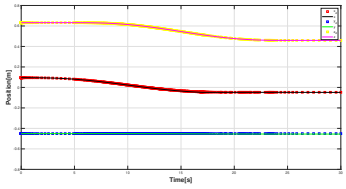

(a) Block Trajectory ($x-y-z$)

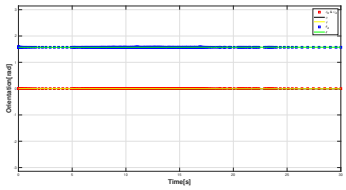

(b) Block Orientation ($\phi-\theta-\psi$)

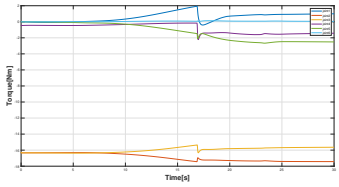

(c) Torques Motor Robot

Figure 2: Simulation Results

References

[1] Siciliano, Bruno, et al. Robotics: modelling, planning and control. Springer Science & Business Media, 2010.

Towards model-based control of divertor detachment

J.T.W. Koenders[1,2]
[1] Energy Systems and Control Group, DIFFER, Eindhoven, the Netherlands
[2] Control Systems Technology Group, Eindhoven University of Technology, Eindhoven, the Netherlands
J.T.W.Koenders@differ.nl

1 Introduction

The heat and particle exhaust in tokamaks, the leading reactor design for economically viable clean energy production through thermonuclear fusion, is guided to a dedicated region called the divertor. Here, the plasma interacts with the divertor surface material causing erosion and hence impurities to enter the plasma. Unmitigated, the expected power fluxes impacting the divertor target during reactor operations exceed present-day engineering limits [1]. Real-time feedback control of plasma detachment, a regime characterized by a large reduction of plasma temperature and pressure at the divertor target, is required to obtain and maintain low target fluxes. A systematic approach to achieve this reduction was recently developed and experimentally demonstrated [2] on the Tokamak à Configuration Variable (TCV) at the EPFL [3]. This approach uses dedicated system identification experiments for controller design enabling control of the CIII emission front position, which is related to a relatively low temperature (<10 eV) region along the divertor leg [4]. We aid controller design by investigating the system identification results and extracting a dominant physical process. This is the first step to obtain a scalable control-oriented model of the CIII emission front position based on physical parameters.

2 Method

The control problem can be reduced to an input: fueling of deuterium molecules by a gas valve Γ_{puff} [#/s], and an output: the CIII emission front location L_{pol} [m]. Real-time (800 Hz) tracking of the CIII emission front was implemented using a detection algorithm [5] applied to spectrally filtered images originating from the multi-spectral imaging diagnostic MANTIS [6]. Figure 1 shows the MANTIS camera view, a visual representation of the detection algorithm and the definition of the parameter L_{pol}. The gas valve is located at the bottom of the machine. System identification experiments were performed by injection of a multisine perturbation on the input Γ_{puff} and measuring L_{pol}. Due to the low signal to noise ratio environment it was chosen to excite three to six frequencies per experiment. Additionally the gas valve system limits the frequencies to <50 Hz. Extraction of a physical process was done by fitting first-principle physics models on the obtained FRF measurements. Steady-state behavior of the system was estimated using the established time-independent equilibrium code SOLPS-ITER.

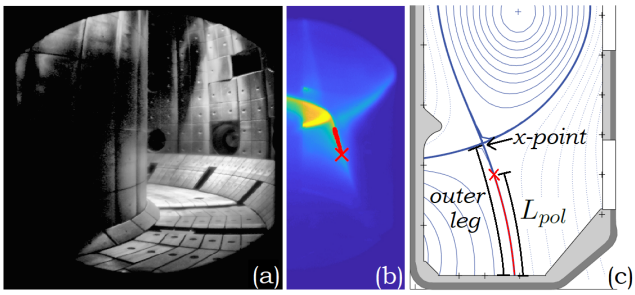

Figure 1: (a) MANTIS camera view in the TCV Tokamak [6]. (b) Identified CIII front location by the detection algorithm, indicated by the red X [5]. (c) Geometric representation of the front location L_{pol} along the outer leg.

3 Results and Discussion

The identification experiments show phase behavior reminiscent of a diffusive system, we find a 1D diffusion dominated transport model to accurately describe the obtained FRF measurements. We present a novel control-oriented grey-box model describing the dynamics of input Γ_{puff} to output L_{pol}. The model accurately reproduces experimental observations and can be used for controller design within the identified operating regime.
The underlying physics responsible for the diffusive like behavior is to be investigated, we hypothesize the process is dominated by plasma-neutral interactions the injected deuterium molecules undergo until they are ionised.

4 Acknowledgments

The author thanks Marco de Baar, Matthijs van Berkel, Basil Duval, Olivier Février, Cristian Galperti, Ricky van Kampen, Artur Perek, Timo Ravensbergen, Christian Theiler, the TCV Team, and the EUROfusion MST1 team.

References

[1] R. Pitts et al., Nucl. Mat. Ener. **20**, (2019)
[2] T. Ravensbergen et al., Nat. Commun. **12**, (2021)
[3] S. Coda et al., Nucl. Fusion **59**, (2019)
[4] C. Theiler et al., Nucl. Fusion **57**, (2017)
[5] T. Ravensbergen et al., Nucl. Fusion **60**, (2020)
[6] A. Perek et al., Rev. Sci. Instrum. **90**, (2019)

Physics–Guided Neural Networks for Inversion–based Feedforward Control applied to Linear Motors

Max Bolderman[1], Mircea Lazar[1] and Hans Butler[1,2]
[1] Control Systems Group, Dept. of Electrical Engineering, Eindhoven University of Technology, 5600 MB Eindhoven, The Netherlands. [2] ASML, 5504DR Veldhoven, The Netherlands
Email: m.bolderman@tue.nl

1 Introduction

Ever–increasing throughput specifications in semiconductor manufacturing require operating high–precision mechatronics, such as linear motors, at higher accelerations. This creates higher nonlinear parasitic forces that cannot be handled by conventional feedforward controllers. We develop a general framework for inversion–based feedforward controller design using physics–guided neural networks (PGNNs).

2 Problem Statement

Consider the discrete–time nonlinear autoregressive exogenous (NARX) dynamics

$$y(t) = f\big(y(t-1),\ldots,y(t-n_y),u(t-n_k),\ldots,u(t-n_u)\big), \tag{1}$$

with output $y(t)$, input $u(t)$, and $f(\cdot)$ a nonlinear mapping describing the forward dynamics. The goal of inversion–based feedforward is to find $f^{-1}(\cdot)$, after which substituting $y(t) = r(t)$ gives the feedforward. The universal approximation capabilities of multi–layer perceptrons (MLP) can be used to parameterize $f^{-1}\big(x(t)\big) \approx f_{MLP}\big(x(t),\theta\big)$, with $x(t)$ the relevant inputs and outputs, and θ the network weights. However, it was shown in [3] that the MLP easily fails to learn underlying physical laws.

3 Main Results

Physics–informed neural networks were proposed in [2]. These introduce physical knowledge during training by adding a regularization term in the cost function that penalizes physical inconsistencies. We take a different approach by embedding physical knowledge in the network structure, see the blue parts in Fig. 1. This gives the PGNN output

$$u(t) = f_{MLP}\Big(T_{PGT}\big(x(t)\big),\theta\Big) + W_{PGL}T_{PGL}\Big(T_{PGT}\big(x(t)\big)\Big), \tag{2}$$

with $\{\theta, W_{PGL}\}$ the PGNN weights. The *physics–guided input transform* $T_{PGT}(\cdot)$ preprocesses the network input, e.g., reconstruct velocity and acceleration, and is similar to basis function identification, see, e.g., [1]. The *physics–guided layer* $T_{PGL}(\cdot)$ can be used to embed structural physical knowledge, such as mass–acceleration. Effectiveness of the PGNN inversion–based feedforward controller was tested in simulation in [3] on a CLM tracking a third order reference in closed–loop. Fig. 2 shows the generated feedforward and resulting tracking error when using two hidden layer neurons. Currently, we are investigation conditions for PGNNs to consistently identify nonlinear inverse dynamics, by exploring links with nonlinear system identification.

This work is part of the research programme 9654 with project number 17973, which is (partly) financed by the Dutch Research Council (NWO).

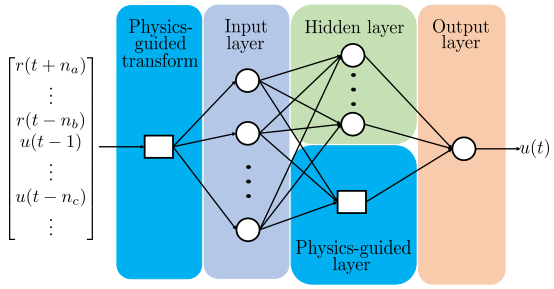

Figure 1: Physics–guided neural network architecture.

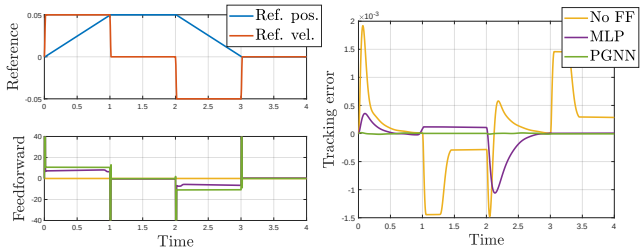

Figure 2: Generated feedforward and resulting tracking error.

References

[1] L. Blanken, S. Koekebakker, and T. Oomen, "Data–driven feedforward tuning using non–causal rational basis functions: With application to an industrial flatbed printer," *Mechatronics,* vol. 71, 102424, 2020.

[2] J. Stiasny, G. S. Misyris, and S. Chatzivasileiadis, "Physics–informed neural networks for non–linear system identification applied to power system dynamics," *arXiv preprint arXiv:2004.04026*, 2020.

[3] M. Bolderman, M. Lazar, and H. Butler, "Physics–guided neural networks for inversion–based feedforward control applied to linear motors," *arXiv preprint arXiv:2103.06092,* 2021.

On Closed-loop Fault Diagnosis of Complex Mechatronic Systems

Koen Classens[1], W.P.M.H. (Maurice) Heemels[1] and Tom Oomen[1]

[1]Dept. of Mechanical Engineering, Eindhoven University of Technology, The Netherlands

{K.H.J.Classens,W.P.M.H.Heemels,T.A.E.Oomen}@tue.nl

1 Background

The economic value of production equipment in the high-precision industry is to a large extent determined by its productivity. It is essential to minimize downtime caused by malfunction and the associated unscheduled maintenance. To this end, digital-twin-assisted fault diagnosis systems are crucial, exploiting cheap operational data and its physics-based structure to isolate the root-cause.

2 Problem

Many fault diagnosis systems are based on parametric first principle models of the open-loop system. For instance, based on parametric models, nullspace-based fault detection and isolation (FDI) methods enable fault diagnosis for large-scale multi-input multi-output (MIMO) systems [1]. In sharp contrast, for precision mechatronics, first principle modeling is ineffective compared to data-driven modeling, which is fast, accurate, and inexpensive [2]. In addition, precision mechatronics operate in closed loop, which is often claimed not to affect the FDI system design. Given the importance for these high-precision mechatronic systems, the aim of this abstract is to develop a closed-loop and closed-loop dynamic modeling view of fault diagnosis.

3 Approach

For FDI, data-driven modeling and closed-loop interconnections are investigated. For this purpose, the consequences of interacting submodules and closed-loop operators are examined and its effect on identification and residual generator design is evaluated through a numerical analysis and experimental case study.

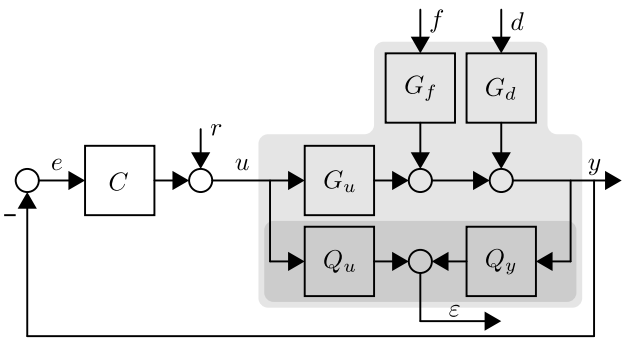

Figure 1: Closed-loop configuration for fault detection by means of the residual signal ε. The residual generator, $Q(s)$ (■), and the open-loop problem (■) are indicated.

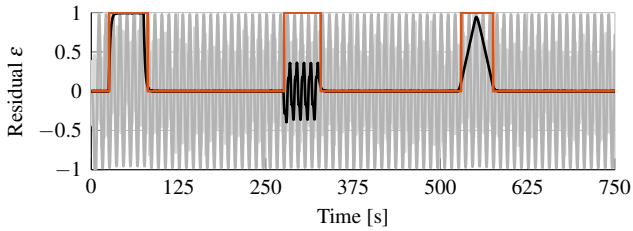

Figure 2: Comparison between normalized effective residual (—) with fault flag (—), and residual signals based on classical design techniques (—), (—).

4 Results

By means of an experimental setup, exhibiting flexible behavior similar to next-generation positioning systems, it is shown that neglecting interaction between closed-loop controlled submodules results in a severely compromised fault diagnosis system [3]. A solution is proposed in which submodules are identified and used as basis for the fault diagnosis system.

5 Outlook

The presented approach addresses ambiguity in fault detection for closed-loop systems since the operation of MIMO systems in closed-loop configuration has major implications for FDI and related system identification. Further details are communicated in [4]. The developed procedure shows that the framework for fault detection, in the form of a digital twin, can serve as the basis to maximize productivity through predictive maintenance for complex mechatronic systems.

References

[1] A. Varga, *Solving Fault Diagnosis Problems*. Springer International Publishing, 2017.

[2] T. Oomen, "Advanced Motion Control for Precision Mechatronics: Control, Identification, and Learning of Complex Systems," *IEEJ J. Ind. Appl. IA*, vol. 7, no. 2, 2018.

[3] K. Classens, W. P. M. H. Heemels, and T. Oomen, "A Closed-Loop Perspective on Fault Detection for Precision Motion Control: With Application to an Overactuated System," in *2021 ICM*, Kashiwa, Japan, 2021.

[4] K. Classens, W. P. M. H. Heemels, and T. Oomen, "Closed-loop Aspects in MIMO Fault Diagnosis with Application to Precision Mechatronics," in *2021 ACC*, New Orleans, USA, 2021.

This work is supported by Topconsortia voor Kennis en Innovatie (TKI), and is supported by ASML Research, Veldhoven, The Netherlands.

Accurate $\mathscr{H}_\infty$-Norm Estimation via Finite-Frequency Norms of Local Parametric Models

Paul Tacx, Tom Oomen
Eindhoven University of Technology
Department of Mechanical Engineering
Control Systems Technology group
P.O. Box 513, 5600 MB Eindhoven, The Netherlands
Email: p.j.m.m.tacx@student.tue.nl & t.a.e.oomen@tue.nl

1 Background

Accurate $\mathscr{H}_\infty$-norm estimation is of critical importance for robust control design. Selecting an appropriate size of the uncertainty is crucial for the performance of the resulting robust controller. On the one hand, if the uncertainty is underestimated, there are no stability nor performance guarantees. On the other hand, if the uncertainty is overestimated, the system may become overly conservative.

2 Problem Formulation

Traditional algorithms to estimate the $\mathscr{H}_\infty$ norm consider a discrete frequency grid. Hence, the $\mathscr{H}_\infty$-norm estimate is based solely on the at-grid frequencies which causes inter-grid errors. Consequently, potential resonances may be overlooked. This research aims to develop an algorithm to accurately and reliably determine the $\mathscr{H}_\infty$ norm with a limited amount of data and limited user effort.

3 Approach

The key idea is the exploit the local smoothness over frequency by identifying local parametric models [1]. Since these local models are parametric, they can be evaluated continuously in their local frequency range, which enable the estimation of the inter-grid behavior [2]. The main idea is to estimate the global $\mathscr{H}_\infty$ norm by estimating the finite-frequency L_∞ norm of the local models through the generalized KYP lemma [3].

4 Results

The developed approach is applied to a multivariable motion system. The resulting model uncertainty is shown in Fig. 1. In Fig. 2, the maximum singular values of the uncertainty and the resulting local models are depicted for a large frequency range. When studying the interpolation performance of the local models, it is clear that the true inter-grid behavior is accurately modeled. Moreover, the simulation shows that the $\mathscr{H}_\infty$ norm is accurately estimated. Overall, the simulation example shows that the method proposed in this paper offers an accurate and reliable approach to estimate $\mathscr{H}_\infty$ norm.

This work is part of the research programme VIDI with project number 15698, which is (partly) financed by the Netherlands Organisation for Scientific Research (NWO).

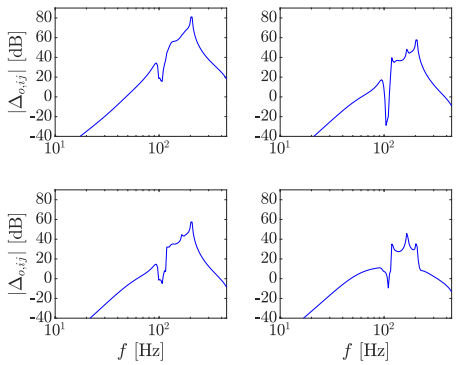

Figure 1: Bode magnitude diagram of the uncertainty Δ (——).

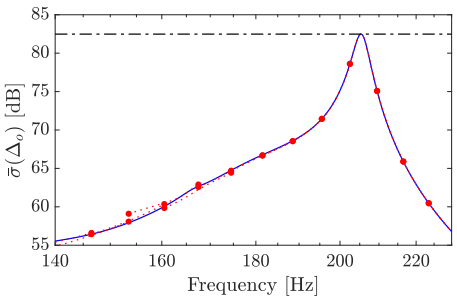

Figure 2: Bode magnitude diagram of the singular values: true uncertainty $\bar{\sigma}(\Delta)$ (——), local modeling estimate $\bar{\sigma}(\tilde{\Delta}_k)$ (•···•).

References

[1] R. Pintelon, J. Schoukens, G. Vandersteen, and K. Barbé, "Estimation of nonparametric noise and frf models for multivariable systems—part i: Theory," Mechanical Systems and Signal Processing, 24(3):573–595, 2010.

[2] E. Geerardyn, and T. Oomen, "local rational model approach for $\mathscr{H}_\infty$-norm estimation: With application to an active vibration isolation system," Control Engineering Practice, 68:63-70, 2017.

[3] R. Iwasaki, and S. Hara, "Generalized KYP lemma: Unified frequency domain inequalities with design applications," IEEE Transactions on Automatic Control, 50(1):41–59, 2005.

Learning Linear Surrogate Models of Nonlinear Systems

Lucian Cristian Iacob, Roland Tóth and Maarten Schoukens
Control Systems Group, Eindhoven University of Technology
P.O Box 513, 5600 MB, Eindhoven, The Netherlands
Email: {l.c.iacob, r.toth, m.schoukens}@tue.nl

1 Introduction

In general, most dynamical systems exhibit some sort of nonlinear behavior. However, most control and identification applications rely on LTI models, which are only valid locally. In recent years, the Koopman framework [1] has gained popularity within the control and identification communities, proposing a global linear representation of nonlinear systems. This is achieved through the embedding of the nonlinear state-space into a possibly infinite-dimensional lifted space where the dynamics are linear and governed by the Koopman operator. In practice, only a finite number of lifting functions is used and, while the choice of the dictionary heavily impacts the representation quality of the resulted linear model, there are little to no systematic methods for the selection. We address this by combining a Least Squares Support Vector Machine (LS-SVM) regression [2], to estimate the nonlinear state transition map, with the linearity condition of the Koopman form.

2 Methodology

Consider the discrete-time autonomous nonlinear system:

$$x_{k+1} = f(x_k) \tag{1}$$

with $x_k \in \mathbb{R}^{n_x}$ and the bounded nonlinear state-transition map $f : \mathbb{R}^{n_x} \to \mathbb{R}^{n_x}$. Our objective is to obtain a linear representation of (1) where the observable functions are chosen automatically.

2.1 Koopman operator

The Koopman concept is to lift the nonlinear dynamics to a possibly infinite-dimensional linear space, through so-called observable functions $\phi : \mathbb{R}^{n_x} \to \mathbb{R}$, with $\phi \in \mathcal{F}$ and $\mathcal{F}$ being a function space. The Koopman operator advances the observables one step forward in time:

$$\mathcal{K}\phi(x_k) = \phi(x_{k+1}). \tag{2}$$

Often, a finite number of observables is used $\{\phi_j\}_{j=1}^{n_f}$, spanning a n_f-dimensional linear subspace $\mathcal{F}_n \subset \mathcal{F}$. The main reason for this transformation is that, when we introduce the lifted state $z_k = \Phi(x_k)$, with $\Phi(x_k) = \left[\phi_1(x_k) \ \dots \ \phi_{n_f}(x_k)\right]^\top$, the lifted dynamics can be described using a linear Koopman matrix representation $A \in \mathbb{R}^{n_f \times n_f}$:

$$z_{k+1} = Az_k. \tag{3}$$

However, due to the immaturity of the theory, very little is known on how to chose Φ analytically such that (3) exists. Hence, approximations are often used to compute an approximative Koopman matrix A, based on data matrices $Z = \left[\Phi(x_1) \ \dots \ \Phi(x_N)\right]$ and Z^+ (the latter represents Z shifted one step forward in time). The goal is to minimize:

$$\frac{1}{2}\|Z^+ - AZ\|_F^2, \tag{4}$$

which has a closed-form solution $A = Z^+Z^\dagger$, where $Z^\dagger$ denotes the pseudoinverse. Due to noise and numerical errors, a regularization is generally needed to correctly preserve properties of (1), like stability. However, the main difficulty of this framework is the choice of $\Phi(x_k)$. To address this, the next subsection presents a LS-SVM based method for the selection of the observables.

2.2 LS-SVM

The LS-SVM approach for function estimation represents f as an expansion of feature maps $\Psi : \mathbb{R}^{n_x} \to \mathbb{R}^m$. The optimization problem is formulated as a Ridge regression :

$$\begin{aligned} \min_{w,e} J &= \frac{1}{2}\sum_{i=1}^{n}\|w^{(i)}\|_2^2 + \frac{1}{2}\sum_{i=1}^{n}\gamma_i\sum_{j=1}^{N}(e_j^{(i)})^2 \\ \text{s.t. } e_j^{(i)} &= f^{(i)}(x_j) - (w^{(i)})^\top\Psi(x_j). \end{aligned} \tag{5}$$

By writing the Lagrangian and solving the KKT conditions, the nonlinear function f is represented in dual form as:

$$f(x_k) = C\overline{\Psi}(x_k), \tag{6}$$

where $\overline{\Psi}(x_k) = \left[k(x_1^{\text{train}}, x_k) \ \dots \ k(x_N^{\text{train}}, x_k)\right]^\top$ is a kernel slice with $k(x_q, x_p) = \Psi(x_q)^\top\Psi(x_p)$ and $C \in \mathbb{R}^{n_x \times N}$ contains the Lagrangian multipliers. Note that the kernel function $k(x_q, x_p)$ is parametrized by a set of kernel parameters θ. The dual form (6) can be related to (3) by choosing the lifted state as the kernel slice $\left(z_k = \overline{\Psi}(x_k)\right)$ and minimizing (4) using the resulted data matrices. This gives a linear surrogate model of dimension N (nr. of training points) of the nonlinear system, that can be used for prediction and analysis:

$$z_{k+1} = Az_k \qquad x_{k+1} = Cz_k, \tag{7}$$

with $z_0 = \overline{\Psi}(x_0)$. To obtain a good representation of the nonlinear system and reduce overfit, the hyperparameters (regression parameters γ_i and kernel parameters θ) need to be tuned. To this end, we jointly solve (5) and (4) in the hyperparameter tuning step.

3 Future work

Future work aims to extend the proposed method to systems with inputs and investigate the representation in the lifted form of different classes of actuated nonlinear systems. Furthermore, the effect of different error measures on the quality of the resulted model will be explored.

References

[1] A. Mauroy et al, "The Koopman Operator in Systems and Control", Springer International Publishing, 2020.

[2] J. A. K. Suykens et al, "Least Squares Support Vector Machines", World Scientific, 2002.

This work has received funding from the European Research Council (ERC) under the European Union's Horizon 2020 research and innovation programme (grant agreement nr. 714663).

Dynamical system identification from video using sub-space encoders

Gerben Izaak Beintema[a], Roland Tóth[a,b], Maarten Schoukens[a]
[a]Control Systems Group, Electrical Engineering, Eindhoven University of Technology
[b]Systems and Control Laboratory, Institute for Computer Science and Control, Budapest, Hungary.
Emails: g.i.beintema@tue.nl (Seconds Year PhD), r.toth@tue.nl, m.schoukens@tue.nl

1 Introduction

The availability and affordability of high-quality cameras have increased substantially in recent years. However, modelling non-linear systems using video, network or spacial (e.g. PDE) signals is currently an open problem. Our contribution is to improve compact state-space modelling by co-estimating a deep non-linear state encoder together with the state and output functions directly from video footage.[1]

2 The Sub-space Encoder Approach

In short, the encoder method randomly selects a number of starting times t_i and employs an encoder structure displayed in (Figure 1) on the data to calculate a batch multiple-step-ahead loss to estimate a non-linear state-space model employing three ANNs using batch optimization.

Estimating the initial state using a non-linear state encoder e_θ contributes to multiple advantages over conventional methods, for instance, the computation cost of the proposed approach scales well with data size. Moreover, the encoder can be used as an observer to jump-start simulations and aid in control.

3 Experimental Results

We show the potential of the sub-space encoder method by modelling a numerical example that consists of a controllable ball (Gaussian inputs) confined within a box by non-linear potential walls with some background friction. The video is constructed by using 25 by 25 pixel greyscale images of the resulting motion of the ball as seen in Figure 2. Lastly, we generated 30000 train, 5000 validation and 5000 test samples. The video frames are flattened into vectors, normalized before passed through the appropriate neural networks f_θ, h_θ and e_θ of the encoder method. All three networks are 2 hidden layer neural feedforward networks with tanh activation and 64 hidden nodes per layer with a linear bypass. Furthermore, we use the following hyperparameters of $n_x = 6$ states, past length of $n_a = n_b = 5$, $n_f = 50$ future steps and the Adam optimizer. For further details on implementation see [1].

[1]Code is available at
https://github.com/GerbenBeintema/SS-encoder-video

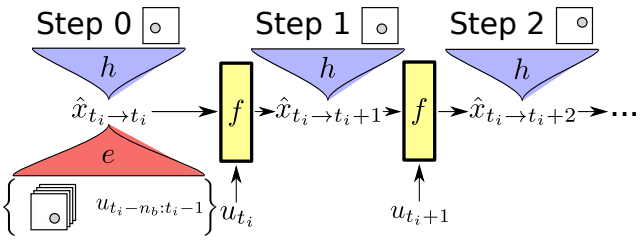

Figure 1: The sub-space encoder applied on a single subsection of the dataset. Here e_θ estimates the state based on past inputs and video images, $f_\theta(\hat{x}_{t_i \to t_i+k}, u_{t_i+k})$ increments the state up to n_f times and $h_\theta(x_{t_i \to t_i+k})$ estimates the output $\hat{y}_{t_i \to t_i+k}$. Output sequences from multiple sections are combined to form a batched multiple-step-ahead loss.

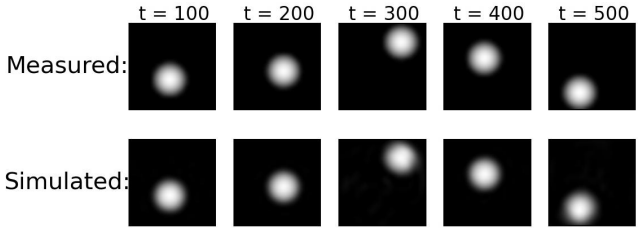

Figure 2: Output frames of both the measured output of the system and the simulated output of the sub-space encoder method for different instances of time in the test set. (Supplementary Video: https://youtu.be/L_zCwzpMZUc)

The resulting compact state-space model has been tested in simulation as can be seen in (Figure 2) where the encoder is used to initialize the state. The figure shows that the estimated model is able to accurately mimic the numerical system on long time scales.

4 Conclusion

We showed that the sub-space encoder method is able to find compact non-linear state-space models directly from datasets with high-dimensional output data. Physical experimental applications and the development of controllers based on the proposed modelling approach are subject to future work.

References

[1] G. I. Beintema, R. Toth, and M. Schoukens, "Nonlinear state-space model identification from video data using deep encoders," *Submitted to SysID 21: 2012.07721*, 2020.

A Control-Theoretic Approach to Dynamic-Pricing Strategies Using First-Principles Models

Coen Hutters
Delft Center for Systems and Control
Delft University
Mekelweg 2628 CD Delft, Netherlands
Email: C.Hutters-1@tudelft.nl

Max Mendel
Delft Center for Systems and Control
Delft University
Mekelweg 2 2628 CD Delft, Netherlands
Email: M.B.Mendel@tudelft.nl

1 Introduction

In dynamic pricing strategies agents vary their prices with respect to an economic goal, e.g. maximum profit or desired inventory levels. Here, the challenge is to take into account the effect that price adjustments have on the behavior of the rest of the market. Currently, prices are analyzed with static equilibrium models or with historic data. These models are unfit to predict dynamic market behavior analytically. We propose the use of first-principles models of the dynamics of prices and economic goods. The interaction between agents in economic markets will be modeled as closed-loop control systems. The resulting dynamical models can be used to incorporate price dynamics in economic optimal control problems.

2 Economic-Engineering Principles

To model price dynamics we use economic-engineering principles, a recent development by the second author. Economic-engineering principles extend the analogy between physical domains (for example between mechanics and electronics) to economics. Considering a mass-spring-damper system, we define prices as the analog of momenta and stock quantities as the analog of positions. The laws of supply and demand are analogous to inertia, inventories to springs, and operational costs to dampers. From these analogs we obtain causal relationships that describe the dynamics of prices and stock quantities from first principles.

3 Theory of Supply and Demand as Closed-Loop System

We illustrate our approach with the law of supply and demand [1], shown in Figure 1. The suppliers adjust their price $p(t)$ based on the difference between in supply $Q_S(p(t))$ and demand $Q_D(p(t))$. We reformulate this as the feedback-control loop in Figure 2 in which the supply curve serves as the process, the demand curve as a state-dependent source, and the quantity supplied and quantity demanded as the corresponding output and reference signals, respectively. The price adjustment is executed by the controller that attempts to reject the excess demand $e(t)$, which serves as error signal, by adjusting the price with the control input $u(t)$. The pricing strategy can for instance be modeled as a PID controller, resulting in a control law with clear economic interpretations:

$$\underbrace{u(t)}_{=\frac{dp}{dt}} = \underbrace{K_p e(t)}_{speed-of-adjustment} + \underbrace{K_I \int e(t)dt}_{inventory-management} + \underbrace{K_D \frac{d}{dt} e(t)}_{speculation}$$

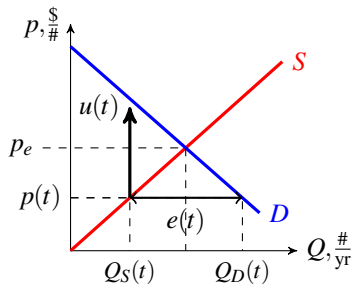

Figure 1: Applying closed-loop dynamics to the law of supply and demand. The control input $u(t)$ drives the prices towards market equilibrium where $p(t) = p_e$ and $e(t) = 0$.

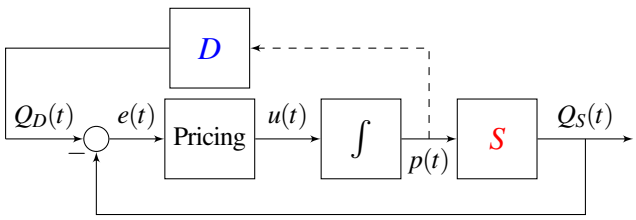

Figure 2: Supply and demand in a closed-loop with pricing as a controller.

4 Subjecting Economic MPC to Price Dynamics

The use of first-principles pricing models allows us to include price dynamics in Economic Model Predictive Control (EMPC) algorithms [2]. EMPC is used in process industry to control production with respect to the economic profit, which serves as the objective function. However, price dynamics are currently not included in EMPC optimization. By using economic-engineering models, we are able to take into account the price dynamics that result from interactions between the controlled process (e.g. a business) and its environment (e.g. the market). This enables the application of EMPC to purely economic processes such as trade, investments, and risk management in which prices and profits are key variables.

References

[1] A. Marshall, *Principles of Economics*, 8th Ed., London: Palgrave Macmillan, 2013, pp. 281-291

[2] M. Ellis, H. Durand, and P. D. Christofides, A tutorial review of economic model predictive control methods, *Journal of Process Control*, vol. 24 (8), pp. 1156-1178, 2014.

Maturing FLORIS towards a Dynamic Wind Farm Model: The inclusion of time-dependent wake propagation, time-varying atmospheric conditions and heterogeneous inflow conditions

Marcus Becker
Delft University of Technology, NLD
marcus.becker@tudelft.nl

Bart Doekemeijer
Delft University of Technology, NL
now with National Renewable Energy Laboratory, USA

Bastian Ritter
Technical University of Darmstadt, DE
now with Wölfel Wind Systems GmbH, DE

Daan van der Hoek
Delft University of Technology, NL

Jan-Willem van Wingerden
Delft University of Technology, NL

1 Motivation

To reduce the costs of offshore wind energy, wind turbines are built in large wind farms. By extracting energy from the wind, turbines influence their downstream neighbours and reduce the efficiency of the farm. A wind farm wide model-based control strategy which takes the turbine interactions into account can compensate for some of these effects. It has to overcome several challenges: complex flow interactions between the turbines, large delays between state changes and effects and spatially heterogeneous wind conditions which change over time. Model Predictive Control (MPC) approaches have shown promising results in the past. Their surrogate model has to be computational cheap enough to allow real time control and accurate enough to facilitate an improved performance also under realistic conditions. The so-called Flow Redirection and Induction in Steady State (FLORIS) models for instance have proven to be an easy to use, easy to tune, computationally inexpensive and powerful wake modelling tool. However, it is lacking dynamical effects by design.

2 The Gaussian FLORIDyn model

In the presented work, a dynamic version of the widely used Gaussian FLORIS model [1] is developed. It is adapted to take spatially heterogeneous wind conditions into account. Time-varying dynamic behaviour is achieved by introducing so-called Observation Points at the rotor plane of each turbine. These propagate through the wake with the free wind speed and simulate the delayed effect of turbine state changes. The chosen approach is a modified version of the Zone FLORIDyn model [2]. A basic, computationally inexpensive wind field model is developed to provide spatially heterogeneous wind field conditions including wind shear.

3 Validation

The new FLORIDyn model is validated in two, three and nine turbine cases and compared to the high fidelity CFD simulation SOWFA. Tested scenarios include a yaw sweep, stepwise increase of the yaw angle, changing C_T and C_P coefficients and a wind direction change. In the steady state cases, FLORIDyn meets the average generated power by the turbines with relative errors between -0.82 % and 22.15 %. In a flow field comparison FLORIDyn lacks accuracy in the near wake area but has a very good agreement with SOWFA in the far wake area which is practically more relevant for the purpose of model-based wind farm control.

4 Conclusion

The presented version of FLORIDyn provides very promising results in terms of model accuracy and computational performance. It provides a unique feature set with the ability to simulate dynamic parametric wake models in a changing, heterogeneous environment. The findings lay the groundwork for a dynamic wind farm model which can be part of a real time wind farm control strategy.

References

[1] Bastankhah, Majid, and Fernando Porté-Agel. “Experimental and Theoretical Study of Wind Turbine Wakes in Yawed Conditions.” Journal of Fluid Mechanics 806 (November 10, 2016): 506–41. https://doi.org/10.1017/jfm.2016.595.

[2] Gebraad, Pieter M. O., and J. W. van Wingerden. “A Control-Oriented Dynamic Model for Wakes in Wind Plants.” Journal of Physics: Conference Series 524 (June 2014): 012186. https://doi.org/10.1088/1742-6596/524/1/012186.

A configurator for supervisory controllers of roadside systems

J.J. Verbakel[1], M.E.W. Vos de Wael[1], J.M. van de Mortel-Fronczak[1], W.J. Fokkink[2], J.E. Rooda[1]

[1] Department of Mechanical Engineering, Eindhoven University of Technology, Eindhoven, The Netherlands.

[2] Department of Computer Science, Vrije Universiteit Amsterdam, Amsterdam, The Netherlands.

1 Introduction

To efficiently use the available highway infrastructure and to improve traffic safety, traffic management systems (TMSs) are used. Nowadays, about one third of the Dutch highways is equipped with around 6000 Roadside units (RSUs). They measure the traffic speed and intensity and control the traffic streams by showing legends, such as speeds or red crosses which are used to close off a lane.

2 Traffic management system

The TMS is structured as follows: An operator monitors the road and can request legends, which are then implemented by a central controller and sent to all involved RSUs. Each RSU has a local controller, which controls all components at its location, such as MSIs, which show legends and detector loops which measure the traffic. The RSU shows the requested legends. In addition, each RSU monitors the traffic speed to detect incidents. If the measured speeds drop below a certain threshold, a speed legend is automatically shown to warn oncoming traffic.

3 Model

RSUs have clearly discernible components, such as detector loops and MSIs. Modules are used to model a component or a collection of related components. Each module is modeled as one or more extended finite automata (EFAs), as was also done in, e.g., [1]. In addition, a module can contain requirements, in the form of logical expressions, and other modules, which describe a part of this module. These models can then be used to synthesize a supervisor, using the algorithm from [2].

4 Configurator

It is not feasible to manually design a controller for each RSU. There are slight differences between all RSUs. Therefore, it is useful to apply a configurator to generate the controller for an RSU. The configurator uses input parameters to model a specific configuration, such as the number of components, the division of lanes into carriageways, information on neighboring RSUs and the speed thresholds that define an incident. Based on the parameters, modules are instantiated and requirements are added to obtain the complete models. Separate models are created for synthesis, simulation and controller generation.

5 Case study

For this case study, a representative RSU is used, as given in Fig. 1. The RSU contains two MSIs and eight detectors, which are divided over three detector rows. At the location of the RSU, there are two lanes. At each detector row, the detectors are divided into two TSs, as shown in the figure. When an incident is detected on one of the first two detector rows, speed 50 km/h is recommended and 70 km/h is recommended for an incident on the last detector row.

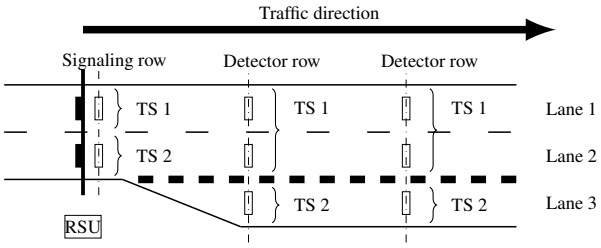

Fig. 1: Typical RSU. Traffic streams are marked by TS for each detector row.

The resulting model has 74 EFAs, all with at most four locations, 72 variables and 68 requirements. The generated discrete-event model can be used to synthesize a supervisor for this specific system. Using the simulation model, the behavior of the supervisor can be validated. If the supervisor behaves as intended, a controller can be derived from the supervisor. This controller can then be implemented on the computation platform, as described in [1].

Model generation reduces the possibility of man-made errors. In addition, unnecessary requirements are automatically omitted. When creating a small number of systems (five to ten), it is faster to create the models and verify there are no errors manually. For larger numbers of system, as is the case for 6000 RSUs, it is faster to create a configurator and ensure that it generates the desired models.

References

[1] F. F. H. Reijnen, M. A. Goorden, J. M. van de Mortel-Fronczak, and J. E. Rooda, "Modeling for supervisor synthesis–a lock-bridge combination case study," *Discrete Event Dynamic Systems*, vol. 30, no. 3, pp. 499–532, 2020.

[2] L. Ouédraogo, A. Khoumsi, and M. Nourelfath, "A new method for centralised and modular supervisory control of real-time discrete event systems," *International Journal of Control*, vol. 83, no. 1, pp. 1–39, 2010.

A Study on Potential of Data-driven Approaches for Efficient and Robust Engine Control Development

Prasoon Garg* Shreyas Sastry* Emilia Silvas* Frank Willems*,†
*Dept. of Mechanical Eng., Eindhoven University of Technology (TU/e), The Netherlands
†TNO Automotive, Helmond, The Netherlands (p.garg.1@tue.nl)

1 Introduction

Increasingly strict legislation for greenhouse gas and pollutant emissions, and growing attention for real-world performance makes it necessary to develop robust, fuel-efficient, cost efficient control solutions for future automotive engines. Traditional map-based control approaches employ numerous fixed maps and require large calibration effort [1]. The current industry standard model-based control development approach has led to reduced development time, however, this approach is sensitive to model uncertainties. Both these approaches employ numerous fixed maps to address robustness, which requires large calibration effort and do not guarantee robustness for all the operating conditions.

Self-learning powertrains show potential to reduce the calibration effort and guarantee robust performance [2], as shown in Figure 1. In the last two decades, Artificial Intelligence (AI) methods have received increasing attention due to availability of more data and successful applications for other complex problems. This approach promises much potential for efficient and robust engine control development. Until now, limited research has been conducted on using AI for learning control in engine control development. This presentation gives an overview of the state-of-the-art in Machine Learning (ML)-based engine control calibration based on the literature and patent search. From this study, identified promising directions for future ML-based engine control research to develop learning control approaches are presented.

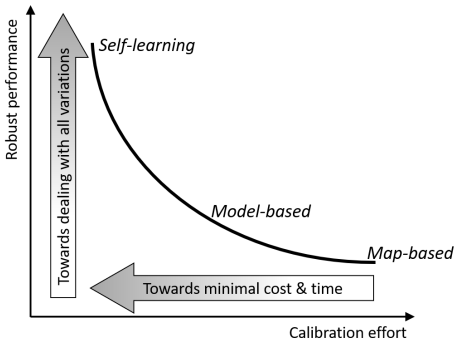

Figure 1: Trade-off between calibration effort and robust performance for applied approaches.

2 ML-based engine control development- State-of-the-art and promising directions

From the current literature and patents, it is seen that most studies have investigated ML, especially supervised learning (SL) methods to develop accurate engine models and observers. A limited number of studies have recently investigated probabilistic regression methods to model uncertainties for robust control performance. Reinforcement learning (RL) has recently gained attention for automated engine controller calibration. However, the impact of employing AI in place of conventional methods on calibration effort has not been dealt with in depth in the literature.

ML-based methods promise much potential to develop efficient and robust control solutions. SL methods show potential to reduce number of calibration parameters by parametrizing embedded maps and models in controllers. Probabilistic SL methods can be utilized in environment modeling and prediction, which can further be used for developing robust control solutions. RL methods can reduce the expert effort by automating the calibration process and achieve robustness by adaptive control solutions. Hybrid modeling approaches i.e. combined physics-based and data-driven models, can be used to achieve robustness at the boundary operating conditions of the engine (i.e., engine torque and speed limits). However, multiple challenges are involved when using AI for engine control development mainly high sensitivity to data quality, high computational requirement and poor extrapolation in boundary conditions.

3 Outlook

The future research of this work focuses on development and demo of ML methods on engines and vehicles. We will present the initial results from our current research on parametrizing embedded maps and models in engine controllers using SL methods.

Acknowledgement

We thank DENSO for providing financial support and the Powertrain R&D team at DENSO Aachen Engineering Centre (AEC) for the constructive discussions for this study.

References

[1] C. Atkinson, "Fuel efficiency optimization using rapid transient engine calibration (no. 2014-01-2359)," *SAE Technical Paper*, 2014.

[2] F. Willems, *The self-learning powertrain : towards smart and green transport*. Technische Universiteit Eindhoven, Mar. 2017, inaugral lecture.

Transformational Supervisor Synthesis for Evolving Systems

Sander Thuijsman, Michel Reniers
Eindhoven University of Technology, Eindhoven, The Netherlands
s.b.thuijsman@tue.nl, m.a.reniers@tue.nl

1 Introduction

Supervisory control theory is a model-based approach to control discrete-event systems. Given a specification that contains a plant model (defining all possible behavior) and a requirement model (defining what behavior is allowed or not), a supervisor can be computed algorithmically *(synthesized)* that restricts the plant's behavior so that it is in accordance with the requirements. Depending on the synthesis algorithm, the supervised system has some useful properties, such as *safety*, *nonblockingness*, *controllability* and *maximal permissiveness*. One of the barriers to industrial acceptance of the technique is *state space explosion*; when the size of the system grows, the time- and space (memory) required for synthesis grows exponentially.

We consider the situation as sketched in Fig. 1; A supervisor has been synthesized for a particular specification: the *base model*. Later, an adaptation is made to the specification, creating the *variant model*, so that a new supervisor is required. In state of practice, a completely new synthesis would be performed on the variant model. We investigate how to reuse the base model and synthesis results, to *transformationally* synthesize a new supervisor, while the supervisor's properties are retained.

2 Synthesis method

The problem is solved using the following three steps:

1) Storing information: From the input plant and requirement model a state space is constructed. Supervisor synthesis consists out of a number of reachability searches over this state space, and in this process several sets of states are constructed. These sets of states have different properties, therefore it is beneficial to remember them to facilitate reuse. For example, we remember what states are *nonblocking*, i.e., can reach the desired (marked) states and do not uncontrollably lead to a blocking state.

2) Modeling the evolution: A *model delta* is constructed that explicitly defines all differences between the base and variant model. Any modification to the base model that constructs a properly defined variant model is allowed.

Research leading to these results has received funding from the EU ECSEL Joint Undertaking under grant agreement n° 826452 (project Arrowhead Tools) and from the partners national programs/funding authorities.

This is an abstract of the following paper: Thuijsman, S.B. and Reniers, M.A. (*under review*) "*Transformational Supervisor Synthesis for Evolving Systems*," Journal of Discrete Event Dynamic Systems, Springer

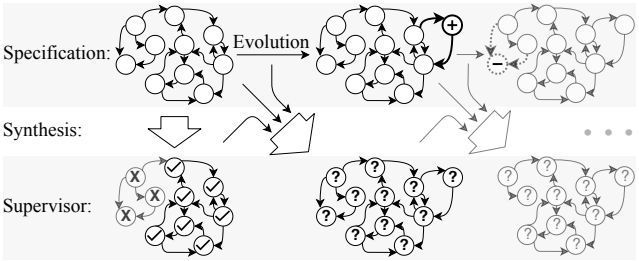

Figure 1: Schematic overview synthesis for evolving system.

3) Transformational supervisor synthesis: We first consider model deltas that are *atomic model adaptations*, which are single indivisible changes in the state space, e.g., adding a sole transition. All atomic model adaptations can regard one or more statesets of the base model. Exhaustively for each possible atomic adaptation and its possible containments in the statesets, an algorithm is made that constructs the supervisor (and according statesets) for the variant model. This result is the same as if synthesis was directly applied to the variant model, only requiring less calculations.

If the model delta is larger than an atomic model adaption, we can divide it into atomic parts and iteratively apply the algorithms to those; called *Iterative Transformational Supervisor Synthesis (ITSS)*. It turned out that these model deltas often contain a large number of very similar atomic adaptations. When these atomic adaptations require the same calculations, they can be grouped and applied at once, which gives the *Grouped Transformational Supervisor Synthesis (GTSS)* algorithm.

3 Results, conclusions, and future work

A proof-of-concept implementation of the transformational synthesis algorithms is made. These were evaluated for both an academic and industrial use case. For each variant model a supervisor is synthesized three times; by applying a completely new supervisor synthesis, ITSS, and GTSS. Computational effort is measured for each synthesis. GTSS is a lot more efficient than ITSS because of the grouping of adaptations. In some, but not all, cases GTSS is more efficient than applying a new supervisor synthesis. This depends on the size of model delta and the type of adaptations in it. Future work contains an implementation of the algorithm for symbolic supervisor synthesis, and investigating similar methods for decomposed systems.

Measurement-based Control Barrier Functions for Safety-Critical Control Systems

Ming Li and Zhiyong Sun
Department of Electrical Engineering, Eindhoven University of Technology, Eindhoven, The Netherlands
Email: {m.li3; z.sun}@tue.nl

I. Introduction

Existing control barrier functions (CBFs) for safety-critical control systems are often constructed based on a common assumption that the system states are directly available [1], [2], which may not be satisfied for practical control systems. In this paper, assuming that the measurement is the only accessible information of a control system, we propose to reformulate the state-based CBF in a measurement-based form and define a measurement-based CBF (MB-CBF) for safety control. This idea is motivated by the recent paper [3]. The major difference between [3] and our paper is that the MB-CBF derived in [3] is dependent on the estimated state recovering from the measurement model, while we use the measurement directly in constructing a MB-CBF. Besides, by considering measurement model uncertainties, a measurement-robust CBF (MR-CBF) is further developed.

II. Problem Statement

Consider a dynamic system with state $\mathbf{x} \in \mathcal{X} \subseteq \mathbb{R}^n$ and control input $\mathbf{u} \in \mathcal{U} \subseteq \mathbb{R}^m$. We assume that the dynamics of the system are continuous in time and affine in the control input, described by

$$\dot{\mathbf{x}} = \mathbf{f}(\mathbf{x}) + \mathbf{g}(\mathbf{x})\mathbf{u} \tag{1}$$

where the drift term $\mathbf{f} : \mathbb{R}^n \to \mathbb{R}^n$ and input gain $\mathbf{g} : \mathbb{R}^n \to \mathbb{R}^{n\times m}$ are locally Lipschitz continuous. Consider a closed convex set $\mathcal{C} \subset \mathbb{R}^n$ being the 0-superlevel set of a continuously differentiable function $h : \mathbb{R}^n \to \mathbb{R}$, which is defined as $\mathcal{C} \triangleq \{\mathbf{x} \in \mathbb{R}^n : h(\mathbf{x}) \geq 0\}$, where we assume that $\mathcal{C}$ is nonempty and has no isolated points. A state-dependent sensor measurement expressed in the form of $\mathbf{y} = \mathcal{I}(\mathbf{x})$ is available in practice, where $\mathcal{I} : \mathbb{R}^n \to \mathbb{R}^k$ is a continuous differentiable function, and $\mathbf{y} \in \mathbb{R}^n$. Considering the system governed (1), the projected (measurement-based) dynamics can be expressed as:

$$\dot{\mathbf{y}} = \mathbf{f}_{\mathbf{y}}(\mathbf{x}) + \mathbf{g}_{\mathbf{y}}(\mathbf{x})\mathbf{u}, \tag{2}$$

where $\mathbf{f}_{\mathbf{y}} : \mathbb{R}^n \to \mathbb{R}^k$ and $\mathbf{g}_{\mathbf{y}} : \mathbb{R}^n \to \mathbb{R}^{k\times m}$ are Lipschitz continuous on $\mathbb{R}^n$, which can be computed via $\mathbf{f}_{\mathbf{y}}(\mathbf{x}) = \frac{\partial \mathcal{I}}{\partial \mathbf{x}}(\mathbf{x})\cdot \mathbf{f}(\mathbf{x})$ and $\mathbf{g}_{\mathbf{y}}(\mathbf{x}) = \frac{\partial \mathcal{I}}{\partial \mathbf{x}}(\mathbf{x})\cdot\mathbf{g}(\mathbf{x})$. We assume that $\boldsymbol{\varphi}(\mathbf{y}) = \mathbf{f}_{\mathbf{y}}(\mathbf{x})$ and $\boldsymbol{\zeta}(\mathbf{y}) = \mathbf{g}_{\mathbf{y}}(\mathbf{x})$. Our objective is to rewrite the CBF in a measurement-based form, and develop a measurement-robust CBF (MR-CBF) is developed.

III. Main Results

Theorem 1. *Consider a set $\mathcal{C} \subset \mathbb{R}^n$ for a continuously differentiable function $h : \mathbb{R}^n \to \mathbb{R}$. If the compatible projection M defined by*

$$\underline{\eta}(h(\mathbf{x})) \leq M(\mathcal{I}(\mathbf{x})) \leq \bar{\eta}(h(\mathbf{x})), \tag{3}$$

exists ($\underline{\eta}$ and $\bar{\eta}$ are class $\mathcal{K}$ functions) and satisfies

$$\sup_{\mathbf{u}\in\mathbb{R}^m} \dot{M}(\mathbf{y},\mathbf{u}) \triangleq \mathcal{L}_{\boldsymbol{\varphi}} M(\mathbf{y}) + \mathcal{L}_{\boldsymbol{\zeta}} M(\mathbf{y})\cdot\mathbf{u} > -\alpha(M(\mathbf{y})),$$

the system (1) renders safety on $\mathcal{C}$.

The following is a measurement model which takes the measurement model uncertainties into consideration,

$$\widehat{\mathbf{y}} = \mathcal{I}(\mathbf{x}) + \mathbf{e}(\mathbf{x}), \tag{4}$$

where $\mathbf{e}(\mathbf{x}) \in \mathbb{R}^m$ and we assume that $\mathbf{e}(\mathbf{x}) = \mathbf{e}_{\mathbf{y}}(\mathbf{y})$. Given a locally Lipschitz function $\varepsilon(\mathbf{y}) : \mathbb{R}^k \to \mathbb{R}_+$ such that for all $\mathbf{y} \in \mathcal{I}(\mathcal{C})$, assume that $\sup_{\mathbf{y}\in\mathbb{R}^m} \|\mathbf{e}_{\mathbf{y}}(\mathbf{y})\|_\infty \leq \varepsilon(\mathbf{y})$.

Theorem 2. *Consider a set $\mathcal{C} \subset \mathbb{R}^n$ for a continuously differentiable function $h : \mathbb{R}^n \to \mathbb{R}$. Suppose the compatible projection defined in (3) exists and it satisfies the condition*

$$\begin{aligned}\sup_{\mathbf{u}\in\mathbb{R}^m} \mathcal{L}_{\boldsymbol{\varphi}} M(\mathbf{y}) + \mathcal{L}_{\boldsymbol{\zeta}} M(\mathbf{y})\cdot\mathbf{u} + \big(C_p + C_q\|\mathbf{u}\|_2 \\ + C_m + C_n\big)\varepsilon(\mathbf{y}) > -\alpha(M(\mathbf{y})),\end{aligned} \tag{5}$$

where C_p is a Lipschitz coefficient, which is given by

$$p(\mathbf{y}) \triangleq \mathcal{L}_{\boldsymbol{\varphi}} M(\widehat{\mathbf{y}}) - \mathcal{L}_{\boldsymbol{\varphi}} M(\mathbf{y}) \leq C_p\|\widehat{\mathbf{y}} - \mathbf{y}\|, \tag{6}$$

and the Lipschitz coefficients C_q, C_m and C_n can be obtained in a similar manner as (6), where $q(\mathbf{y}) \triangleq \mathcal{L}_{\boldsymbol{\zeta}} M(\widehat{\mathbf{y}}) - \mathcal{L}_{\boldsymbol{\zeta}} M(\mathbf{y})$, $m(\mathbf{y}) \triangleq \alpha(M(\widehat{\mathbf{y}})) - \alpha(M(\mathbf{y})$ and $n(\mathbf{y}) \triangleq \iota(\|\boldsymbol{\xi}(\widehat{\mathbf{y}})\|) - \iota(\|\boldsymbol{\xi}(\mathbf{y})\|)$, and $\iota(\cdot)$ is a class $\mathcal{K}$ function. Then the system (1) renders safety on $\mathcal{C}$.

Advantages of the MB-CBF comparing to [3]: Our construction is more straightforward which also features three main advantages: i) we do not have to introduce an inaccurate state-recovery function (i.e., a predefined function which involves system states from the measurement model), ii) since our approach does not include the recovery operation mentioned in i), thus the assumption for an invertible measurement model is not a necessity, which makes our MB-CBF more general and applicable, and iii) the proposed MB-CBF can be directly employed for ensuring safety in dynamical control systems via only measurements.

References

[1] A. D. Ames, X. R. Xu, J. W. Grizzle, and P. Tabuada, "Control barrier function based quadratic programs for safety critical systems," *IEEE Transactions on Automatic Control*, vol. 62, no. 8, pp. 3861–3876, 2016.
[2] F. Berkenkamp, R. Moriconi, A. P. Schoellig, and A. Krause, "Safe learning of regions of attraction for uncertain, nonlinear systems with gaussian processes," in *2016 IEEE 55th Conference on Decision and Control (CDC)*. IEEE, 2016, pp. 4661–4666.
[3] S. Dean, A. J. Taylor, R. K. Cosner, B. Recht, and A. D. Ames, "Guaranteeing safety of learned perception modules via measurement-robust control barrier functions," *arXiv preprint arXiv:2010.16001*, 2020.

Integrated MPC for urban water supply and crop irrigation

Congcong Sun, Simon van Mourik
Farm Technology Group
Wageningen University
P.O. Box 16, 6700 AA Wageningen
The Netherlands
Email: congcong.sun, simon.vanmourik@wur.nl

Vicenç Puig
Advanced Control Group
Technical University of Catalunya
Llorens i Artigas, 4-6, Barcelona
Spain
Email: vicenc.puig@upc.edu

1 Introduction

Agriculture is the largest user of freshwater and accounts for 70% of total global withdrawal [1]. Climate change, which results in irregular rainfall, makes water management a great challenge for agriculture sector, especially for crop irrigation in open field. Therefore, optimize irrigation to improve water usage efficiency using the most advanced methods and technologies is in need. However, water resource is not only used for irrigation, but also for drinking water supply in urban areas. Water service decisions made in one area may generate negative impact in another, causing inefficiencies and non-optimal for the entire system. Integration is an obvious way to overcome these issues through identifying synergies and conflicts between different components for more efficient and sustainable resource usage in the entire system.

2 Method and material

Under this necessity, this abstract proposes an integrated management approach of urban supply and crop irrigation using model predictive control (MPC). As shown in Figure 1, the integrated approach includes two control components and a feedback coordination strategy, which are: 1) MPC for urban supply to optimize energy cost and balance water usage for both urban and irrigation; 2) MPC for irrigation to optimize water usage while maintain crop yield; 3) a feedback strategy to coordinate different components to ensure global optimal management in water usage and energy cost. In the coordination strategy, irrigation component is aggregated as a water demand for the MPC in urban area. After optimization, control actions in the form of precise irrigation time and dosage is generated.

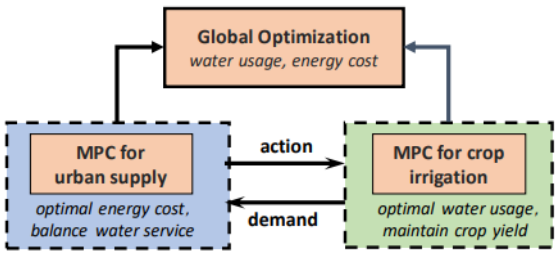

Figure 1: Integrated MPC for urban supply and crop irrigation

A water supply system generally contains pool/dams and a network of pipes with pump/valve or sprinkler to manipulate water flows. The mass balance equation is used to define relation among the stored volume v, manipulated inflows q^j_{in} and outflows q^h_{out} for the i-th pool/dam as follows:

$$v_i(k+1) = v_i(k) + \Delta t \left(\sum_j q^j_{\text{in}}(k) - \sum_h q^h_{\text{out}}(k) \right) \quad (1)$$

A single canal reach is approximated by using IDZ model [2] as a first order plus time delay τ_d as in Equation (2).

$$q_{out,i}(k+1) = \alpha q_{out,i}(k) + \beta q_{in,i}(k-\tau_d) \quad (2)$$

Δt is sampling time, k is time instant, α, β are parameters related to time and gain of canal. Irrigation demands are anticipated by forecasting as a measured disturbance.

3 Result and discussion

The case study to illustrate proposed approach is Catalunya Regional Water Network lies within Catalunya Inland Basins, from which the irrigation (1200 ha) and metropolitan (5.5 million people) area of Barcelona is supplied. An assessment obtained by supply companies in Barcelona shows 81% of the water input came from surface sources, the two rivers Llobregat and Ter. Of the total water input, 90 hm^3 came from Llobregat and 124 hm^3 from Ter river.

After applying integrated control approach, 25% energy cost can be saved (0.4M €/year). Besides, the network can supply 65 days longer before meeting deficit in dry season, which is a benefit for sustainable usage of water resource.

So far, we simplified irrigation component as a measured disturbance by forecasting. Future work will go deep to the irrigation component to develop model regarding water stress, crop growth and drainage reduction.

References

[1] Food and Agriculture Organization of the United Nations, "The Water-Energy-Food Nexus: A new approach in support of food security and sustainable agriculture," 2014.

[2] X. Litrico, and V. Fromion, "Simplified modeling of irrigation canals for controller design," Journal of Irrigation and Drainage Engineering, 130(5):373-383,2004.

Grey-box identification of a SCARA robot

András Retzler[1,2,3], Joris Gillis[1,2], Jan Swevers[1,2], and Zsolt Kollár[3]

[1]MECO Research Team, Dept. of Mechanical Engineering, KU Leuven, B-3001 Heverlee
[2]DMMS-M laboratory, Flanders Make, BE-3001 Heverlee
[3]Dept. of Measurement and Information Systems,
Budapest University of Technology and Economics, H-1521 Budapest
Email: andras.retzler@kuleuven.be

1 Introduction

Modeling mechatronic systems based on physical knowledge can lead to models with inherent nonlinearities. If our model does not fit into a certain class of nonlinear models for which tailored algorithms exist (e.g. PLNSS [1], NLARX [2]), we can easily encounter problems, for example the solver is unable to find a solution within the specified error threshold, or the running time of the solver makes the method practically infeasible. Possible reasons for these can be for example local minimums, or instability of the model for a set of parameter values. As a result, parameter estimation methods that work on a general set of nonlinear models are still a challenge.

In this study the task considered is estimating the parameters of a SCARA robot (in this case limited only to the masses of the links), with the goal to provide an accurate model for control. Having preliminary knowledge about the mechanical structure, the ODEs of the system were derived using the recursive Newton-Euler algorithm.

2 The method

Our approach is based on optimal control problems (OCP) for the simulation of the states of the system. In addition to the single shooting (SS) and multiple shooting (MS) formulations, we are using a hybrid formulation (X_{sim}, see Figure 1) that is in between SS and MS. This is similar to the idea in [1], but there it was limited to the scope of PLNSS models. The recursion depth in the formula can be controlled to find a compromise between memory usage, running time and the robustness of the algorithm.

We use CasADi to formalize the problem in MATLAB and solve it using Ipopt, an off-the-shelf solver for nonlinear programs. For the SS formulation, we also test the Ceres Solver, a solver from Google for nonlinear least-squares problems.

A comparison of running times and the memory usage for different initial parameter values and recursion depths has been carried out on a simulated robot. In addition, using different approximations of the Hessian matrix were also included in the comparison.

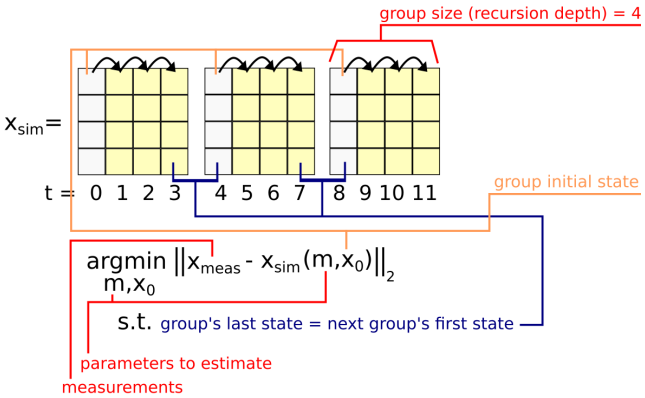

Figure 1: The hybrid formulation of the OCP

3 Results and future work

The simulations show that we can decrease the running time of the algorithm by choosing the appropriate recursion depth. The method will be validated on a model and measurements corresponding to a real system. Furthermore, we are planning a parallelized implementation to speed up the computation of the Hessian matrix.

4 Acknowledgements

This research is supported by Flanders Make: ICON project ID2CON: Integrated IDentification for CONtrol.

References

[1] A. Van Mulders, “Tackling two drawbacks of polynomial state-space models”, PhD thesis, VUB, Jun. 2012

[2] L. Ljung, R. Singh, Q. Zhang, P. Lindskog, A. Iouditski, “Developments in The MathWorks System Identification Toolbox”, IFAC Proceedings Volumes, vol. 42, no. 10, pp. 522-527, Jul. 2009

Improved kernel-based frequency response function estimation

Noël Hallemans, Rik Pintelon and John Lataire
Vrije Universiteit Brussel, Pleinlaan 2, 1050 Elsene, Belgium. e-mail: noel.hallemans@vub.be

1 Problem statement

The problem to be solved is the modelling of the frequency response function (FRF) $G(j\omega)$ of LTI systems from, persistently excited, known input $U(k)$, noisy output $Y(k)$ frequency domain data

$$\mathscr{D} = \{U(k), Y(k)\}_{k=0,1,\ldots,F-1}. \tag{1}$$

The input and output spectra are related as follows

$$Y(k) = G(j\omega_k)U(k) + L(j\omega_k) + V(k), \tag{2}$$

where $\omega_k = 2\pi k/T$, $L(j\omega_k)$ represents the transient and leakage, and $V(k)$ represents the noise. An example is shown in Fig. 1. Note that the problem of estimating $G(j\omega_k)$ from the data $\mathscr{D}$ is ill-posed: there are twice as many unknowns as equations. That is, each equation (2) has two unknowns; $G(j\omega_k)$ and $L(j\omega_k)$. This problem has yet been solved by imposing a local smoothing operator such as the local rational method (LRM) [1] or by using regularisation [2]. The regularisation solution has a couple of advantages over the LRM; (i) the model order selection is continuously tuneable, (ii) the estimate is a continuous function and (iii) it allows to impose stability, causality and smoothness on the estimate. However, it also has drawbacks over the LRM: it fails for lightly damped systems and it is only applicable when the noise is white. In this research we improve the regularisation method by solving these two drawbacks.

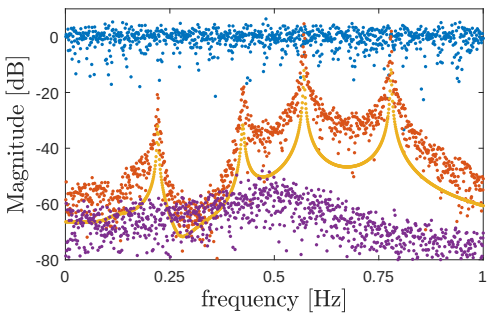

Figure 1: Input-output data. Blue: $U(k)$, red: $Y(k)$, yellow: $L(j\omega_k)$ and purple $V(k)$.

2 Kernel-based approach

The input-output relation (2) is rewritten in stacked notation

$$\mathbf{Y} = \Phi\theta + \mathbf{V} \text{ with } \Phi = \begin{bmatrix} \text{diag}(\mathbf{U}) & 0 \\ 0 & I_F \end{bmatrix} \text{ and } \theta = \begin{bmatrix} \mathbf{G} \\ \mathbf{L} \end{bmatrix}. \tag{3}$$

The optimal parameters are estimated using regularisation;

$$\hat{\theta} = \arg\min_{\theta} V_{WRLLS}, \tag{4}$$

where the weighted regularised linear least squares cost function is given by

$$V_{WRLLS}(\theta, \mathbf{Y}) = (\mathbf{Y} - \Phi\theta)^H W^{-1} (\mathbf{Y} - \Phi\theta) + \theta^H P^{-1} \theta \tag{5}$$

Solving (4) is no longer ill-posed thanks to the regularisation term. The core of the problem, however, is now translated into the choice of the kernel P. This kernel is most of the time obtained in two steps: (i) fixing the structure of the kernel depending on some hyper parameters and (ii) tuning these hyper parameters. In [2], the diagonal correlated (DC) kernel is chosen for P, which imposes smoothness, and hence, is not applicable for lightly-damped systems. Here, we introduce a new kernel which depends on prior knowledge about the resonating poles of the system. This prior knowledge and the weights matrix W can be extracted from an LRM preprocessing step. This improvement of the frequency-domain regularisation method is shown to perform well on simulation (Fig. 2). The MSE is lower compared with the LRM and measurements with colored noise can be processed.

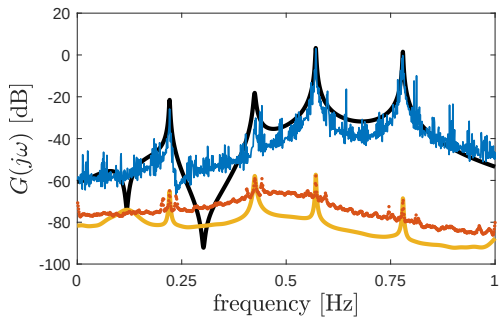

Figure 2: Monte-Carlo simulation. Black: true FRF $G(j\omega)$, red: MSE of the LRM [1], blue: MSE of the kernel-method [2] and yellow: MSE of the improved kernel method.

References

[1] Pintelon, R., Peumans, D., Vandersteen, G., & Lataire, J. (2020). Frequency Response Function Measurements via Local Rational Modeling, Revisited. *IEEE Transactions on Instrumentation and Measurement*, 70, 1-16.

[2] Lataire, J., & Chen, T. (2016). Transfer function and transient estimation by Gaussian process regression in the frequency domain. *Automatica*, 72, 217-229.

Data-Driven Predictive Control of Linear Parameter-Varying Systems

C. Verhoek[1], R. Tóth[1,2] and S. Haesaert[1]
[1]Control Systems Group, Eindhoven University of Technology, P.O. Box 513, 5600 MB, The Netherlands
[2]Systems and Control Laboratory, Institute for Computer Science and Control, H-1111 Budapest, Hungary
Email: {c.verhoek, r.toth, s.haesaert}@tue.nl

1 Introduction and motivation

Due to the increasing complexity and ever-growing performance demands towards systems in engineering, the involved modelling and control problems are becoming more and more challenging. To overcome the tedious process of obtaining a detailed dynamic model based on first-principles and a suitable model-based controller for such complex systems, data-driven modelling and control are attractive and have been in the focus of intensive research for several decades. However, a data-driven approach is associated with important questions: 1. When do we know that the data represents the *full* system behaviour? And, 2. How to generate an *optimal* control action based on the available data? One particular approach that in the Linear Time-Invariant (LTI) case has been successfully addressing these questions is the data-driven approach of the behavioural theory. This method characterises the full behaviour of the LTI system using a single sequence of input-output (IO) data [1], where the input is persistently exciting, covering question 1. The single data sequence can be reformulated as a data-based predictor, which can be used to determine an optimal control map or to synthesize an optimal control sequence, answering the second question. In a noise-free environment, such a Data-driven Predictive Controller (DPC) and a Model Predictive Controller (MPC) (which uses an accurate system model) yield the same result for LTI predictive control problems (see also the results on DeePC). Hence, a DPC can control the system efficiently and exactly as the MPC, without any information of the system other than a single earlier obtained data sequence. However, so far extensions of this promising theory have not been made for nonlinear systems. As a first step in this direction, we extend the aforementioned LTI results to a subset of nonlinear systems that can be modelled as affine Linear Parameter-Varying (LPV) systems.

2 Approach

We use the behavioural system theory for LPV systems [2]. The main idea of our approach is to rewrite the LPV system in a linear, constrained form, for which we can generalize the LTI results (see also [4]). Consider a data-generating LPV system, given by the following IO representation:

$$y_k + \sum_{i=1}^{n_\mathrm{a}} a_i(p_{k-i})y_{k-i} = \sum_{i=1}^{n_\mathrm{b}} b_i(p_{k-i})u_{k-i}, \qquad (1)$$

This work has received funding from the European Research Council (ERC) under the European Union's Horizon 2020 research and innovation programme (grant agreement nr. 714663), and financial support in the scope of the AI4GNC project with SENER Aeroespacial S.A., contract nr. 4000133595/20/NL/CRS

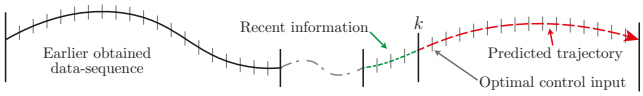

Fig. 1: Schematic representation of information used by the DPC.

with $u_k \in \mathbb{R}^{n_\mathrm{u}}$, $y_k \in \mathbb{R}^{n_\mathrm{y}}$ and $p_k \in \mathbb{P} \subseteq \mathbb{R}^{n_\mathrm{p}}$ the input, output and scheduling signal, respectively. Suppose that the functions a_i and b_i in (1) have *affine* dependence, i.e. $a_i(p_{k-i}) = a_{i,0} + a_{i,1}p_{k-i,1} + \cdots + a_{i,n_\mathrm{p}}p_{k-i,n_\mathrm{p}}$. Then we can rewrite the system (1) in the *implicit* IO form,

$$\begin{bmatrix} I & 0 \end{bmatrix}\mathscr{Y}_k + \sum_{i=1}^{n_\mathrm{a}} \begin{bmatrix} a_{i,0} & \cdots & a_{i,n_\mathrm{p}} \end{bmatrix}\mathscr{Y}_{k-i} = \sum_{i=1}^{n_\mathrm{b}} \begin{bmatrix} b_{i,0} & \cdots & b_{i,n_\mathrm{p}} \end{bmatrix}\mathscr{U}_{k-i}, \quad (2)$$

where $\mathscr{Y}_k := \begin{bmatrix} y_k^\top & (p_k \otimes y_k)^\top \end{bmatrix}^\top$ and $\mathscr{U}_k := \begin{bmatrix} u_k^\top & (p_k \otimes u_k)^\top \end{bmatrix}^\top$, and '$\otimes$' denotes the Kronecker product. Thus the considered LPV system, can be represented as a *constrained* LTI system, with constraints $\mathscr{U}_k$ and $\mathscr{Y}_k$. This allows the extension of the behavioural theory [1] to (2), without loosing the attractive properties and the simplicity of the data-driven predictor. The resulting LPV data-driven predictor can be incorporated in a predictive control scheme, which uses the earlier obtained data-sequence and recent information (to account for the initial condition) to generate an optimal control input for the system at hand, as shown in Fig. 1.

3 Preliminary results and outlook

In [3], we use an example to show that with the aforementioned predictor a fully data-driven predictive controller yields the same optimal behaviour as a model-based MPC scheme. However, these results were limited to the imposed affine parametrization of the LPV system. In the future, we plan to extend the results for general LPV systems (see [4]).

References

[1] J. C. Willems, et al., "A note on persistency of excitation," *Systems & Control Letters*, 2005.

[2] R. Tóth, *Modeling and Identification of Linear Parameter-Varying Systems*, 1st ed. Springer-Verlag, 2010.

[3] C. Verhoek, et al. , "Data-Driven Predictive Control for Linear Parameter-Varying Systems," *Accepted for the 4th IFAC Workshop on Linear Parameter-Varying Systems (LPVS)*, 2021.

[4] C. Verhoek, et al. , "Fundamental Lemma for Data-Driven Analysis of Linear Parameter-Varying Systems," *Submitted to the 60th IEEE Conference on Decision and Control*, 2021. Preprint available: arXiv:2103.16171

Underwater Localisation Using Magnetic Field Distortions

Frida Viset
DCSC, TU Delft
Mekelweg 2, 2628CD
F.M.Viset@tudelft.nl

Rudy Helmons
MTT, TU Delft
Mekelweg 2, 2628CD
R.L.J.Helmons@tudelft.nl

Manon Kok
DCSC, TU Delft
Mekelweg 2, 2628CD
M.Kok-1@tudelft.nl

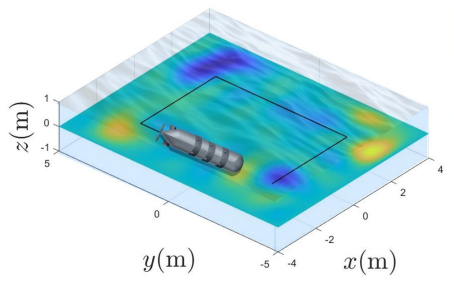

Figure 1: An underwater vehicle driving in a simulated trajectory. The trajectory and magnetic field distortions are simulated in two dimensions.

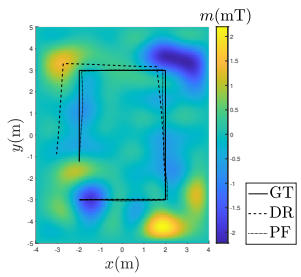

Figure 2: Comparison of an accelerometer dead reckoning (DR), and a particle filter (PF) trajectory estimate to the ground truth (GT) trajectory, where the PF uses information about the magnetic field distortions.

1 Introduction

Autonomous underwater vehicles can inspect and maintain underwater cables and structures, but they need accurate position estimates to be truly autonomous. The most popular position estimation methods for vehicles in air and on land are not usable underwater, as light conditions are poor, and GPS signals decay a few centimetres below the sea surface. Inspired by recent advances in indoor localisation, which exploits the informational value in magnetic field distortions [1], we propose the use of magnetic field distortions to improve underwater position estimates.

2 The underwater magnetic field

The global underwater magnetic field has spatial variations that are described in open-source online maps [2]. In addition, sub-sea metallic structures and electric cables cause additional local nonlinear spatial distortions in the magnetic field. When the magnetic field is distorted, we can use it as a source of position information. Magnetic field distortions tend to be slowly varying spatially, as illustrated by the simulated field strength m in Figure 2.

3 Localisation in a magnetic field

Figure 2 shows simulation results for how magnetic field anomalies can improve a position estimate. The trajectories show the x and y positions of the vehicle relative to the coordinate system in Figure 1. One estimate is obtained by integrating acceleration measurements (dead reckoning), and the other is obtained by using acceleration and magnetic field measurements in a particle filter. A particle filter is a Monte-Carlo based approach to estimate states that are a nonlinear function of available measurements. The dead reckoning estimate drifts away from the actual position, because it integrates erroneous measurements. Since the magnetic field distortions are stationary, they give information about an underwater vehicle's absolute position that the particle filter can use to remedy the drift. Through simulations in three dimensions (not illustrated here), we observe indications that the position of an underwater vehicle for a short mission can be determined near known magnetic field distortions using only accelerometer, gyroscope and magnetometer measurements, when these measurements are accurate enough, and when the information about the magnetic field disturbances is accurate.

4 Future work

The next step towards magnetic field navigation underwater is to test the algorithms in small-scale experiments. The experiments will be carried out in a controlled environment, using an accelerometer, gyroscope and magnetometer mounted on a small underwater vehicle.

References

[1] F. Viset, J. T. Gravdahl, and M. Kok, "Magnetic field norm SLAM using Gaussian process regression in foot-mounted sensors," *in Proceedings of the Europen Control Conference 2021*, 2021.

[2] J. Dyment et al., "Global equivalent magnetization of the oceanic lithosphere," *Earth and Planetary Science Letters*, vol. 430, pp. 54 – 65, 2015.

A hybrid neural network Kalman filter for vehicle state estimation

Alberto Bertipaglia
Cognitive of Robotics
Delft University of Technology
Mekelweg 2, 2628 CD Delft
Email: A.Bertipaglia@tudelft.nl

Barys Shyrokau
Cognitive of Robotics
Delft University of Technology
Mekelweg 2, 2628 CD Delft
Email: B.Shyrokau@tudelft.nl

1 Introduction

Automated driving is the automotive research field that aims to eliminate human error from driving to enhance passenger safety. Despite immense improvements promoted by deep learning, automated vehicles still struggle to be reliable in hazardous driving scenarios. The lack of data affects the data-driven approach. However, even physical vehicle models struggle in the edge cases because vehicle dynamics and tires enter a nonlinear working range. Especially in this range, the standard sensor set in conventional passenger vehicles cannot measure all the necessary parameters and variable. This study aims to enhance the safety of the automated vehicle in hazardous scenarios estimating the vehicle states (sideslip angle and tire-road forces) accurately in real-time and in various road conditions (friction variation, slope, or bank angle). Two innovative concepts are adopted: load sensing bearings to estimate the tire forces and the development of a new filter architecture that combines a deep neural network with a nonlinear Kalman filter. The proposed algorithm will be compared to the current state of the art, such as the unscented Kalman filter and deep neural network alone.

2 Review of sideslip angle estimation

The collision avoidance controller needs to know the value of the vehicle sideslip angle and the tire-road forces. Still, the sensor set regularly installed in a conventional passenger vehicle cannot measure them. Thus, engineers develop various filters to estimate vehicle states, avoiding the installation of expensive sensors. Two filter categories are distinguishable: model-based approach and learning-based approach. The first category is further divisible in kinematic and dynamic modelling.

Kinematic modelling relies on a simple model which correlates vehicle velocities with vehicle accelerations [1]. The main advantage is that it does not require any knowledge of tire parameters and road grip, but it is sensitive to sensor noise, sensor bias, and the system is not observable in a steady-state condition. A possible solution to the problem is introducing a conditional logic that merges the kinematic model with empirical knowledge [1]. For instance, it forces the sideslip angle to zero when the vehicle is driving straight. Thus, it requires relevant manual tuning. Furthermore, it supposes that the vehicle cannot have lateral drifting without a yaw moment which is unlikely but still feasible.

Dynamic modelling fully describes the lateral dynamics, so it needs extensive knowledge of tire parameters. Its accuracy is very high when vehicle and tires behave linearly. The main problem is that as soon as tires enter a nonlinear working range, their parameters need to be adapted. A possible solution is an adaptive tire model in which the cornering stiffness is a random walk model [2]. Authors present reliable results when tires are highly excited, but the filter loses accuracy in the other cases. Although a linear tire model can work together with an adaptive tire model, defining a threshold between the two in the mild range condition is not easy.

The learning-based approach relies just on the information coming from the data, and it can overcome the model structure limitation [3]. Despite good accuracy, it lacks a physical interpretation, so it is arguable its use in a safety application. Moreover, the learning-based approach still struggles with generalization.

In this project, the authors propose a new filter architecture combining the universal approximation properties of artificial neural network with the interpretability of a model-based approach. The measured strains at the wheel hub bearing are transformed in tire forces thanks to a recurrent neural network [4]. The computed forces are used as measurements in the Kalman filter to improve its accuracy.

References

[1] Selmanaj, D., et al. Vehicle sideslip estimation: A kinematic based approach, Control Engineering Practice, 2017, 67: 1-12.

[2] van Aalst, S., et al. An adaptive vehicle sideslip estimator for reliable estimation in low and high excitation driving, IFAC-PapersOnLine, 2018, 51(9): 243-248.

[3] Bonfitto, A., et al. Combined regression and classification artificial neural networks for sideslip angle estimation and road condition identification, Vehicle System Dynamics, 2020, 58(11): 1766-1787.

[4] Kerst, S. et al. Reconstruction of wheel forces using an intelligent bearing, SAE Int. J. of Passenger Cars-Electronic and Electrical Systems, 2016, 9: 196-203.

Nonlinear sample-based MPC in a Greenhouse with Lettuce and uncertain weather forecasts

Sjoerd Boersma
Farm Technology Group
Wageningen University
The Netherlands
Email: sjoerd.boersma@wur.nl

Simon van Mourik
Farm Technology Group
Wageningen University
The Netherlands
Email: simon.vanmourik@wur.nl

1 Introduction

Model predictive greenhouse climate control employs weather forecasts for energy efficient crop production. It has been a research subject for several decades [1]. By regulating the greenhouse's climate, the crop is indirectly also regulated and can consequently be optimized. A common objective is to minimize energy use per kg yield. For this, optimal predictive control solutions are proposed (for example, [2, 3]). These assume the weather forecasts to be deterministic even though it is uncertain. The exact impact of this uncertainty on the control results is not clear yet. In this work, a nonlinear model predictive controller is proposed that deals with this uncertainty. The controller allows for investigating the effect of uncertain weather forecasts on the control results.

2 Methodology

The model described in [2] is considered in this work:

$$x(k+1) = f\big(x(k), u(k), \hat{d}(k)\big), \qquad y(k) = g\big(x(k)\big), \quad (1)$$

with discrete time $k \in \mathbb{R}$ and $f(\cdot), g(\cdot)$ nonlinear functions. The measurement $y(k) \in \mathbb{R}^4$ contains the dry matter content of the lettuce crop in g m^{-2}, greenhouse's carbon dioxide concentration in g m^{-3}, the air temperature in °C and air's humidity content in g m^{-3}. The controllable signal $u(k) \in \mathbb{R}^3$ contains the supply rate of carbon dioxide in g m^{-2} s^{-1}, energy supply by the heating system in W m^{-2} and ventilation rate through the vents in mm s^{-1}. The uncertain disturbance (outside climate) $\hat{d}(k) \in \mathbb{R}^4$ contains the outside radiation in W m^{-2}, the outside's carbon dioxide concentration in kg m^{-3}, air temperature in °C and air humidity content outside the greenhouse in kg m^{-3}. These are assumed to be uniformly distributed with the true climate value $d(k)$ as its mean and variance $\sigma_{\hat{d}} = \frac{1}{12}(\hat{d}_{\max}(k) - \hat{d}_{\min}(k))^2$ with $\hat{d}_{\max}(k) = (1+\sigma)d(k)$ and $\hat{d}_{\min}(k) = (1-\sigma)d(k)$. The following optimization problem is solved at each sample period:

$$\min_{u(k)} \frac{1}{N_s}\sum_{j=1}^{N_s} -q_0 \cdot y_1^j(N_p) + \sum_{k=k_0}^{k_0+N_p}\sum_{i=1}^{3} q_i \cdot u_i(k),$$
$$\text{s.t. } (1), \quad y_{\min}(k) \le y(k) \le y_{\max}(k), \quad x(k_0) = x_0$$
$$u_{\min} \le u(k) \le u_{\max}, \quad |u(k) - u(k-1)| \le \delta u,$$

with prediction horizon N_p, weights $q_i \in \mathbb{R}$ and number of samples taken from the uniform distribution N_s. Note that $y_1^j(k)$ depends on $\hat{d}^j(k)$, which is a realization of the disturbance signal from the uniform distribution. The optimization aims at minimize the energy use per kg yield. The constraints $y_{\min}(k), y_{\max}(k) \in \mathbb{R}^4$ are set such that the greenhouse temperature during the night is lower than during the day. Additional constraints $(u_{\min}, u_{\max}, \delta u)$ are included to bound the control signal and its change.

3 Results

Each simulation has a time-span of 40 days. Table 1 shows percentages from the deterministic case (where $\hat{d}(k) = d(k)$). For the control signals, the rms values are compared (for example, $\delta\text{rms}(u_i) = 10$ implies a 10% higher rms value of $u_i(k)$ with respect to the deterministic case). It can be observed that an uncertainty increase results in an increased energy usage and decreased dry weight yield. Note that -4.2% dry weight is approximately half a lettuce less per square meter, which is significant. Overall, the results show that uncertain weather forecasts should be taken into account when a grower wants to invest in a predictive controller.

Table 1: Simulation results: percentages are with respect to the deterministic case where $\hat{d}(k) = d(k)$ is assumed.

σ	δW %	$\delta\text{rms}(u_1)$ %	$\delta\text{rms}(u_2)$ %	$\delta\text{rms}(u_3)$ %
0.1	-0.5	0.6	36.3	1.3
0.2	-1.4	1.6	77.7	2.6
0.3	-1.9	1.8	110.5	3.8
0.4	-4.2	3.7	199.1	5.4

References

[1] G. van Straten, G. van Willigenburg, E. J. van Henten, and R. van Ooteghem. *Optimal control of greenhouse cultivation*. CRC Press, 2011.

[2] E. J. van Henten. *Greenhouse climate management: an optimal control approach*. PhD thesis, University Wageningen, 1994.

[3] W. J. P. Kuijpers, D. Katzin, S. van Mourik, D. J. Antunesa, S. Hemming, and M. J. G. van de Molengraft. Lighting systems and strategies compared in an optimally controlled greenhouse. *Biosystems Engineering, vol. 202, pp. 195-216*, 2021.

Impact of essential tremor on saccadic adaptation

Florence Blondiaux[1,2], Louisien Lebrun[2], Bernard Hanseeuw[2], and Frédéric Crevecoeur[1,2]

[1]*Institute of Information and Communication Technologies, Electronics and Applied Mathematics, Université Catholique de Louvain, Louvain-la-Neuve, Belgium*

[2]*Institute of Neuroscience, Université Catholique de Louvain, Brussels, Belgium*

Corresponding author: Florence Blondiaux, INMA, Avenue Georges Lemaître 4-6/L4.05.01, 1348 Louvain-la-Neuve, Belgium. E-mail: florence.blondiaux@uclouvain.be

Essential Tremor (ET), one of the most common movement disorders, is characterized by involuntary oscillations of the limbs, mainly during movement. Although its origin remains unclear, there is a consensus on a neurogenic cause originating from a dysfunction of the cerebello-thalamo-cortical loop. A recent neuroimaging study reported reduced connectivity between the cerebellum and other brain regions [1], providing additional evidence for an implication of cerebellum in the generation of the tremor. From a different point of view, recent theoretical work in the field of systems theory showed that oscillations, consistent with the properties of ET, could arise from an erroneous estimation of transmission delays, inherent to the conduction of neural signals from sensory organs to the brain and back to muscles ($\sim$ 50-100 ms in human depending on the sensory system) [2]. Interestingly, this process of state estimation in human motor control has also been associated to cerebellum. These two findings led us to investigate the fingerprint of Essential Tremor on motor adaptation, an ability known to rest on the integrity of the cerebellum. More specifically by investigating the performances of patients affected by ET in a saccadic adaptation task,which involves processing of delayed sensory feedback. We hypothesized that if the tremor is linked to cerebellar deficits, then a deficit in saccadic adaptation could be observed. We recruited 33 participants (18 ET patients (13 F) and 15 healthy aged-matched controls (9 F)) to perform a standard saccadic-adaptation task. They were first assessed with standard clinical evaluation (Fahn-Tolosa-Marin tremor rating scale) to confirm their inclusion in the study. During the task, a visual target presented laterally (eccentricity: 20°) jumped vertically during the saccade (5°), see Fig. A. The target shift was typically not perceived but it resulted in a final error in the vertical direction that participants learned to anticipate with practice. After adaptation (300 trials), the final position of the saccade became closer to the goal target after the jump. The protocol included baseline trials composed of oblique and horizontal saccades (Fig: Ob., Horiz.) without any jump for control analyses (60 trials in total). There was no significant difference between the two groups during these trials. Regarding the adaptation trials, ET patients showed reduced adaptation captured by the extent of vertical component of the saccade and by the peak vertical velocity of partially adapted saccades, see Fig. B. Linear mixed models analysis of these

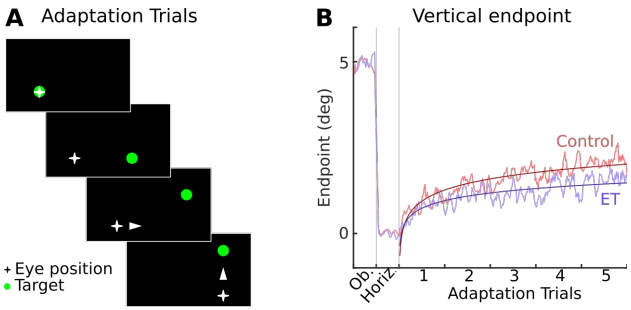

A: Chronology of one adaptation trial. Arrows indicate saccade direction. **B** Evolution of the vertical endpoint of the saccade. ET patients showed a smaller but significant adaptation to the perturbation.

two parameters revealed strong interaction between groups and the trial indices, revealing slower adaptation for the ET group ($p < 0.001$). The curvature of saccades from ET patients after adaptation also differed from the control group, showing an adaptation mainly towards the end of the saccade, in contrast with the control group who showed more gradual change in saccade curvature within each movement. These results show impairments in saccadic adaptation, for which no effect of the tremor itself was expected. Indeed, participants did not exhibit any nystagmus or eye oscillation, and their behaviour during fixation prior to saccades was similar to the control group. The monitoring of sensory feedback plays a key role in the control and adaptation of saccades, and the integration of this neural signal involves the cerebellum. The saccadic adaptation impairements shown by this study support the hypothesis of a cerebellar origin of ET. Because the same feedback integration mechanism is involved in other tasks such as upper limb control, we suggest that its deficit is a candidate cause of limb oscillations. Assessing motor adaptation deficits could represent a new quantitative behavioural marker of the disorder.

References

[1] Tikoo, S., Pietracupa, S., Tommasin, S., Bologna, M., Petsas, N., Bharti, K., Berardelli, A., & Pantano, P. (2020). Journal of Neurology.

[2] Crevecoeur, F., & Gervers, M. (2019). 2925–2954.

Selection of Elementary Flux Modes for the Development of Reduced Macroscopic Models

Maton Maxime[1*], Philippe Bogaerts[2], Alain Vande Wouwer[1]
[1]Systems, Estimation, Control and Optimization, University of Mons, Belgium
[2]3BIO - Modeling and Control of Bioprocesses, University of Brussels, Belgium
*Email: Maxime.Maton@umons.ac.be

1 Abstract

Over the years, mathematical modelling of mammalian cell cultures has received an ever increasing attention for the optimization of the production of biopharmaceuticals, such as monoclonal antibodies, viral vaccines and recombinant proteins. The development of dynamic macroscopic models from the knowledge of detailed metabolic networks relies on the concept of elementary flux modes (EFMs) regarded as the simplest metabolic pathways linking substrates to products. With the complexity and the size of the network, the number of elementary modes explodes and a selection of the most informative modes is required. In this connection, the present study proposes an algorithm called REM, i.e., Reducer of Elementary Modes, to cut the initial set of modes and to pick the most informative ones for the purpose of deriving reduced macroscopic models. The REM algorithm is a two-step procedure. First, the initial set of EFMs is drastically reduced by enlarging the concept of the cosine-similarity algorithm introduced in [1]. Then, the methodology is pursued by extracting the most informative modes from the first reduced set by means of a series of optimisation problems. This work makes use of experimental data of hybridoma cultures in batch and perfusion modes and two metabolic networks of different sizes illustrate the performance of the whole procedure.

2 REM algorithm

Fig.1 depicts the reduction algorithm used to select a minimal set of elementary modes, $K_{reduced}$, from an initial set K, this latter obtained on the basis of the metabolic network knowledge and the measurements of extracellular fluxes. The REM algorithm is an iterative method based on an optimisation problem where SSR_q represents the sum of squared residuals and determines if the observed phenotypes are part of the solution space. The whole procedure is mainly composed of two steps : (i) a pre-filtering exploiting the cosine similarity for collinearity identification and (ii) a further reduction to identify and retain the most informative modes according to a target number fixed beforehand. These steps involve a number of checks where a user-defined tolerance value guides the selection.

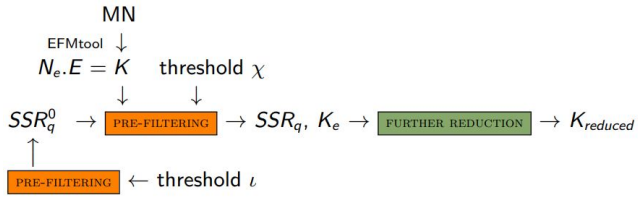

Figure 1: REM algorithm

3 Results

The present study relies on two metabolic networks and different measurements scenarios. The first network includes only 24 reactions leading to 11 EFMs, the second considers 70 reactions and leads to more than 22 thousands modes justifying the use of reduction algorithms. In that respect, when the methodology is applied to the more detailed network, the pre-filtering step allows cutting the initial set of EFMs from 22'563 to 476 and the subsequent steps allow a further reduction to 22 modes or less - depending on the measurements scenario and the fixed target number. Fig.2 shows the evolution of lactate concentration deduced from 476 modes (orange line) and from 22 modes (green line). This figure illustrates the merits of the REM algorithm.

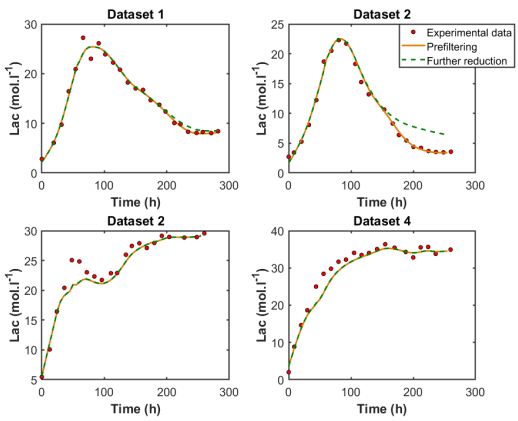

Figure 2: Time evolution of lactate concentration

References

[1] L. Hebing, T. Neymann, T. Thüte, A. Jockwer, and S. Engell, "Efficient generation of models of fed-batch fermentations for process design and control," IFAC-PapersOnLine, 2016. Vol.49(7) 621-626

On the Modelling of Behaviour in Epidemic Network Models for Sexually Transmitted Infections

Kathinka Frieswijk
University of Groningen
ENTEG
9747 AG Groningen
The Netherlands
Email: k.frieswijk@rug.nl

Lorenzo Zino
University of Groningen
ENTEG
9747 AG Groningen
The Netherlands
Email: lorenzo.zino@rug.nl

Ming Cao
University of Groningen
ENTEG
9747 AG Groningen
The Netherlands
Email: m.cao@rug.nl

1 Abstract

Without a cure, sexually transmitted infections (STIs) such as gonorrhoea, syphilis, chlamydia, and trichomoniasis can cause health problems, including chronic neurological problems, stillbirths, infertility, and cancer [1]. After the discovery of a cure in 1928, however, the severe facial deformities caused by syphilis predominantly became things of the past. After having relieved society of such horrific visual reminders of the consequences of unprotected sexual encounters, common STIs have been underestimated enemies for decades, and presently, their prevalence is rising. Each day, more than one million individuals become infected with a common STI [1]. In 2018, the combined prevalence of chlamydia, gonorrhoea, and syphilis in the United States came to an all-time high [2]. Since STIs — in particular gonorrhoea — are developing antibiotic resistance [3], this rise is very concerning. Adding fuel to the fire is the current COVID-19 crisis, which caused a disruption in STI services, and additionally a relocation of resources to the response to COVID-19 [4].

Although condoms are a very effective tool in the prevention of spreading of STIs, they are used at differing degrees. In order to construct more effective control policies, it is necessary to increase our knowledge of the underlying dynamics behind the prevailing trends of risky sexual behaviour. Potent means to study the underlying dynamics of the spreading of infections, are mathematical models of epidemic spreading on networks. The insights they produce can subsequently be used to inform control strategies. Here, we propose a model for the spreading of common STIs. The model is constructed within the framework of continuous-time activity-driven networks (ADNs) [5], in which each individual is assigned an activity rate, representing the individual's tendency to have sexual encounters with others. The ADN framework allows to model the time-varying pattern of encounters and the individuals' heterogeneity in their predisposition to initiate them. By adding extra compartments to the traditional susceptible–infected–susceptible (SIS) model, which is standardly used to model STIs such as gonorrhoea, we include individuals' behavioural preferences with regard to the use of protection during sexual encounters, and the presence of asymptomatic, unaware — but infectious — individuals. Behavioural preferences of individuals are evolving according to a nontrivial mechanism that accounts for the persuasive effect of encounters with individuals who have a different behavioural preference, the cost of adopting protective measures, and the perceived risk, which depends on the detected infection prevalence. If individuals with differing behavioural preferences interact, then it depends on the outcome of a probabilistic negotiation process whether the sexual encounter takes place or not. Here, we consider two negotiation processes: i) a process in which the other individual either rejects or accepts the proposal with a certain probability; and ii) a negotiation process in which a counterproposal can be made after rejection. In order to obtain analytical results, we take a mean-field approach to derive the epidemic threshold of a homogeneous ADN, and examine the effect of two control measures on the spreading of STIs: (i) condom marketing campaigns; and (ii) routine screening for STIs at high-volume sites. By employing simulations we expand our theoretical results, and introduce heterogeneities. Our results reveal the important effect of both marketing campaigns and routine screening for STIs.

References

[1] J. Rowley *et al.*, "Chlamydia, gonorrhoea, trichomoniasis and syphilis: global prevalence and incidence estimates, 2016," *Bull. World Health Organ.*, vol. 97, pp. 548–562, Aug. 2019.

[2] Centers for Disease Control and Prevention, "Sexually transmitted disease surveillance 2018.," *Atlanta: U.S. Department of Health and Human Services*, Okt. 2019.

[3] T. Wi *et al.*, "Antimicrobial resistance in neisseria gonorrhoeae: Global surveillance and a call for international collaborative action," *PLOS Med*, vol. 14, July 2017.

[4] World Health Organization, "Disruption in HIV, Hepatitis and STI services due to COVID-19," July 2020.

[5] L. Zino, A. Rizzo, and M. Porfiri, "Continuous-time discrete-distribution theory for activity-driven networks," *Phys. Rev. Lett.*, vol. 117, Nov. 2016.

An SIR-type model for COVID-19 hospitalization forecasts

Ousmane Diao, P.-A. Absil
ICTEAM Institute, UCLouvain, Belgium
{ousmane.diao,pa.absil }@uclouvain.be

Mouhamadou Diallo
Bacteriology & Virology, Cheikh Anta DIOP University of Dakar, Senegal
mouhamdiallo@gmail.com

1 Introduction

Compartmental models, and in particular the well-known SIR model [1], have been widely used to model infectious diseases since the early 20th century; see [2] and references therein. In [3], an SEIR model is proposed to predict hospitalization cases based on real data and to predict the resurgence of the COVID-19 epidemic taking into account the age structure of the population and different strategies of the government policies (physical distancing, quarantine, lockdown, school closure, work at home and transport closure, etc.) to fight against the pandemic. Gabor Vattay [4] uses the common SIR model to show how the cumulative number of deaths can be regarded as a master variable and estimates some epidemiological parameters such as the reproduction number R_0, the size of the susceptible population and the infection rate. In the present work, we use the SIR model as in [2], given by:
$\dot{S}(t) = -\frac{\beta}{N}S(t)I(t)$, $\dot{I}(t) = \frac{\beta}{N}S(t)I(t) - \gamma I(t)$ and $\dot{R}(t) = \gamma I(t)$
where $S(t)$, $I(t)$, and $R(t)$ are the number of susceptible, infectious and removed (or recovered) individuals at time t with the condition that the population $N = S(t) + I(t) + R(t)$ is constant. We denote by $\dot{S}(t)$, $\dot{I}(t)$ and $\dot{R}(t)$ their time derivatives, β is the contact rate (i.e., contacts sufficient for transmission) and $1/\gamma$ is the average infectious period. In this paper, we adapt the SIR model to the situation where S, I and R are hidden variables but $I(t)$ is observed through a "proxy" $H(t) = \alpha I(t)$, the number H of hospitalized patients. Furthermore, α is unknown but constant and β, γ and N (the total concerned population) are unknown.

2 Model formulation

The proposed adapted SIR model has two state variables ($\bar{S}$—a scaled version S—and H) and two parameters ($\bar{\beta}$—which lumps together the parameters β, N, and α—and γ) which we term the SH model. We leverage the proposed SH model as follows in order to make hospitalization forecasts. Letting $\bar{S} = \alpha S$ and $\bar{\beta} = \frac{\beta}{N\alpha}$, we obtain the simplified SIR model

$$\dot{\bar{S}}(t) = -\bar{\beta}\bar{S}(t)H(t) \text{ and } \dot{H}(t) = \bar{\beta}\bar{S}(t)H(t) - \gamma H(t).$$

We denote by $E(t) = \bar{\beta}\bar{S}(t)H(t)$ the number of patients entering the hospital by unit of time and by $L(t) = \gamma H(t)$ the number of patients leaving the hospital by unit of time. Considering t_i and t_c the initial and end time of the training set, given observed values $(H_o(t))_{t=t_i,\dots,t_c}$, $(E_o(t))_{t=t_i,\dots,t_c}$ and $(L_o(t))_{t=t_i,\dots,t_c}$, we estimate the parameters $\bar{\beta}$, γ, and the initial conditions $\bar{S}(t_i)$ and $H(t_i)$ of the SH model by using the sum-of-squared-errors objective function

$$\phi(\bar{\beta}, \bar{S}(t_i)) = c_H \sum_{t=t_i}^{t_c}(H(t) - H_o(t))^2 + c_E \sum_{t=t_i}^{t_c}(E(t) - E_o(t))^2 + c_L \sum_{t=t_i}^{t_c}(L(t) - L_o(t))^2$$

where the c coefficients are parameters, all set to 1 in our experiments unless otherwise stated, and a ratio of means:

$$\hat{\gamma}^{\mathrm{RM}} = \frac{\sum_{t=t_i}^{t_c} L_o(t)}{\sum_{t=t_i}^{t_c} H_o(t)}$$

Then we simulate the SH model in order to predict $(H(t))_{t=t_{c+1},\dots,t_f}$ for a specified final prediction time t_f. This approach thus relates to the areas of parameter estimation, data assimilation (for the generation of the initial conditions) and machine learning (for the train set and test set approach).

3 Results

We show in [5] that when the model is trained on a suitable three-week period around the hospitalization peak for Belgium, it forecasts the subsequent two months with mean absolute percentage error (MAPE) under 4%. The statistical table shows that more than half of the Belgian provinces have an MASE_test below 3 where MASE denotes the mean absolute scaled error,

$$\mathrm{MASE} = \frac{t_b - t_a}{t_b - t_a + 1} \frac{\sum_{t=t_a}^{t_b} |H_o(t) - H(t)|}{\sum_{t=t_a}^{t_b - 1} |H_o(t+1) - H_o(t)|},$$

and $H_o(t)$ and $H(t)$ are the observed and predicted number of hospitalized patients.

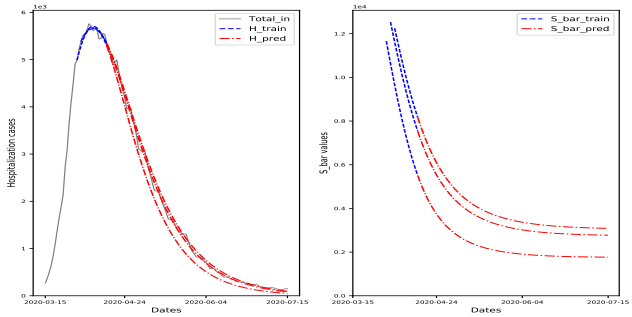

Figure 1: Belgium, train period around the peak. Fitting and predictions with the SH model.

Table 1: Belgium provinces

Percentiles	min	P_{25}	P_{50}	P_{75}	max
MASE	0.61	1.10	1.31	1.75	6.69
MASE_train	0.65	0.76	0.85	0.94	1.27
MASE_test	1.51	2.20	2.84	3.30	11.18

References

[1] William O. Kermack and al., 'A contribution to the mathematical theory of epidemics", Proceedings of the Royal Society of London. Series A, *Containing Papers of a Mathematical and Physical Character*, 115(772):700-721, 1927.

[2] Hethcote and Herbert W., The Mathematics of Infectious Diseases, *SIAM Review*, 42(4),599-653, 2000.

[3] Steven Abrams and al., "Modeling the early phase of the Belgian COVID-19 epidemic using a stochastic compartmental model and studying its implied future trajectories", medRxiv, 2020.

[4] Gabor Vattay, "Forecasting the outcome and estimating the epidemic model parameters from the fatality time series in COVID-19 outbreaks", arXiv, 2020.

[5] P.-A. Absil, O. Diao and M. Diallo, "Assessment of COVID-19 hospitalization forecasts from a simplified SIR model", eprint arXiv:2007.10492, 2020.

Model Predictive Control of Modular Multilevel Converter for Ultra-Fast charging stations

Victor Daniel Reyes Dreke[1], Mircea Lazar[1]
[1] Control Systems Group, Eindhoven University of Technology, 5600 MB Eindhoven, The Netherlands
Email: v.d.reyes.dreke@tue.nl

1 Introduction

Next-generation Charging Stations for Electrical Vehicles (EVs) are envisioned to be more efficient, cheaper and accessible. These new stations should reduce the charging time, which is one of the main limitations of EVs. Aiming for this goal, many researchers are exploring the benefits of replacing two-level AC/DC bidirectional converters with Modular Multilevel Converters (MMCs). In similar applications, MMCs had shown lower losses and higher quality of the output waveform. Besides, there is not need for a transformer when MMCs are employed.

2 Motivation

The basic component of the MMC in Figure 1 is called submodule (SM), consisting of a half-bridge (HB) with a capacitor buffer. Each phase leg of the converter has two arms, the upper and lower arms, which are constituted by a number (N) of series connected submodules. The number of the output steps (voltage levels) depends on the number of submodules available in each arm.

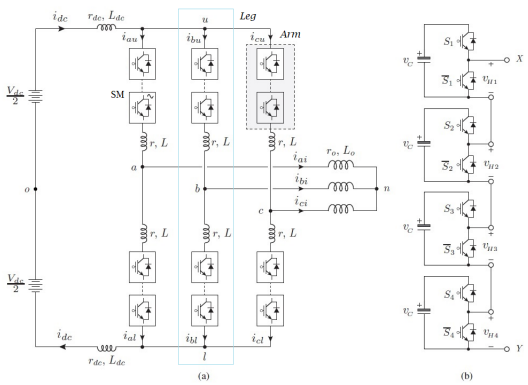

Figure 1: Modular multilevel converter and arm configuration: (a) MMC with passive load and (b) connection diagram of HB submodule within the arm.

Based on Figure 1, each arm behaves as a dependent voltage source defined as

$$v_{XY} = v_{H1} + ... + v_{HN} = S_1 v_c + ... + S_N v_c = \mathbf{v_c} \cdot S_{XY}, \quad (1)$$

where v_c is the voltage of the capacitor buffer, $S_N \in \{0,1\}$ is the state of the Nth submodule of the arm, v_{XY} is the arm voltage, $X \in \{l,u\}$ determines the arm, $Y \in \{a,b,c\}$ determines the phase. Applying Kirchoff's law, we calculate the phase voltage as $\mathbf{v_Y} = v_{lY} - v_{uY}$, and the line current $\mathbf{i_Y}$ as

$$\frac{d\mathbf{i_Y}}{dt} = [\frac{-r_m + 2r_o}{L_m + 2L_o}] \cdot \mathbf{i_Y} + [\frac{-1}{L_m + L_o}] \cdot [2v_{no}\mathbf{1_{3x1}}] + [\frac{1}{L_m + L_o}] \cdot \mathbf{v_Y}, \quad (2)$$

Traditionally, the most popular control technique used among industrial practitioners is PI control. However, better performance could be achieved if Model Predictive Control (MPC) is used, as in [1]. Based on (1), the control of the MMC is define as Mixed Integer Nonlinear Problem (MINLP). The manipulated variables are the switch positions in each leg i.e., $(u_a, u_b, u_c) \in \mathscr{U} \times \mathscr{U} \times \mathscr{U}$

$$\mathscr{U} = \{-2^{N-1}+1, ..., 0, ..., 2^{N-1}-1\} \quad (3)$$

where each values of $\mathscr{U}$ is a switching state combination for each leg. To the author's best knowledge, this MINLP for MMC applications had only been solved using MPC with unitary prediction horizon. However, there is evidence, such as [2], that using a long prediction horizon significantly increases the performance of the MPC in Power Electronics (PE) applications. In comparison with other PE circuits, the number of control actions for MMCs is considerably higher. Hence, the computational burden of the current MPC implementations is too heavy, making difficult for real time implementation in the considered MMCs application.

3 Approach

Aiming to research the benefits of using Long Prediction Horizon MPC, different optimization methods like Branch and Bound, Sphere Decoding [2] and Sampling -Based MPC [3] will be compared. For these methods, the computational burden does not increase exponentially when the prediction horizon increases.

References

[1] A. Dekka, B. Wu, V. Yaramasu, R. L. Fuentes, and N. R. Zargari, "Model Predictive Control of High-Power Modular Multilevel Converters - An Overview," *IEEE Journal of Emerging and Selected Topics in Power Electronics*, vol. 7, pp. 168–183, 3 2019.

[2] P. Karamanakos, E. Liegmann, T. Geyer, and R. Kennel, "Model Predictive Control of Power Electronic Systems: Methods, Results, and Challenges," *IEEE Open Journal of Industry Applications*, vol. 1, pp. 95–114, 8 2020.

[3] R. V. Bobiti and M. Lazar, "Towards Parallelizable Sampling–based Nonlinear Model Predictive Control," *IFAC-PapersOnLine*, vol. 50, pp. 13176–13181, 7 2017.

Pinning synchronization of heterogeneous multi-agent nonlinear systems via contraction analysis

Hao Yin, Bayu Jayawardhana, and Rodolfo Reyes-Báez
ENTEG, University of Groningen, 9747 AG Groningen, The Netherlands.
hao.yin@rug.nl, b.jayawardhana@rug.nl and r.reyes.baez@rug.nl

1 Introduction

Using recent results on the incremental stability analysis via contraction and on internal model principle, we revisit the pinning synchronization problem in nonlinear multi-agent systems (MAS) [1]. We provide sufficient and necessary conditions for both the pinned agents as well as the rest of the agents to guarantee the state synchronization. For the non-pinned agents, we present a distributed control framework based only on the relative local state measurement and we give sufficient conditions for the contractivity of the individual virtual systems in order to achieve pinning synchronization. Numerical simulation is given to illustrate the main results.

2 Problem formulation

The oscillator dynamics at node v_0 is given by

$$\dot{w} = S(w), \tag{1}$$

We consider (non-identical) agents described by

$$\dot{x}_i = f_i(x_i) + g_i(x_i)u_i, \quad \forall i \in \mathscr{V}, \tag{2}$$

The dynamic controller for i-th agent is given by

$$\begin{cases} \dot{\xi}_i &= \hat{C}_i(\xi_i, e_i) \\ u_i &= \hat{D}_i(\xi_i) \end{cases} \tag{3}$$

where $e_i = \sum_{j\in N_i} a_{ij}(x_i - x_j)$. Based on the previous systems' description, we can formulate the pinning synchronization problem as follows.

Pinning synchronization problem: For a given exosystem and agents' dynamics given by (1) and (2), respectively, design the controller (3) for the nodes $\mathscr{V}\backslash\mathscr{V}_{\text{pin}}$ such that 1) The origin of the closed-loop systems is locally exponentially stable; and 2) For all initial conditions $w(0), x_i(0), \xi_i(0)$ which contains the origin, the trajectories of the closed-loop systems are bounded and satisfy

$$\lim_{t\to\infty}(x_i(t) - w(t)) = 0, \qquad \forall i \in \mathscr{V}. \tag{4}$$

3 Main Result

proposition 1 *The synchronization problem is solvable if and only if for all $i \in \mathscr{V}\backslash\mathscr{V}_{pin}$ there exist mappings $x_i = w$, $\xi_i = \hat{\sigma}_i(w)$ with $\hat{\sigma}_i(0) = 0$ satisfying*

$$\left.\begin{aligned} S(w) &= f_i(w) + g_i(w)\hat{D}_i(\hat{\sigma}_i(w)) \\ \hat{\sigma}^i_w S(w) &= \hat{C}_i(\hat{\sigma}_i(w), 0). \end{aligned}\right\} \tag{5}$$

If pinning synchronization problem is solvable, the variational system is

$$\begin{pmatrix} \delta\dot{q}_i \\ \delta\dot{\xi}_i \end{pmatrix} = \underbrace{\begin{pmatrix} \frac{\partial(f_i(q_i)+g_i(q_i)\hat{D}_i(\xi_i))}{\partial q_i} & g_i(q_i)\hat{D}^i_{\xi_i} \\ \hat{C}^i_{e_i}\sum a_{ij} & \hat{C}^i_{\xi_i} \end{pmatrix}}_{\hat{A}_i} \begin{pmatrix} \delta q_i \\ \delta\xi_i \end{pmatrix} \tag{6}$$

proposition 2 *Assume that for the pinned agents $i \in \mathscr{V}_{pin}$, for the rest of the agents, consider the variational system* (6) *satisfying* (5). *If there exists a symmetric matrix $P_i(q_i, \xi_i)$ s.t. $c_1 I \le P_i(q_i, \xi_i) \le c_2 I$, and*

$$\hat{A}_i^T P_i + \dot{P}_i + P_i\hat{A}_i \le -\lambda P_i \tag{7}$$

holds for some $\lambda > 0$ and for all $(q_i, \xi_i) \in Q_0 \times \Xi_0$ with $W_0 \cup X_{i0} \subset Q_0$, $i \in \mathscr{V}$ then the closed-loop systems (1), (2) *and* (3) *satisfy 1) and 2).*

4 Simulation Results

The phase plot of each agent's trajectories is shown in Figure 1 where pinning synchronization is achieved as expected.

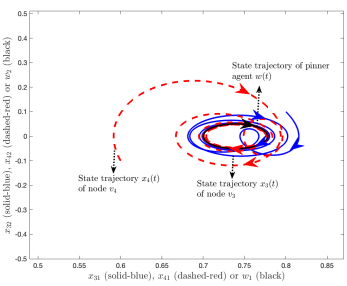

Figure 1: The phase plot of pinning agents' state x_1, x_2, x_3, x_4 and of the pinner agent w.

References

[1] Yin H, Jayawardhana B, Reyes-Báez R. Pinning synchronization of heterogeneous multi-agent nonlinear systems via contraction analysis. IEEE Control Systems Letters. 2021 Jan 21.

On Consensus Control of Uncertain Multi-Agent Nonlinear Systems in Power-Chained Form

Maolong Lv
Delft Center for Systems and Control
Delft University of Technology
Email: M.Lyu@tudelft.nl

Bart De Schutter
Delft Center for Systems and Control
Delft University of Technology
Email: B.DeSchutter@tudelft.nl

Simone Baldi
Southeast University and
Delft University of Technology
Email: S.Baldi@tudelft.nl

1 Introduction

Recent years have witnessed a tremendous progress in the field of distributed control of nonlinear multi-agent systems. Such results can be categorized according to two large families of nonlinear dynamics: strict-feedback and pure-feedback dynamics. At the same time, another family of dynamics, namely power-chained form (also called high-order systems or p-normal form) [1], has been attracting great attention. The reason is twofold: first, power chained dynamics are a generalization of strict-feedback and pure-feedback dynamics since they include more general integrators (with positive odd-integer-powers); second, dynamics in power-chained form can describe relevant classes of practical systems such as dynamical boiler-turbine units, or hydraulic dynamics [1]. Besides, [1] has shown that some classes of under-actuated, weakly coupled mechanical systems with cubic force-deformation relations (nonlinear spring forces) can also be captured by power-chained form. The adding-one-power-integrator technique was successfully proposed in [2] to handle the power-chained form. Based on this approach, several control methods have been proposed to achieve stabilization and output tracking for the power-chained form.

2 Open Problems in Multi-Agent Control of Power-Chained Form

In this presentation, we will discuss three major open problems in multi-agent control of power-chained form.

Problem 1: The extension of the standard adding-one-power-integrator technique to a distributed setting is not very meaningful due to the following two complex aspects: (a) the high-power terms in the power-chained form must be separated from the control gain functions via separation lemmas that make the power of the virtual control gains grow exponentially with the power of the system; (b) the control gain of each virtual control law is incorporated into the next virtual control law iteratively, thus increasing the control complexity at each step. Such issues result in high-complexity and high-gain designs which might be prohibitive for multi-agent systems with low computational power and limited actuation. Therefore, the first research question arises: *how to design a reduced-complexity distributed control methodology overcoming above-mentioned high control gains for nonlinear multi-agent systems in power-chained form?*

Problem 2: State-of-the-art results rely on the assumption that the agents' control directions (i.e. the signs of the control gain functions) are known *a priori* and are available for control design. When such *a priori* knowledge is not available, an established approach is continuous parameter adaptation via Nussbaum functions. Thus, the second research question arises: *how to design Nussbaum functions-based techniques for handling nonlinear multi-agent control systems in power-chained form in the presence of unknown control directions?*

Problem 3: It is well-recognized [3] that Nussbaum functions-based methods require additional complexity in the control design. This may lead to large learning transients: therefore, logic-based adaptation was employed for strict-feedback dynamics to overcome the conventional Nussbaum approach. State-of-the-art logic-based mechanisms in [3] for strict-feedback systems rely on monitor functions that monitor whether asymptotic tracking can be achieved. Unfortunately, the same mechanisms cannot be adopted for the power-chained form due to the fact that asymptotic tracking is impossible since the linearized dynamics contain uncontrollable modes whose eigenvalues are in the right half plane. Hence, the third research question arises: *how to design a new logic-based mechanism for nonlinear multi-agent control in power-chained form with unknown control directions?*

References

[1] C. Qian and W. Lin, "Practical output tracking of nonlinear systems with uncontrollable unstable linearization," *IEEE Transactions on Automatic Control*, vol. 47, no. 1, pp. 21-35, 2002.

[2] W. Lin and C. Qian, "Adding one power integrator: a tool for global stabilization of high-order lower-triangular systems," *Systems & Control Letters*, vol. 39, pp. 339-351, 2000.

[3] C. Huang and C. Yu, "Tuning function design for nonlinear adaptive control systems with multiple unknown control directions," *Automatica*, vol. 89, pp. 259-265, 2018.

Distributed Control for Distribution Network-Constrained Prosumers in Real-time market

Xiupeng Chen
ENTEG
University of Groningen
Nijenborgh 4, 9747 AG Groningen
The Netherlands
Email: xiupeng.chen@rug.nl

Jacquelien M. A. Scherpen
ENTEG
University of Groningen
Nijenborgh 4, 9747 AG Groningen
The Netherlands
Email: j.m.a.scherpen@rug.nl

Nima Monshizadeh
ENTEG
University of Groningen
Nijenborgh 4, 9747 AG Groningen
The Netherlands
Email: n.monshizadeh@rug.nl

1 Introduction

Driven by growing environmental and climate concerns, power systems are undergoing a fundamental transition due to the rapid increase of distributed energy resources including rooftop PV generation, storage batteries, plug-in vehicles and controllable loads. Traditional consumers are becoming prosumers who are able to manage their flexible energy resources actively to rapidly response to fluctuating supply/demand and provide voltage support in smart grid [1]. Traditionally, power networks are kept stable and secure by centralized control actions. However, this centralized network architecture is of great concern, because sending all this information to a independent system operator(ISO) introduces scalability, complexity and privacy issues. Consequently, more distributed network control and optimization techniques are required to support the energy management for large numbers of prosumers [2].

2 Practical issues and requirements

The coordinated control of prosumers relies on a well-designed market mechanism, the existing research about energy sharing mechanism design for prosumers can be classified into two categories: distributed optimization based method and game theory based method. In the former approach, all prosumers are willing to collaborate to achieve a certain goal, e.g. maximizing social welfare. A non-profit agent is programmed to set prices and the individual prosumers choose their corresponding strategies as price takes. The interaction between prosumers with the ISO is privacy preserving as only energy sharing preferences are communicated. In the latter approach, the conflicting interests of prosumers are characterized. The key point here is to model the decision-making processes of prosumers and find the Nash equilibrium so that each prosumer maximizes their profits while ensuring the system supply and demand balance.

Prosumers are generally connected by an alternating current(AC) distribution nerwork, so the network energy losses and energy transmission limitation can significantly impact the power balance and power sharing among prosumers. So we should consider not only the economic issues of energy trading, but also the technical issues of system operation, e.g. line congestion and voltage violation may occurring in distribution network. Optimal power flow(OPF) technique plays an important role in dealing with these issues. Additionally, incorporating OPF technology into energy trading could discover the distribution locational marginal prices(DLMPs). A variety of distributed optimization and control algorithms for solving OPF problems are shown in [3].

3 Main results

A market based control mechanism in the real-time market is proposed to coordinate the energy sharing among prosumers economically while ensuring the stability and security of system operation. Considering the dynamic characteristics of storage batteries and responsive demands, a model predictive control(MPC) method is used to handle constraints between different time intervals and incorporate the future generation and consumption predictions. Moreover, due to the computational burden and individual privacy issues, an efficient distributed algorithm is developed for solving the optimal power flow(OPF) problem and the strong coupling between prosumers through power networks is decoupled by introducing auxiliary variables to get DLMPs including not only energy component, but also congestion and loss components.

References

[1] Y. Parag, et al, "Electricity market design for the prosumer era," Nature energy 1.4 (2016): 1-6.

[2] A. Nedic, et al, "Distributed optimization for control," Annual Review of Control, Robotics, and Autonomous Systems 1 (2018): 77-103.

[3] D.K. Molzahn, et al, "A survey of distributed optimization and control algorithms for electric power systems," IEEE Transactions on Smart Grid 8.6 (2017): 2941-2962.

Angle-based formation with bearing and velocity information

Ningbo Li, J.M.A. Scherpen and A.J. van der Schaft
Jan C. Willems Center for Systems and Control, ENTEG, University of Groningen, The Netherlands
ningbo.li@rug.nl, j.m.a.scherpen@rug.nl and a.j.van.der.schaft@rug.nl

1 Motivation

In terms of the sensing capability, using partial information, such as distance or bearing, needs less onboard sensors, which has more practical meaning in formation control. There is also many literature on this topic in recent years. In this talk, we study the case where the sensing capability of agents is based on bearing and velocity measurement and the interaction topology of agents is constrained by angle. Compared with the interaction topology constrained by bearing, it enables formation to track the time-varying orientations. However, the resulting control law for this case in energy-based approaches usually contains a negative gradient of the energy function, which implies that the agents need the full information of relative position even if the sensing capability and the interaction topology of agents are both only bearing or distance. To solve this problem, we extend the passive adaptive compensator proposed in [1] to estimate the unavailable distance information by relative velocity.

2 Methodology

We consider the triangular formation as in Fig.1. For the link k between agent a and agent b, we have

$$z_k = q_a - q_b, r_k = ||z_k||, s_k = \frac{z_k}{||z_k||}, cos\angle 1 = (s_k^T s_j).$$

where $q_a, q_b \in \mathbb{R}^2$ are positions of agent a and b, $z_k \in \mathbb{R}^2$ is the relative position associated with the link k. $r_k \in \mathbb{R}^+$ is the distance, $s_k \in \mathbb{R}^2$ is the bearing and $(s_k^T s_j) \in \mathbb{R}$ is the angle. The dynamics of the agents are simplified to a double integrator, modeled in port-Hamiltonian form as

$$\begin{pmatrix} \dot{q}_i \\ \dot{p}_i \end{pmatrix} = \begin{pmatrix} 0 & I_2 \\ -I_2 & D_i \end{pmatrix} \begin{pmatrix} \frac{\partial H_i}{\partial q_i} \\ \frac{\partial H_i}{\partial p_i} \end{pmatrix} + \begin{pmatrix} 0 \\ I_2 \end{pmatrix} u_i. \quad (1)$$

We consider the triangular formation determined only by angle constraints. As shown in Fig.1, a, b, c are agents. i, j, k are the edges. Angle 1 and 2 are the constrained angles. If angle 1 and 2 are both controlled to a desired value, all the inner angles are invariant to the angle constraints.

Now we consider the controller of agent a. Since the motion of agent a affects both angle 1 ad 2, the controller of agent a consist of two parts. One is used to satisfy the constraint angle 1, the other part is used to satisfy constraint angle 2. For the controller of agent a to satisfy angle 1, the resulting

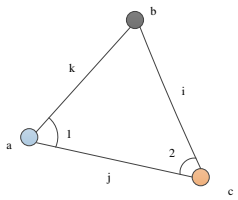

Figure 1: Triangular formation

control law is derived as

$$u_{1,a} = [\frac{1}{\hat{r}_{1,k}}(I_3 - s_k {s_k}^T)^T s_j + \frac{1}{\hat{r}_{1,j}}(I_3 - s_j {s_j}^T)^T s_k] \\ [c_{1,a}\widetilde{(s_k^T s_j)} + d_{1,a}\dot{\widetilde{(s_k^T s_j)}}]. \quad (2)$$

Furthermore, the dynamics of the estimator for $r_{1,k}$ is given by

$$\dot{\hat{r}}_{1,k} = \dot{r}_k + \dot{\tilde{r}}_{1,k} = s_k^T \dot{z}_k - \frac{\gamma_{1,a}^T}{c_{1,k}\hat{r}_{1,k}}(\dot{s_k^T} s_j). \quad (3)$$

Similarly, we can derive the controllers for all agents a, b, c and estimators for all edges i, j, k. In general, the controller is given by the following theorem.

Theorem 1. Consider three agents are modeled as (1) and the three agents will not overlap, i.e., $r_i, r_j, r_k \neq 0$. Using controller for all agents where each part is designed similarly to (2) and (3), the agents satisfy the inner angle constraints.

3 Conclusion

In this abstract, we consider the formation control of three agents modeled in Hamiltonian form where the sensing capability is based on bearing and velocity measurement and the interaction topology is constrained by angle. To solve this problem in such a way, the resulting control law contains the distance term. Therefore, we extend the passive adaptive compensator to estimate the unavailable bearing or distance information by relative velocity.

References

[1] G. Stacey and R. Mahony, "A passivity-based approach to formation control using partial measurements of relative position," *IEEE Transactions on Automatic Control*, vol. 61, no. 2, pp. 538–543, 2015.

A Linear Least Squares Approach to Estimate Space-Dependent Parameters in Heat and Mass Transport

Ricky van Kampen[1,2], Amritam Das[3], Siep Weiland[4], Matthijs van Berkel[1,2]
[1] Energy Systems and Control Group, DIFFER, Eindhoven, the Netherlands
[2] Control Systems Technology Group, Eindhoven University of Technology, Eindhoven, the Netherlands
[3] Control Group, University of Cambridge, Cambridge, United Kingdom
[4] Control Systems Group, Eindhoven University of Technology, Eindhoven, the Netherlands
R.J.R.vanKampen@differ.nl

1 Introduction

Heat and mass transport are important to solve various problems in physics and chemistry. For example, in the field of nuclear fusion transport determines the reactor's efficiency. For this reason, the physical parameters that dictate the transport are often studied by perturbative experiments. Here, the transport is modeled by a linear one-dimensional parabolic partial differential equation (PDE) and the goal is to estimate the unknown physical parameters utilizing measured data. This is known as an inverse problem or grey box identification problem.

As PDEs are infinite dimensional models, these are typically approximated by a finite dimensional model such that the parameters are estimated by minimizing the difference between the model output and the measured data, i.e. output error criterion. This minimization problem is primarily solved with iterative optimization methods that suffer from two problems: 1) they are solved iteratively, which is time consuming and in many cases the problem is non-convex, i.e. no guarantee for convergence to an optimal solution; 2) as only the output error is optimized and the unknown parameters are unconstrained, the parameters can start oscillating due to spatial aliasing of the state.

In this work, we discuss the method to write the problem as a linear least squares problem, using the equation error instead of the output error as presented in [1]. The optimum of a linear least squares problem is given by a closed-form solution, avoiding computational expensive optimization methods and guaranteeing the optimal solution.

2 Problem Formulation

Consider the following 1D linear parabolic partial differential equation

$$\frac{\partial T}{\partial t} = D(x)\frac{\partial^2 T}{\partial x^2} + V(x)\frac{\partial T}{\partial x} + K(x)T + P(x)s(t), \qquad (1)$$

that governs the temperate $T(x,t)$ in the spatial domain $x \in [0,L]$ and time t. The functions $D(x)$, $V(x)$ and $K(x)$ represent the unknown physical parameters for the diffusivity, convectivity and reactivity. The input consists of the unknown spatial deposition profile $P(x)$ and the known modulation signal $s(t)$. Furthermore, the *boundary* and *initial* conditions are considered to be unknown.

The goal is to simultaneously estimate $D(x)$, $V(x)$, $K(x)$ and $P(x)$ based on $s(t)$ and the measurements $y(t) = \mathrm{col}\big(T(x_1,t),\ldots,T(x_M,t)\big)$ on $M > 2$ locations.

3 Methodology

The general outline of the methodology as proposed in [1] is as follows: (i) the data obtained from the experiment is prepossessed such that noise and transients (non steady-state) contributions are removed; (ii) the infinite dimensional problem is approximated by a finite dimensional model by first taking a frequency domain approach, then linear parameterization of the unknown parameters, and finally using a finite difference as a semi-discretization; (iii) The extremum measurements are used as boundary conditions; (iv) Under the conditions that the semi-discretization grid equals the measurement grid, the commonly used output error criterion is rewritten as the equation error criterion such that the problem results in linear least squares. If the semi-discretization grid does not equal the measurement grid, one can estimate the state at the required locations, e.g. by interpolation or Gaussian process regression.

4 Results

The proposed method results in fast estimates that guarantees to be optimal for the chosen parameterization and discretization. If the parameterization of the unknown functions have sufficient freedom and the discretization grid is sufficiently dense, the true parameter values are found.

References

[1] R. J. R. van Kampen, A. Das, S. Weiland, and M. van Berkel, "A Closed-Form Solution to Estimate Spatially Varying Parameters in Heat and Mass Transport," *IEEE Control Syst. Lett.*, vol. 5, pp. 1681–1686, Nov. 2021.

Random coordinate descent algorithm for open multi-agent systems

Charles Monnoyer de Galland[1] Renato Vizuete[2,3] Julien M. Hendrickx[1] Paolo Frasca[3]
Elena Panteley[2]

[1]ICTEAM, UCLouvain, Belgium: {charles.monnoyer,julien.hendrickx}@uclouvain.be
[2]L2S CentraleSupélec, France: {renato.vizuete,elena.panteley}@l2s.centralesupelec.fr
[3]GIPSA-lab, France: paolo.frasca@gipsa-lab.fr

1 Introduction

Optimal resource allocation is an important problem in many networks, where a budget must be distributed among different agents such that each agent minimizes a local cost function. Most gradient-based distributed methods to solve this problem, such as that introduced in [1], require the computation of the full gradient at each iteration. In [2], a random coordinate descent algorithm is proposed, and requires only partial computations of that gradient. However, while those methods assume a constant composition of the system, it is expected in the real world that the agents constantly enter and leave the system. In such open systems, it is common to assume that each new agent has a different cost function, so that the location of the global minimizer changes. Optimization in open multi-agent systems was investigated for the first time in [3], where the authors studied the stability of the decentralized gradient descent where the agents try to achieve agreement.
In this work, we study the optimization of a function subject to a budget constraint in open multi-agent systems. We analyze the stability of the minimizer and the rate of convergence in expectation of the algorithm introduced in [2] when the cost functions of the agents change during the iterations.

2 Problem statement

We consider the minimization problem of the form

$$\min_{x\in\mathbb{R}^n} f(x) = \sum_{i=1}^{n} f_i(x_i) \quad \text{subject to} \quad \langle a,x\rangle = b, \qquad (1)$$

for some $b \in \mathbb{R}$ and some vector $a \in \mathbb{R}^n$, where each function $f_i : \mathbb{R} \to \mathbb{R}$ is α-strongly convex and β-smooth.To this problem we associate a network composed of n agents that each have access to a local objective function f_i and a variable $x_i \in \mathbb{R}$. Agents can exchange information according to an undirected and connected communication graph $G = (V,E)$, where $V = \{1,\dots,n\}$ and $E \subseteq V \times V$. We consider that agents can be replaced in the process, so that the local functions f_i can change in a discontinuous manner.

We analyze the stability and convergence in expectation of the Random Coordinate Descent algorithm introduced in [2], defined by the update rule (2) whenever the pair of agents $(i,j) \in E$ is randomly selected. For that purpose, we assume that for each $i \in V$, the local minimizer of f_i denoted as x_i^* is inside a ball $B(0,1)$ and $f_i(x_i^*) = 0$.

$$\begin{bmatrix} x_i^+ \\ x_j^+ \end{bmatrix} = \begin{bmatrix} x_i \\ x_j \end{bmatrix} - \frac{1}{\beta} \begin{bmatrix} 1-\frac{a_i^2}{a_i^2+a_j^2} & -\frac{a_i a_j}{a_i^2+a_j^2} \\ -\frac{a_i a_j}{a_i^2+a_j^2} & 1-\frac{a_j^2}{a_i^2+a_j^2} \end{bmatrix} \begin{bmatrix} \nabla f_i(x_i) \\ \nabla f_j(x_j) \end{bmatrix}. \qquad (2)$$

3 Results

In order to analyze the stability of the algorithm, we first characterize the location of the global minimizer:

$$\operatorname*{arg\,min}_{x:\langle a,x\rangle=b} f(x) \in B(0,R_\kappa)^n, \qquad R_\kappa := 1 + (1+\tfrac{|b|}{n})\sqrt{\kappa n}, \quad (3)$$

where $\kappa = \beta/\alpha$ is the condition number of the functions f_i. We proved linear convergence of the method for fully connected graphs. Using the result above, we aim at showing it in expectation for the open case, guaranteeing a monotonic progress towards the minimizer at every step so that:

$$\mathbb{E}\|x^+ - x^*\|^2 \le \gamma \mathbb{E}\|x - x^*\|^2, \qquad \gamma \in (0,1). \qquad (4)$$

Moreover, under some assumptions on the initial conditions, we have shown that the algorithm remains inside a ball of specific diameter for the case $n = 2$. We expect that this result can be extended for $n \ge 2$ such that the stability of the algorithm for open multi-agent systems can be derived.

4 Acknowledgements

Charles Monnoyer de Galland is a FRIA fellow (F.R.S.-FNRS). This work is supported by the "RevealFlight" ARC at UCLouvain and in part by ANR via grant HANDY, number ANR-18-CE40-0010.

References

[1] L. Xiao and S. Boyd, "Optimal scaling of a gradient method for distributed resource allocation," *Journal of optimization theory and applications*, 2006.

[2] I. Necoara, "Random coordinate descent algorithms for multi-agent convex optimization over networks," *IEEE Transactions on Automatic Control*, 2013.

[3] J. M. Hendrickx and M. G. Rabbat, "Stability of decentralized gradient descent in open multi-agent systems," in *59th IEEE Conference on Decision and Control*, IEEE, 2020.

Select controlled nodes to reduce network synchronization

Martin Moriamé
University of Namur ASBL
Rue de Bruxelles 61 - 5000 Namur
Belgium
Email: martin.moriame@unamur.be

Timoteo Carletti
University of Namur ASBL
Rue de Bruxelles 61 - 5000 Namur
Belgium
Email: timoteo.carletti@unamur.be

Abstract

In the framework of dynamical interactions between entities, synchronization-desynchronization patterns are widely studied. For instance, brain activity can be seen as a succession of synchronized and desynchronized states linking certain cerebral regions. Networks of coupled Kuramoto oscillators determine a paradigmatic model to study these patterns.

In some settings, a particular state can occur, called hypersynchronized state, which may induce system malfunctioning. For instance, some people suffer from a disorder that sometimes prevents their neurons to recover their normal activity after a synchronization period. Instead, their synchronization grows ever more strongly. These phenomena cause epilepsy seizures or uncontrollable Parkinson shakings, for example. A way to prevent such events is to perturb the dynamics to force desynchronization.

Asllani M. et al. developed a control function that avoids excessive synchronization in a Kuramoto network by acting on some of the nodes (see [1]). It simulates the effect of microelectrodes implanted in some brain region that mesure their activity and inject electrical signal to disturb it when they synchronize too much. Their model also take in account the effect of the electromagnetic field that perturbs dynamics of neighboring regions. This method has the great advantage of being minimally invasive. That is to say that it needs only a few controlled nodes, i.e. a few microelectrodes, and a low signal strength to be effective. Moreover, its order of magnitude is significative only when it's necessary.

We here examined how to select nodes (i.e. oscillators) to be controlled to decrease the invasivity of the above control method. Indeed, some nodes in a network are more influent on the global dynamics than the others. Controlling them allows us to decrease the required number of controlled nodes and signal strength while keeping the control efficiency, i.e. its ability to reduce the synchronization phenomenon (what is measured by some order parameter) by a fixed amount. In order to achieve our goal, we tried to use a new centrality measure developed by Rossel-Tarago G. and Diaz-Guilera A., i.e. the functionability (see [2]). Its aim is to find the nodes with most influence on the synchronized state of a Kuramoto system when we apply a phase shift on them. It is a particular centrality measure because it is the result of the competition of two antagonist forces: high degree and nonbetweenness. We compared the functionability-based selection of nodes with a random one as well as a degree-based method, the whole using different network topologies.

We found that in the case of networks exhibiting scale-free topology, functionability- and degree-based selections provide better results than the ones obtained using a random selection. In this kind of networks, controlling the high degree nodes, that are also the most functional nodes and are few in number, is sufficient to make the control efficient.

In the case of small-world networks, we found that functionability-based selection does not provide good results and degree-based selection only slightly improves what is obtained with random-based selection. The latter outcome can be explained by the fact that degree and random selections allow to maximize the control effect by selecting widely dispersed nodes through the network. In contrast, functionability seems to be a local property in small-world topologies. Therefore, this selection prevents the control to have a global impact.

These results can help us to enhance the control method mentioned above. In a further work, we would like to analyze network features such as rich clubs or high modularity to improve our understanding of what makes a selection method better than the others and generalize our results. Other future developments will also focus on natural frequencies associated to controlled oscillators because they seem to play a role in the control efficiency. Indeed, when there are groups of nodes with the same natural frequencies, distributing the controlled nodes evenly among these groups give rise to better results. We plan to analyze more various frequency distributions to shed new ligths on it.

References

[1] Asllani M., Expert P. and Carletti T. (2018), *A minimally invasive neurostimulation method for controlling abnormal synchronisation in the neuronal activity*, . PLoS Comput Biol 14(7): e1006296.

[2] Rossel-Tarago G. and Diaz-Guilera A., *Functionability in complex networks: Leading nodes for the transition from structural to functional networks through remote asynchronization*, Chaos **30**, 013105 (2020).

Model Predictive Control of 4th Generation District Heating Systems with Building Model and Forecasting Uncertainty[1]

Ilham Naharudinsyah
Department of Process and Energy
Delft University of Technology
Email: I.Naharudinsyah@tudelft.nl

Ivo Pothof
Department of Process and Energy
Delft University of Technology
Email: I.W.M.Pothof@tudelft.nl

Tamas Keviczky
Delft Center for Systems and Control
Delft University of Technology
Email: T.Keviczky@tudelft.nl

1 Abstract

4th generation district heating systems (DHS) are characterized by the integration of smart control approaches and renewable energy sources (RES), such as geothermal energy. As opposed to conventional heat sources with high supply temperatures, renewable energy sources tend to produce heat with lower or limited temperatures [1]. To overcome this drawback, some optimal control strategies were proposed to exploit DHS flexibility, such as thermal storage, network flexibility, and building thermal inertia [1], [2].

The plausibility of the utilization of the building thermal inertia as a source of thermal flexibility has been investigated in various works [1], [2]. However, most of the results assume the availability of the dynamical model of the building. This assumption contradicts the real-world situation, where dynamical model of the building is unavailable to the DHS authority. Therefore, a model identification measure is required to approximate the dynamical model of the building. Additionally, due to the limitation on the RES temperature, the future heat demand forecast is important to prevent undesired undersupply of heat that may jeopardize the thermal comfort in buildings. By noting that both approximate building model and demand prediction suffer from uncertainty, proper treatment of the uncertainty is necessary to ensure the reliability of the resulting optimal controller.

In this work, we present a robust model predictive control (RMPC) scheme to deal with the building model and heat forecasting uncertainty in a DHS. The RMPC framework accounts for the error or uncertainty on the model by introducing additional chance constraints to the optimization problem, yielding a robust optimization problem [3].

Firstly, we discuss the dynamical model of a small-scale DHS based on the physical description and constraints. Subsequently, we formulate a robust optimal control problem that considers the building model and forecasting uncertainties. As part of the formulation of the optimal control problem, we quantify the building model uncertainties by using the bootstrap method [4]. Meanwhile, for the forecasting uncertainty, we construct a prediction interval by adopting the strategies proposed in [5]. Finally, we transform the robust optimal control problem by utilizing the scenario approach and chance constraint approximation [3]. The last step is crucial considering that most of the available solvers cannot directly solve a robust optimization problem with chance-constraints.

In future work, we will extend the approach to handle a large-scale district heating network. We will develop a distributed version of the robust model predictive control framework to distribute the computational burden of the large-scale optimal control problem. The efficacy of the results will be demonstrated through a numerical simulation based on a real-world DHS setting.

[1]Research supported by Netherlands Enterprise Agency, Ministry of Economic Affairs and Climate Policy as part of the WarmingUP programme with grant reference TEUE819001.

References

[1] S. v. d. Zwan, I. Pothof, “Operational optimization of district heating systems with temperature limited sources,” in *Energy & Buildings*, vol.226, 2020.

[2] A. Vandermeulen, B. v. d. Heijde, L. Helsen, “Controlling district heating and cooling networks to unlock flexibility: A review,” in *Energy*, vol.151, pp. 103-115, 2018.

[3] X. Geng, L. Xie, ”Data-driven decision making in power systems with probabilistic guarantees: Theory and applications of chance-constrained optimization,” *Annual Reviews in Control*, Vol. 47, pp. 341-363 2019.

[4] S. Dean, *et. al*, ”On the sample complexity of the linear quadratic regulator,” *Foundations of Computational Mathematics*, Vol. 20, pp. 633-679, 2019.

[5] A. Khosravi, S. Nahavandi, D. Creighton, ”Quantifying uncertainties of neural network-based electricity price forecast,” *Applied Energy*, Vol. 112, pp. 120-219, 2013.

Optimal System Design for Active Vibration Isolation Systems

S.T. Spanjer, W.B.J. Hakvoort
University of Twente
s.t.spanjer@utwente.nl, w.b.j.hakvoort@utwente.nl

1 Introduction

Vibration isolation systems are used to attenuate the effects of disturbances on a sensitive payload. These disturbances can be separated into direct and indirect disturbances. Direct disturbances work directly on the sensitive payload, where indirect disturbances generate forces on the payload through the suspension. Examples of both disturbances are acoustic waves and floor vibrations respectively. In the design of vibration isolation systems with only passive elements, a clear trade-off exists between the sensitivity to these two types of disturbances. This trade-off can be circumvented by adding a control loop to the system [1].
To implement the control loop for Active Vibration Isolation Systems (AVIS) inertial motion measurements are required. Since the amplitude of the vibrations, especially on the isolated payload, are inherently small, the noise introduced by the sensors and the actuators is an important limiter of the performance of AVIS. Given the spectra of the disturbances and the noise of the used sensors, a system can be designed that minimizes the total resulting acceleration. This work considers the method and results of simultaneously optimizing the mechanical design as well as the control.

2 Method

The blockscheme that describes an AVIS system with feedback (C_{FB}) en feedforward (C_{FF}) can be seen in figure 1. P_1 and P_2 represent a typical mechanical system and are defined as

$$P_1(s) = \frac{ds+k}{ms^2+ds+k} \cdot PD(s), \quad P_2(s) = \frac{s^2}{ms^2+ds+k} \cdot PD(s), \tag{1}$$

where $PD(s)$ is the high frequency parasitic dynamics. The acceleration a_1 can be expressed in Laplace domain as

$$a_1(s) = T(s)a_0(s) + C(s)n_a(s) + S_0(s)n_0(s) + S_1(s)n_1(s), \tag{2}$$

where $T(s)$, $C(s)$, $S_0(s)$ and $S_1(s)$ are the closed loop sensitivity functions. These sensitivity functions can be obtained from the blockscheme in figure 1. The optimal design can be captured into the minimization problem

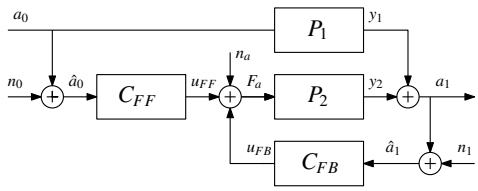

Figure 1: AVIS system. a_0 are the floor accelerations, a_1 the accelerations of the sensitive payload, n_0 and n_1 the sensor noise of the floor and the payload sensor respectively. n_a is a compound of the noise introduced by the actuators and other direct disturbances.

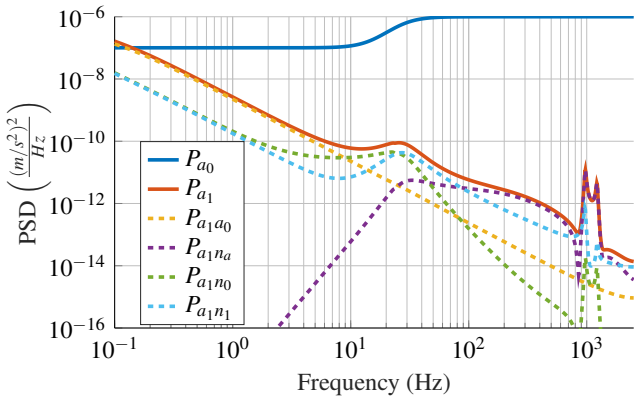

Figure 2: Power spectral densities (PSD) of a_0 (P_{a_0}) and optimized PSD of a_1 (P_{a_1}). $P_{a_1a_0}$ is the part of P_{a_1} due to a_0, etc.

$$J = \arg\min_{\boldsymbol{\theta}\in\boldsymbol{\Theta}} \int_{f_0}^{f_1} (a_1(\boldsymbol{\theta}, j2\pi f))^2 df, \tag{3}$$

where a_1 is the acceleration of the sensitive payload in the frequency band of interest, from f_0 to, f_1. $\boldsymbol{\Theta}$ is the total admissible parameter space. The parameter vector $\boldsymbol{\theta}$ can be separated into $\boldsymbol{\theta} = [\boldsymbol{\theta}_m^T, \boldsymbol{\theta}_c^T]^T$, where $\boldsymbol{\theta}_m^T$ is related to the mechanical design of the system and $\boldsymbol{\theta}_c^T$ to the control parameters.
The mechanical parameters $\boldsymbol{\theta}_m$ contains the suspension stiffness, while the optimal control parameters and structure are determined by the H_2 synthesis. The minimization is performed by alternating gradient descent based minimization to find the optimal $\boldsymbol{\theta}_m$, and H_2 synthesis for $\boldsymbol{\theta}_c$.

3 Conclusion and Result

A method for combined optimization of the control loop and the mechanical system is presented here, which yields an optimal and stable system. The resulting PSD of a_1 can be seen in figure 2. In this figure, the different contributions to the acceleration of the sensitive payload are optimally balanced.

References

[1] Beijen, M.A., Heertjes, M.F., Butler, H. and Steinbuch, M., 2017. H_∞ feedback and feedforward controller design for active vibration isolators. IFAC-PapersOnLine, 50(1), pp.13384-13389.

A Bayesian approach for efficient large-scale data representation

Clara Menzen
DCSC, TU Delft,
Mekelweg 2, 2628 CD Delft
c.m.menzen@tudelft.nl

Manon Kok
DCSC, TU Delft,
Mekelweg 2, 2628 CD Delft
m.kok-1@tudelft.nl

Kim Batselier
DCSC, TU Delft,
Mekelweg 2, 2628 CD Delft
k.batselier@tudelft.nl

An efficient representation of data

To efficiently treat large-scale data sets, we need powerful methods to store data and perform operations on it. Take, for example, a matrix of size one million times one million. On a conventional laptop, its storage already becomes problematic. But what if we could treat this large matrix with a fraction of the original complexity? One way to approximately represent a large matrix are tensor decompositions (TD). TDs exploit the correlation in data, forming an approximation with a considerably lower number of elements. Figure 1 shows the matrix mentioned above expressed as a tensor train (TT) decomposition [1]. The nodes represent small multidimensional arrays, called TT-cores, which, like train wagons, form a tensor train. The TT-cores share indices with other cores, depicted by the connected edges. The edges that stick out of the nodes are the indices that split the large number of rows and columns: Since $1,000,000$ can be factorized as $8 \cdot 8 \cdot 5 \cdot 5 \cdot 5 \cdot 5 \cdot 5$, the row and column indices have the size of those factors.

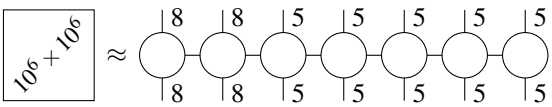

Figure 1: Depiction of a matrix of size $10^6 \times 10^6$ and its diagrammatic representation as a tensor train.

The workhorse algorithm to find a TD for a given large matrix is an iterative scheme called the alternating linear scheme (ALS). The ALS has been extensively studied and successfully applied to compute a tensor train decomposition [2]. The novelty of our approach is to solve a Bayesian inference problem to find a TT decomposition while taking inspiration from the ALS.

Bayesian inference of tensor decompositions

Solving the tensor decomposition problem in a Bayesian way has the following benefits. Prior knowledge on each of the TD components can be explicitly taken into account. Furthermore, assumptions on measurement noise are considered when deriving uncertainties of the TD components and thus the resulting tensor approximation comes with a measure of uncertainty.

As discussed in the previous section, the main players in finding a TD are its components and the large matrix that we want to represent efficiently. While taking a Bayesian perspective we treat all players as Gaussian random variables. In this way, finding a TD can be solved as a Bayesian inference problem: given the prior distributions of the TD components $p(\mathbf{g}_i)$ and the large matrix $\mathbf{y}$, the posterior distribution $p(\{\mathbf{g}_i\} \mid \mathbf{y})$ can be found by applying Bayes' rule

$$p(\{\mathbf{g}_i\} \mid \mathbf{y}) = \frac{p(\mathbf{y}|\{\mathbf{g}_i\})p(\{\mathbf{g}_i\})}{p(\mathbf{y})},$$

where $\{\mathbf{g}_i\}$ denotes the collection of all TD components. We solve the inference problem by dividing it into sub-problems where we sequentially infer the posterior distribution of one TD component at a time. To perform a tractable inference, we assume that the likelihood and prior are Gaussian and, alike in the ALS, we apply the optimization technique called block coordinate descent. Figure 2 shows the application of this method to a noisy image reconstruction problem.

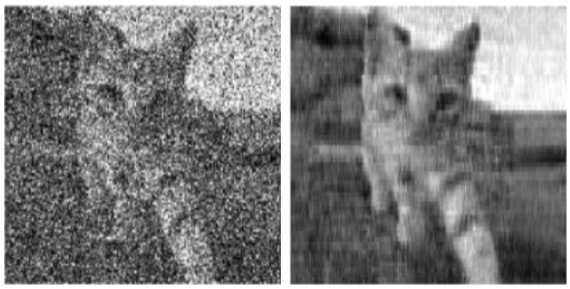

Figure 2: Noisy cat image, reconstructed image.

A more extensive treatment of this approach can be found in [3].

References

[1] I. V. Oseledets. Tensor-train decomposition. *SIAM J. Sci. Comput.*, 33(5):2295–2317, 2011.

[2] S. Holtz, T. Rohwedder, and R. Schneider. The alternating linear scheme for tensor optimization in the tensor train format. *SIAM J. Sci. Comput.*, 34, 2012.

[3] C. Menzen, M. Kok, and K. Batselier. Alternating linear scheme in a bayesian framework for low-rank tensor approximation. *arXiv:2012.11228*, 2020.

A Novel Fast SQP Method for Nonlinear Model Predictive Control

David Kiessling, Ben Hermans, Joris Gillis, and Jan Swevers
MECO Research Team, Department Mechanical Engineering, KU Leuven
DMMS-M lab, Flanders Make, Leuven, Belgium
Email: david.kiessling@kuleuven.be

1 Introduction

In industrial applications such as robotics, mechatronics, or power system control, Nonlinear Model Predictive Control (NMPC) enjoys more and more popularity, since it is capable of considering both the underlying model dynamics and additional constraints. The strategy of NMPC is to solve an optimal control problem (OCP) in each control interval. A key challenge therefore is the real-time constraint, where a possibly complicated optimization problem needs to be solved within a sampling period. Moreover, solvers need to run on resource-constrained embedded hardware.
The Direct Multiple Shooting Method gives a powerful tool to find a solution of the underlying OCP, discretizing it into a nonlinear program (NLP). NLPs of the form

$$\begin{aligned} \min_{x\in\mathbb{R}^n} \quad & f(x) \\ \text{s.t.} \quad & x_{\text{lb}} \leq x \leq x_{\text{ub}} \\ & g_{\text{lb}} \leq g(x) \leq g_{\text{ub}} \end{aligned}$$

with $f\colon \mathbb{R}^n \to \mathbb{R}$, $g\colon \mathbb{R}^n \to \mathbb{R}^m$, $x_{\text{lb}}, x_{\text{ub}} \in \mathbb{R}^n$, and $g_{\text{lb}}, g_{\text{ub}} \in \mathbb{R}^m$ are considered. The Sequential Quadratic Programming (SQP) method presented in [1] has advantageous properties for solving optimization problems exploiting the NLP problem structure. Thus, the aim of our work is to develop a new fast and efficient SQP solver providing feasible solutions and global convergence by exploiting typical properties of the NMPC context such as a feasible initial state and an extensive offline-study of the underlying NLP.

2 The Methodology

In the SQP method a trust-region technique combined with a ℓ_1 merit function in order to obtain global convergence is considered. The trust-region model subproblem has as objective the quadratic approximation of the lagrangian function $\mathscr{L}(x,\lambda)$ with lagrangian multiplier $\lambda \in \mathbb{R}^m$ and a ℓ_1 penalty term of the linearized constraints with penalty parameter $\mu > 0, \mu \in \mathbb{R}$ subject to a trust region constraint with trust-region radius $\Delta \in \mathbb{R}$ [2, chapter 18]. A non-smooth problem can be avoided by introducing slack variables $v^x, w^x \in \mathbb{R}^n$, $v^g, w^g \in \mathbb{R}^m$. At the k-th iteration this yields the following QP:

$$\begin{aligned} \min_{\substack{p,\, v^x,\, w^x \in \mathbb{R}^n \\ v^g,\, w^g \in \mathbb{R}^m}} \quad & \nabla f(x_k)^T p + \frac{1}{2} p^T \nabla^2_{xx} \mathscr{L}(x_k, \lambda_k) p \\ & + \mu \sum_{i=1}^{n} (v_i^x + w_i^x) + \mu \sum_{i=1}^{m} (v_i^g + w_i^g) \\ \text{s.t.} \quad & x_{\text{lb}} - x_k \leq p + v^x - w^x \leq x_{\text{ub}} - x_k, \\ & g_{\text{lb}} - g(x_k) \leq Dg(x_k)p + v^g - w^g \leq g_{\text{ub}} - g(x_k), \\ & 0 \leq v^x, v^g\, w^x, w^g, \\ & ||p||_\infty \leq \Delta_k. \end{aligned}$$

In order to avoid slow convergence due to the Maratos effect a Second-Order Correction mechanism is applied [2, chapter 18]. Different initialization strategies and update techniques of the trust-region radius as well as the penalty parameter are discussed, aiming at decreasing the iterations needed for converging to an optimal solution. The algorithm is tested on the overhead crane test problem.

3 Outlook

Future work will aim at finding optimal initial trust region radii for the typical OCP NLP problem structure. Smart parameter update strategies will be investigated that yield in fast deterministic convergence rates. Embracing second order information without polluting the QP subproblem with uniform regularization may lead to less needed QP steps. Therefore, different convexification techniques will be explored. The algorithm will be benchmarked on the *CUTEst* problem test set and on typical problems arising in mechatronics applications of NMPC. Finally, the algorithm will be implemented in a high-level programming language solving NLPs of mechatronics applications deterministically in a given problem sampling rate. Exploiting the specific OCP problem structure an efficient implementation with respect to memory and computational resources will be applied.

References

[1] H. G. Bock, K. J Plitt, "A multiple shooting algorithm for direct solution of optimal control problems," *Proceedings of the 9th IFAC World Congress*, 1984.

[2] J. Nocedal, S. Wright, "Numerical Optimization," Springer, 2006.

Acknowledgement: This work has been carried out within the framework of Flanders Make SBO DIRAC: DIRAC - Deterministic and Inexpensive Realizations of Advanced Control and KU Leuven Research project C14/15/067: B-spline based certificates of positivity with applications in engineering. Flanders Make is the Flemish strategic research centre for the manufacturing industry.

Automated Worst-Case Performance Analysis of Decentralized Optimization Methods

Sebastien Colla and Julien M. Hendrickx
ICTEAM, UCLouvain, 1348 Louvain-la-Neuve, Belgium.
Email: { sebastien.colla, julien.hendrickx } @uclouvain.be

1 Introduction

We develop a methodology that automatically provides nearly tight performance bounds for primal first-order decentralized optimization methods on convex functions [3].

Decentralized optimization has received an increasing attention due to its useful applications in large-scale machine learning and sensor networks, see survey [1]. In decentralized methods for separable objective functions, we consider a set of agents $\{1,\dots,N\}$, working together to minimize $f(x) = \frac{1}{N}\sum_{i=1}^{N} f_i(x)$, where f_i is the private local function held by agent i. Each agent i holds its own version x_i of the decision variable x, performs local computations and exchanges local information with its neighbors to seek to reach agreement on the minimizer x^* of the global function f. In the system, the exchanges of information often take the form of a multiplication by a given matrix $W \in \mathbb{R}^{N\times N}$, typically assumed symmetric and doubly-stochastic.

A classical way for evaluating the quality of an optimization method is to obtain worst-case guarantees regarding a chosen quality metric. Obtaining theoretical worst-case performance bounds for decentralized algorithms can often be a challenging task, requiring to combine the effects of the optimization and of the interconnection network. This can result in performance bounds that are not very tight.
In this work, we follow an alternative computational approach that finds the worst-case performance of an algorithm by solving an optimization problem, whose variables are the iterates, functions values and (sub)gradients. This is known as the performance estimation problem - PEP - and has been studied for centralized fixed step first-order methods in [2]. Current PEP theory does not allow matrix multiplications in the methods it analyzes, which are needed for representing communications in decentralized algorithms.

2 Main results

When the communication matrix W is given *a priori*, the performance estimation problem (PEP) can be directly formulated as an SDP, in the same way as presented in [2]. This formulation provides the exact worst-case performance for the given decentralized method and the specific communication matrix given *a priori*. This can be useful for trying different communication matrices and observing their impact on the performance of the algorithm. However, we would like to obtain more general results, valid over entire classes of communication matrices.

We now consider that the matrix W is not *a priori* given, but is one of the decision variables of PEP. As constraints, we impose W to belong to the commonly used set of symmetric, doubly-stochastic matrices with a given range of eigenvalues $[-\lambda,\lambda]$. We also impose this matrix W to represent the different interactions that occur in the given decentralized algorithm. We consider only algorithms in which an interaction k takes the form of a matrix-vector multiplication $y^k = Wx^k$. The vector x^k regroups the N local variables that are subject to a communication, typically the iterates x_i^k of each agent.We suppose the same matrix W is used for each interaction k, then we have $Y = WX$, where $Y = [x^k]$ and $X = [x^k]$, for $k = 1,\dots,K$.
We do not have a direct way for representing these constraints into PEP but we construct a relaxation, that is often close to tight. For that, from these constraints, we derive the following new necessary conditions involving only variables X and Y and allowing to remove W from the problem:

$$\overline{X} = \overline{Y} \qquad \text{and} \qquad Y_\perp^T Y_\perp \preceq \lambda^2 X\perp^T X\perp,$$
$$\text{with} \qquad Y_\perp = Y - \mathbf{1}\overline{Y}^T \qquad X_\perp = X - \mathbf{1}\overline{X}^T,$$

where $\overline{X}$ and $\overline{Y}$ denote the vectors with the agents average of X and Y. In short, these new constraints says the agents average is preserved during a communication, while the variance is reduced by a factor at least λ^2. See [3] for details.

We apply our new PEP formulation to the decentralized gradient descent (DGD) and obtain worst-case performance bounds that largely improve the one from [1]. For DGD, by comparing the second relaxed PEP formulation with the first exact one, it appears to be tight if we allow the communication matrix to have negative elements. See [3] for details.

Acknowledgements

S. Colla is supported by the French Community of Belgium through a FRIA fellowship (F.R.S.-FNRS).

References

[1] A. Nedić, A. Olshevsky and M. G. Rabbat, "Network Topology and Communication-Computation Tradeoffs in Decentralized Optimization,"textitProceedings of the IEEE, vol. 106, no. 5, pp. 953-976, 2018.

[2] A. B. Taylor, J. M. Hendrickx and F. Glineur, "Exact Worst-Case Performance of First-Order Methods for Composite Convex Optimization," *SIAM Journal on Optimization*, vol.27, 2015.

[3] S. Colla, J. M. Hendrickx, "Automated Worst-Case Performance Analysis of Decentralized Gradient Descent", preprint, 2021.

On the minimal and maximal smooth convex interpolating functions

Yassine Kamri, François Glineur and Julien M. Hendrickx
ICTEAM, UCLouvain, 1348 Louvain-la-Neuve, Belgium.
Email : {yassine.kamri,francois.glineur,julien.hendrickx}@uclouvain.be

1 Introduction

Given a list of points with associated function values and gradients, we consider the problem of finding an interpolating smooth convex function, where smooth is defined as

Definition 1. Given a constant $L > 0$, a differentiable function F is said to be L-smooth if and only if it satisfies :

$$\|\nabla F(x) - \nabla F(y)\| \leqslant L\|x-y\| \ \forall x, y \in \mathbf{E}.$$

Formally, the input of the interpolation problem we consider is a set of triplets {(point, gradient, function value)} :

Definition 2. A set of triplets $\{(x_i, g_i, f_i)\}_{i\in I} \in \mathbf{E}\times\mathbf{E}^*\times\mathbf{R}$ is said to be L-smooth convex interpolable if and only if there exists an L-smooth convex function F such as $F(x_i) = f_i$ and $\nabla F(x_i) = g_i \ \forall i \in I$.

Smooth convex interpolation was characterized in [1]:

Theorem 1. A set of triplets $\{(x_i, g_i, f_i)\} \in \mathbf{E}\times\mathbf{E}^*\times\mathbf{R}$; $i \in I$ is L-smooth interpolable if and only if

$$\forall i, j \in I, f_i \geqslant f_j + \langle g_j, x_i - x_j\rangle + \frac{1}{2L}\|g_i - g_j\|^2.$$

In this work, we search for extremal interpolating functions, i.e. we identify the pointwise maximal and minimal smooth convex interpolating functions. Our main result is as follows.

Theorem 2. Consider a set of triplets $\{(x_i, g_i, f_i)\}_{i\in I}$. If this set is L-smooth convex interpolable, there exist two L-smooth convex interpolating functions F_l and F_h such as any L-smooth convex function F interpolating the set $\{(x_i, g_i, f_i)\}_{i\in I}$ satisfies:

$$F_l(x) \leqslant F(x) \leqslant F_h(x) \ \forall x \in \mathbf{E}.$$

2 Extremal smooth interpolating functions

Let us consider a L-smooth convex interpolable set of triplets $\{(x_i, g_i, f_i)\}$ and an interpolating function F. It follows [1, Theorem 2] that the convex conjugate F^* of F is a $\frac{1}{L}$-strongly convex functions that interpolates the new set of triplets $\{(g_i, x_i, \langle g_i, x_i\rangle - f_i)\}$. Defining now the function $h(y) = F^*(y) - \frac{1}{2L}\|y\|^2 \ \forall y \in \mathbf{E}^*$ it follows that h is convex.

Remark 1. h is a convex interpolating function for the set $\{(g_i, x_i - \frac{1}{L}g_i, \langle g_i, x_i,\rangle - f_i - \frac{1}{2L}\|g_i\|^2)\}_{i\in I}$.

From this we reduce our initial problem to that of identifying extremal convex interpolating functions (without the smoothness requirement) [1, Theorem 4], which is given by the following

Theorem 3. If the set $\{(x_i, g_i, f_i)\}$ is interpolable by a convex function, then any convex interpolable function f satisfies $f_l(x) \leq f(x) \leq f_h(x)$ for all x where f_l and f_h are the lowest and highest interpolating functions defined by

$$f_l(x) = \max_{i\in I} f_i + \langle g_i, x - x_i\rangle.$$

$$f_h(x) = \min_{\lambda_i \geqslant 0} \sum_{i\in I} \lambda_i f_i \text{ s.t } \sum_{i\in I}\lambda_i = 1 \text{ and } x = \sum_{i\in I}\lambda_i x_i.$$

Using Remark 1 and Theorem 3, we can find two convex functions h_l and h_h interpolating the set $\{(g_i, x_i - \frac{1}{L}g_i, \langle g_i, x_i,\rangle - f_i - \frac{1}{2L}\|g_i\|^2)\}_{i\in I}$ and such that $h_l(y) \leqslant h(y) \leqslant h_h(y)$ for all $y \in \mathbf{E}^*$. Observe now that F can be recovered by h with $F = (h + \frac{1}{2L}\|y\|^2)^*$. Since this is based on two order-preserving/reversing transformations we can construct from h_l and h_h two extremal L-smooth convex functions F_l,F_h that are guaranteed to bound F:

$$F_h(x) = \sup_{y\in\mathbf{E}^*} \langle y, x\rangle - h_l(y) - \frac{1}{2L}\|y\|^2,$$

$$F_l(x) = \sup_{y\in\mathbf{E}^*} \langle y, x\rangle - h_h(y) - \frac{1}{2L}\|y\|^2.$$

3 Special case : One-dimensional functions

Let us now consider the special case of one-dimensional functions $\mathbf{E} = \mathbf{E}^* = \mathbb{R}$. Assume without loss of generality that points x_i $i \in I$ are ordered such that $x_i \leqslant x_{i+1}$ for all $i \in I$. Using this fact, we find simplified expressions for the bounding functions of Theorem 3 and derive from that closed-form expressions for F_h and F_l.

4 Conclusion and Perspectives

We prove the existence and give explicit expressions for the pointwise maximal and minimal L-smooth convex functions interpolating a given set of triplets. Future work will be devoted to the search for simplified expressions in higher dimensions.

Y. Kamri is supported by the European Union's MARIE SKŁODOWSKA-CURIE Actions Innovative Training Network (ITN)-ID 861137, TraDE-OPT

References

[1] A.B. Taylor, J.M. Hendrickx, F. Glineur *Smooth strongly convex interpolation and exact worst-case performance of first-order methods*. Mathematical Programming , 2017.

3D-printed Flexible Piezoresistive Sensors-based Source Seeking Control of Unicycle Robots

Tinghua Li [1] t.li@rug.nl
Bayu Jayawardhana[1] b.jayawardhana@rug.nl
Amar Kamat[2] a.m.kamat@rug.nl
Ajay Giri Prakash Kottapalli[2] a.g.p.kottapalli@rug.nl

[1] DTPA, [2] APE, ENTEG, Faculty of Science and Engineering, University of Groningen, The Netherlands

1 Abstract

This work proposes source seeking control algorithms for a unicycle mobile robot which is equipped with novel 3D printed flexible graphene-based piezoresistive airflow sensors and validates the same through numerical simulations and experiments. Without the knowledge of robot's position, we propose and analyze a projected gradient ascent algorithm solely based on a local gradient measurement from the airflow sensors. The Extremum-Seeking Control is also combined with our proposed algorithm in case of partial sensor failure. For both of the control laws, we have proved the asymptotic convergence of the robot to the source. The accompanying video of the experimental results is publicly accessible at https://youtu.be/y3OoRu5GX3M.

2 Problem Formulation and Control Design

For our source-seeking control problem, we consider a source that emits (laminar) air flow on the 2D plane whose strength decays with distance to the source. Let the potential function $J(z_1,z_2)$ define the magnitude of the air flow which has a global maximum at the source location (z_1^*,z_2^*). Furthermore, we consider the robot setup where it is able to measure the local gradient of J, denoted by $\nabla J(z_1,z_2)$, using our 3D-printed graphene-based piezoresistive sensors [1]. The robot can drive forward with a longitudinal velocity u and rotate with an angular velocity ω.

Using the unit vector orientation of mobile robot $\vec{v}(\theta)$, the local gradient ∇J and its orthogonal vector $\nabla^{\perp}J$, the proposed projected gradient-ascent control laws for u and ω are given by

$$\begin{aligned} u &= k_1 \langle \vec{v}(\theta), \nabla J(z_1,z_2)\rangle \\ \omega &= -k_2 \left\langle \vec{v}(\theta), \nabla^{\perp} J(z_1,z_2)\right\rangle, \end{aligned} \tag{1}$$

where $k_1>0$ and $k_2>0$ are the longitudinal velocity gain and angular velocity gain, respectively. The closed-loop systems dynamics is given by

$$\begin{bmatrix}\dot{z}_1\\ \dot{z}_2\\ \dot{\theta}\end{bmatrix} = \begin{bmatrix} k_1 \langle \vec{v}(\theta), \nabla J(z_1,z_2)\rangle \vec{v}(\theta) \\ -k_2 \left\langle \vec{v}(\theta), \nabla^{\perp} J(z_1,z_2)\right\rangle \end{bmatrix}. \tag{2}$$

Assume that the potential function J is twice-differentiable, radially unbounded and is a strictly concave function with a maximum at $\begin{bmatrix}z_1^*\\ z_2^*\end{bmatrix}$. Then for any positive gains $k_1,k_2>0$, the control law (1) solves the gradient-based source-seeking control problem globally.

Similarly, consider the unicycle system and assume that the potential function J is quadratic function given by

$$J(z_1,z_2) = J^* - c_1(z_1-z_1^*)^2 - c_2(z_2-z_2^*)^2 \tag{3}$$

where J^* is the local maximum, c_1,c_2 are unknown positive constants and $\begin{bmatrix}z_1^*\\ z_2^*\end{bmatrix}$ is the global maximizer. The extremum seeking control based approximated gradient of potential function J is given by

$$\frac{\partial \hat{J}}{\partial z_1} := J_{z1} = C_{z_1}\Delta\sin(\omega_0 t) + a\omega_0\cos(\omega_0 t), \tag{4}$$

$$\frac{\partial \hat{J}}{\partial z_2} := J_{z2} = -C_{z_2}\Delta\cos(\omega_0 t) + a\omega_0\sin(\omega_0 t). \tag{5}$$

Then, for any positive gains $k_1,k_2,C_{z1},C_{z2},a>0$ and sufficiently large ω_0, the ESC-based projected gradient-ascent control law with $\widehat{\nabla J}$ and $\widehat{\nabla J}^{\perp}$ guarantees that the average trajectories $\begin{bmatrix}z_{1,\text{avg}}\\ z_{2,\text{avg}}\end{bmatrix}$ are bounded and $\lim_{t\to\infty}\left\|\begin{bmatrix}z_{1,\text{avg}}(t)-z_1^*\\ z_{2,\text{avg}}(t)-z_2^*\end{bmatrix}\right\| = 0$ holds for all initial conditions in the neighborhood of $\begin{bmatrix}z_1^*\\ z_2^*\end{bmatrix}$.

3 Main Results

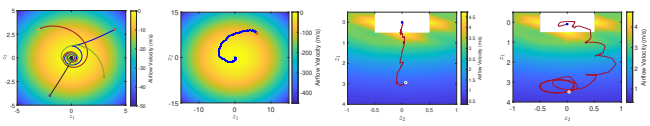

(a) Simulation-1 (b) Simulation-2 (c) Experiment-1 (d) Experiment-2

Figure 1: Simulation and experiment results of the closed-loop system with (a)/(c).the projected gradient-ascent control law, and (b)/(d). the ESC-based control law.

References

[1] A.M. Kamat, X. Zheng, B. Jayawardhana, A.G.P. Kottapalli, "Bioinspired PDMS-graphene cantilever flow sensors using 3D printing and replica moulding," *Nanotechnology*, vol. 32, no. 9, pp. 095501, 2021.

Digital Control of High Frequency Switched Power Amplifiers

Duo Xu and Mircea Lazar
Control Systems Group, Eindhoven University of Technology
The Netherlands
Email: {d.xu, m.lazar}@tue.nl

1 Introduction

In semiconductor manufacturing, the high precision fast moving stages are utilized to achieve the accurate positioning of wafers. Power amplifiers play an important role in actuating the current reference signal. Thus the error and bandwidth limitation of the output current produced by the amplifier can influence the stationary and dynamic positioning accuracy of the moving stage system.

2 Problem description

In this work, the impact of the power amplifier on the position accuracy of the motion system is analyzed. The outline of this system is described in Figure 1. It consists of the external position control loop and the internal current control loop, where each control loop is designed separately [1].

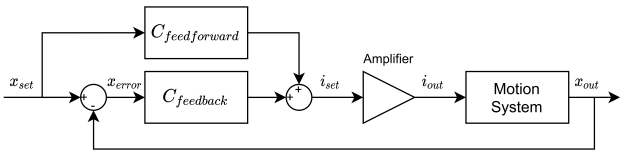

Figure 1: Outline of the position control system.

Figure 2 presents a short stroke power amplifier topology, where the output current i_o is used to actuate the motor [2]. It has four operation modes in total with respect to the switching states (S_1, S_2, S_3, S_4). The averaged dynamic model of the power amplifier is derived for controller design.

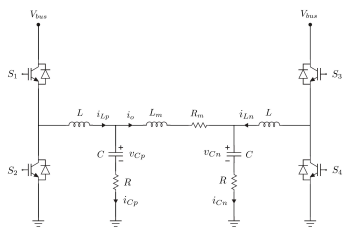

Figure 2: Schematic of a short stroke power amplifier.

The design objective of the power amplifier current control can be divided into two steps. Firstly, the evaluation of the current controller performance is carried out in terms of response speed, reference error and bandwidth; also real-time requirements are evaluated. Second is to analyze the impact of the current controlled amplifier on position accuracy. There are two critical aspects to characterize the position error: moving average (MA) and moving standard deviation (MSD), which they reflect the low-frequency and high-frequency position error respectively.

3 Approach

For the current control of the amplifier, two loops are designed. An inner loop based on an LQR controller is designed to improve bandwidth. Then, an outer loop based on a frequency loop shaping controller is designed to achieve frequency specifications. Figure 3 shows the simulation result of the current control loop. The position error under this configuration are MA=779 pm and MSD=1740 pm, which is an improvement compared to an existing industrial controller.

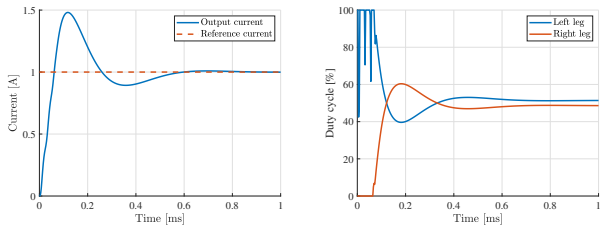

Figure 3: (a) Amplifier step response (b) Duty cycles.

4 Outlook

For future work more advanced constrained control techniques will be investigated such as control invariant sets and MPC, which effectively take into account constraints. Also, since the structure of the power amplifier topology is symmetrical, a reduced order model can be introduced to reduce the computation time.

References

[1] S. J. Settels, J. van Duivenbode and J. L. Duarte, "Impact of amplifier errors on position loop accuracy of high-precision moving stages," 19th European Conference on Power Electronics and Applications, Warsaw, 2017, pp. P.1-P.10.

[2] T.T. Nguyen, "State-Feedback Controller Design for Short Stroke and Long Stroke Power Amplifiers" MSc Internship, Eindhoven University of Technology, 2012.

Modelling Geometrically Nonlinear Flexure Mechanisms With Piezoelectric Vibration Damping

B. Seinhorst, W.B.J. Hakvoort
Department of Mechanics of Solids, Surfaces and Systems (MS3), University of Twente
P.O. Box 217, 7500 AE Enschede, The Netherlands
{b.seinhorst/w.b.j.hakvoort}@utwente.nl

1 Introduction

Flexure mechanisms are widely used in the industry when high accuracy and repeatability are required. However, the lack of friction or any other form of damping results in undamped parasitic dynamics, which can result in high transmissions of vibrations and difficulties with controller design. Traditional damping methods using viscous material can be difficult to implement and introduce unwanted behaviour such as creep and hysteresis. Alternatively, piezoelectric patches can be placed strategically on such flexure mechanisms. Damping can then be added to the mechanism by using the patches to actively suppress the vibrations, or by using passive shunt circuitry to dissipate energy.

2 Large deflection modelling

A variety of linear beam elements with piezoelectric layers is available, several simple models are given in [1]. This leads to a typical linear beam constitutive equations, relating beam strain, curvature and voltage to applied forces, moments and charge.
Similar to the method presented in [2], the linear beam constitutive equations can be used to formulate a geometrically nonlinear beam element with piezoelectric interaction. This element has been implemented in the multibody software SPACAR, which can be used to simulate transient responses of controlled flexure mechanisms. Furthermore, it can also be used to determine the frequency response of mechanisms in the deflected state.

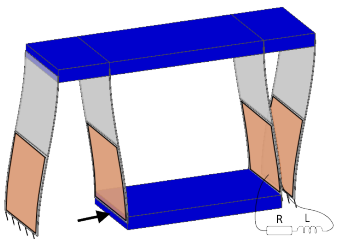

Figure 1: A double parallelogram flexure where voltages can be applied to the piezoelectric patches on the surface of the leaf springs. Force is applied and deformation is measured at the location of the black arrow. Each of the orange piezoelectric patches is attached to the surface of the leaf spring and is shunted with an RL-circuit.

3 Piezoelectric shunting

A double parallelogram flexure, as depicted in Figure 1, is considered. Piezoelectric patches are applied to the bottom half of the flexures and shunted with RL-cirucits. An RL-circuit in series with a piezoelectric patch forms an electric resonance circuit due to the inherent capacitance of the piezoelectric patch. At this resonance frequency mechanical energy is converted to the electric domain and dissipated there. In this case the resistances (R) and inductances (L) have been chosen to suppress resonance of the upper body. The frequency response of the shunted mechanism in the nominal and deflected position is shown in Figure 2. The frequency of the internal mode changes when the mechanism is deflected, making the piezoelectric shunting less effective.
The implemented geometrically nonlinear beam element allows investigation of piezoelectric damping in large stroke flexure mechanisms. This framework will be used for future investigation into alternative control techniques that will be able to robustly reject parasitic dynamics under large deflection.

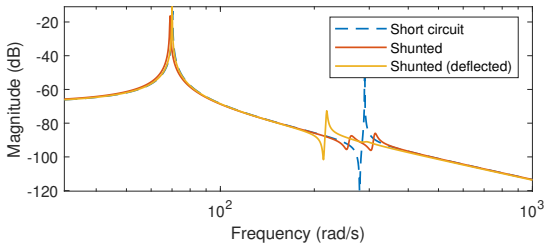

Figure 2: Frequency response function from applied force to displacement of the mechanism in actuation direction, for the nominal and deflected state.

References

[1] L. Luschi, G. Iannaccone, and F. Pieri, "A critical review of reduced one-dimensional beam models of piezoelectric composite beams," *Journal of Intelligent Material Systems and Structures*, vol. 30, no. 8, pp. 1148–1162, 2019.

[2] J. B. Jonker and J. P. Meijaard, "A geometrically nonlinear formulation of a three-dimensional beam element for solving large deflection multibody system problems," *International Journal of Non-Linear Mechanics*, vol. 53, pp. 63–74, 2013.

Hybrid Model-Data Approach for Machine Level FDI

Farhad Ghanipoor[1], Carlos Murguia[1], Nathan van de Wouw[1,2], Peyman Mohajerin Esfahani[3]
[1]Department of Mechanical Engineering, Eindhoven University of Technology, Eindhoven, The Netherlands
[2]Department of Civil, Environmental and Geo-Engineering, University of Minnesota, Minneapolis, MN, USA
[3]Delft Center for Systems and Control, Delft University of Technology, Delft, The Netherlands
Emails: {f.ghanipoor, C.G.Murguia, N.v.d.Wouw}@tue.nl
P.MohajerinEsfahani@tudelft.nl

1 Introduction

The reliable functioning of high-tech systems can only be achieved through predictive maintenance, for which techniques for fault detection (is a fault occurring?) and fault isolation (what is the fault source?) are key prerequisites.
There are two main approaches for fault diagnosis: 1. Hardware redundancy; and 2. Analytical redundancy. In hardware redundancy, the idea is to use various devices to compare duplicated signals with the same source. The analytical redundancy approach uses a software scheme for modeling the system and an estimation technique for Fault Detection and Isolation (FDI). Although this approach is challenging due to the need to ensure robustness against model uncertainties, noise, and disturbances (perturbations), it is more cost-efficient than hardware redundancy [2].
The software scheme can be model-based, or data-driven [1]. We refer to model-based methods when the model comes from first principles (physics-based models). On the other hand, in data-driven strategies, the model can come from AI algorithms or any other technique that uses data without considering a physics-based model. Neither of the model-based and data-driven approaches is suitable to guarantee accurate fault detection for complex systems operating in uncertain and changing environments.
In this project (within the Digital Twin Program), we aim to develop hybrid (physics-AI) FDI schemes that provide superior monitoring performance by combining the strengths of the current model-based and data-driven schemes.

2 Challenges and Research Goals

The challenges of this project include:

- How to achieve robustness of hybrid (physics-AI) FDI schemes against perturbations.
- How to cope with data shortage from the real system for training of data-driven methods.
- How to guarantee the adaptation of the schemes against changes in the system over time.

The project research goals will address these challenges and implement the developed FDI schemes on actual industrial use cases.

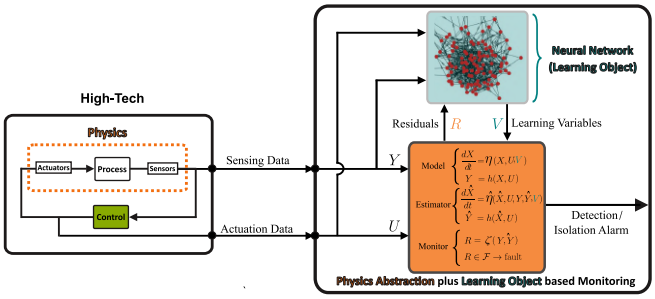

Figure 1: Physics abstraction plus learning object-based monitoring.

3 Research Approach

For developing hybrid physics-AI schemes, three different variants of hybrid (physics-AI) FDI schemes are envisioned:

1. Physics Abstraction plus Learning Object-based Monitoring (hybrid #1)
   The base method is model-based and the learning object is used to learn unknown dynamics (e.g., uncertainties in the model) and for decision making to improve robustness against perturbations (see Fig. 1).
2. Physics Guided/Constrained Data-Driven Monitoring (hybrid #2)
   The base method is data-driven and the first principles model or any other digital twin can generate artificial data for training of the data-driven method.
3. Hybrid of aforementioned variants (hybrid #3)
   A more accurate learning object based on hybrid #2 can be used in hybrid #1.

References

[1] Rahat Iqbal et al. Fault detection and isolation in industrial processes using deep learning approaches. *IEEE Transactions on Industrial Informatics*, 15(5):3077–3084, 2019.

[2] Xiaodong Zhang, Marios M. Polycarpou, and Thomas Parisini. A robust detection and isolation scheme for abrupt and incipient faults in nonlinear systems. *IEEE Transactions on Automatic Control*, 47(4):576–593, 2002.

Kernel-based learning control for iteration-varying tasks applied to a printer with friction[1]

Maurice Poot [2,*], Jim Portegies [3], Tom Oomen [2]

[2]Control Systems Technology Group, Dept. of Mechanical Engineering, Eindhoven University of Technology, The Netherlands

[3]CASA, Dept. of Mathematics and Computer Science, Eindhoven University of Technology, The Netherlands. *Email: m.m.poot@tue.nl

1 Background

Feedforward control is essential in mechatronic systems that perform varying motion tasks with extreme accuracy requirements. In [1, 2], iterative learning control with polynomial basis functions (ILCBF) is introduced to enable extrapolation of the motion tasks. However, polynomial parameterizations are limited in describing flexible system dynamics, hence do not meet the performance requirements. In [3], identification of inverse non-causal LTI systems using kernels [4] is addressed. However, extensions to nonlinear elements and closed-loop systems are not straightforward.

2 Problem formulation

Although developments have been made in iterative learning control for general tasks, at present the use of kernel-based approaches has not been exploited yet. The aim of this research is to develop a kernel-based approach to ILC, and present a specific approach for non-causal and nonlinear basis functions arising in motion feedforward control.

3 Approach

The developed kernel-based ILC (KILC) approach exploits the use of non-causal kernels to regularize the non-causal impulse response parameters and learns these simultaneously with prescribed nonlinear basis functions in closed-loop. Prior knowledge about the system is added through a developed kernel design approach, which enforces model complexity and non-causality to deal with NMP systems.

4 Results

Initial results for positioning of a consumer printer subject to nonlinear friction demonstrate the superior performance of KILC with 201 non-causal impulse response parameters and a non-causal OBF kernel compared to ILCBF with only acceleration as basis. Both methods also have a nonlinear Coulomb friction component. In Fig. 1, the time-domain error and feedforward signals are presented. The results show that KILC automatically identifies impulse response parameters to compensate higher-order dynamics, e.g., the snap parameter.

[1]This work is supported by ASM Pacific Technology. The authors thank Dragan Kostić and Robin van Es for their contributions to this research.

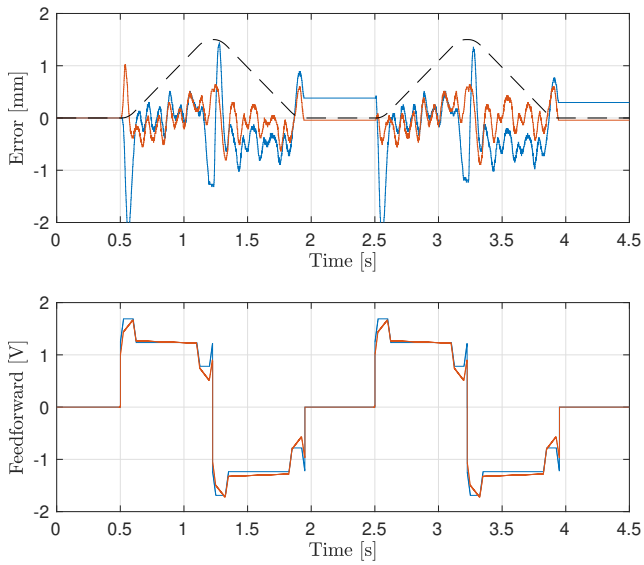

Figure 1: Time-domain error and feedforward signals for the scaled reference (- -) of both ILCBF (—) and KILC using an OBF kernel (—).

5 Conclusion and outlook

The presented KILC framework enables accurate control for a class of non-causal and nonlinear systems. Performance improvements are most prominent for systems with NMP and higher order dynamics. Ongoing research focuses on application to MIMO systems, selecting nonlinear basis functions derived from rigid-body modeling, and modeling position-dependency of the feedforward parameters.

References

[1] D. Bristow, M. Tharayil, and A. Alleyne, "A survey of iterative learning," *EEE Control Syst. Mag.*, vol. 26, no. 3, pp. 96–114, 2006.

[2] J. Van De Wijdeven and O. H. Bosgra, "Using basis functions in iterative learning control: Analysis and design theory," *Int. J. Control*, vol. 83, no. 4, pp. 661–675, 2010.

[3] L. Blanken and T. Oomen, "Kernel-based identification of non-causal systems with application to inverse model control," *Automatica*, vol. 114, p. 108830, apr 2020.

[4] C. Rasmussen and K. Williams, *Gaussian Processes for Machine Learning*. MIT Press, 2006.

Finite Horizon Privacy of Stochastic Dynamical Systems: A Synthesis Framework for Gaussian Mechanisms

Haleh Hayati[1], Carlos Murguia[2], Nathan van de Wouw[3]
Department of Mechanical Engineering, Eindhoven University of Technology
Emails: [1]h.hayati@tue.nl, [2]c.g.murguia@tue.nl, [3]n.v.d.wouw@tue.nl

1 Abstract

We address the problem of synthesizing distorting mechanisms that maximize privacy of stochastic dynamical systems. Information about the system state is obtained through sensor measurements and driving inputs. This data is transmitted to a remote station through an unsecured communication network. We aim to keep part of the system state private (a private output); however, because the network is unsecured, adversaries might access sensor data and inputs, which can be used to estimate private outputs. To prevent an accurate estimation, we pass data through some distorting mechanisms (privacy-preserving mechanisms) before transmission, and send the distorted data to the trusted user. These mechanisms consist of a coordinate transformation and additive dependent Gaussian vectors. We cast the synthesis of the mechanisms as a convex program, where we minimize an information-theoretic metric (our privacy metric) between an arbitrarily large sequence of private outputs and the disclosed distorted data for desired distortion levels.

2 Problem Formulation

We consider stochastic systems of the form:

$$\begin{cases} X(k+1) = AX(k) + BU(k) + T(k), \\ Y(k) = CX(k) + W(k), \\ S(k) = DX(k), \end{cases} \tag{1}$$

where $X \in \mathbb{R}^{n_x}$, $Y \in \mathbb{R}^{n_y}$, $U \in \mathbb{R}^{n_u}$, and $S \in \mathbb{R}^{n_s}$, are state, output, reference signal, and private output, respectively. The initial state $X(1)$, the state perturbation T, and the output perturbation W are mutually independent multivariate gaussian processes.

We aim to prevent adversaries from estimating the stacked private output S^K, accurately. To this end, we randomize stacked measurements Y^K and stacked inputs U^K before transmission, and send the corrupted data to the remote station instead. The randomized vectors $Z(k)$ and $R(k)$ are constructed as $Z(k) = GY(k) + V(k)$ and $R(k) = U(k) + H(k)$, respectively, with matrix $G \in \mathbb{R}^{n_y \times n_y}$ and additive random vectors $V(k)$ and $H(k)$. Vectors $V(k)$ and $H(k)$ are multivariate dependent Gaussian processes with $V(k) \sim \mathcal{N}[\mathbf{0}, \Sigma^V(k)]$ and $H(k) \sim \mathcal{N}[\mathbf{0}, \Sigma^H(k)]$. The randomized vectors $Z(k)$ and $H(k)$ are transmitted over an unsecured communication network to a remote station, see Figure 1.

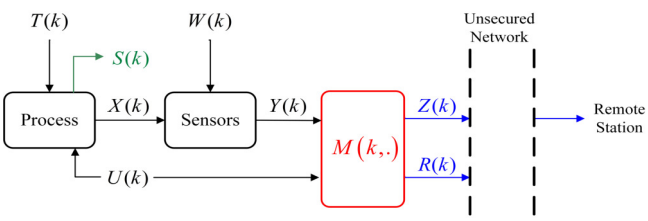

Figure 1: System configuration.

Note, however, that we do not want to make (Y^K, U^K) and (Z^K, R^K) overly different. Hence, we need to consider the *trade-off between privacy and distortion*. As distortion metric, we use the weighted mean squared errors between the original and distorted data, i.e., $E[||W_Y(Z^K - Y^K)||^2]$ and $E[||W_U(R^K - U^K)||^2]$, for some given weighting matrices. As privacy metric, we propose the mutual information between private and disclosed data, $I[S^K; Z^K]$, and the negative differential entropy of the input error, $h[U^K - R^K] = h[H^K]$, as $I[S^K; Z^K] - h[H^K]$. So, we aim at minimizing $I[S^K; Z^K] - h[H^K]$ subject to the weighted second moment constraints $E[||W_Y(Z^K - Y^K)||^2] \leq \epsilon_Y$ and $E[||W_U(R^K - U^K)||^2] \leq \epsilon_U$, for some desired distortion levels ϵ_Y and $\epsilon_U \in \mathbb{R}^+$ and weights $W_Y \in \mathbb{R}^{n_y \times n_y}$ and $W_U \in \mathbb{R}^{n_u \times n_u}$, by designing the mapping variables, that is

$$\begin{cases} \min\limits_{G(k), \Sigma^V(k), \Sigma^H(k), k \in \mathcal{K}} I[S^K; Z^K] - h[H^K], \\ \text{s.t.} \begin{cases} E[||W_Y(Z^K - Y^K)||^2] \leq \epsilon_Y, \\ E[||W_U(R^K - U^K)||^2] \leq \epsilon_U \end{cases} \end{cases} \tag{2}$$

3 Problem Solution

To minimize $I[S^K; Z^K] - h[H^K]$, we write the cost and constraints in terms of our design variables. We prove that the cost $I[Z^K; S^K] - h[H^K]$ and constraints $E[||W_Y(Z^K - Y^K)||^2]$ and $E[||W_U(R^K - U^K)||^2]$ are convex functions of stacked design variables $\tilde{\Sigma}^V$, $\tilde{G}$, and $\tilde{\Sigma}^H$. Hence, we can use of-the-shelf optimization algorithms to find the design variables that minimize $I[Z^K; S^K] - h[H^K]$ subject to the distortion constraints.

Structure-preserving model reduction of interconnected systems

Lars Janssen
Eindhoven University of Technology*
Email: l.a.l.janssen@tue.nl

Rob Fey
Eindhoven University of Technology*
Email: r.h.b.fey@tue.nl

Bart Besselink
University of Groningen†
Email: b.besselink@rug.nl

Nathan van de Wouw
Eindhoven University of Technology*
Email: n.v.d.wouw@tue.nl

1 Introduction

Many complex models of (multi-)physical systems are naturally based on an interconnection of subsystems. These dynamics models of interconnected systems often have high order, which makes analysis computationally expensive or unfeasible. This motivates the need for model order reduction (MOR) techniques. For such interconnected systems, we aim to capture the dynamics in a model that preserves the topology of the system such that we can understand the influence of individual subsystems on this system. This work introduces a potential method that can 1) evaluate the contribution of errors introduced by individual subsystem reduction to the overall model accuracy, and 2) uses this knowledge to determine a model accuracy specification distribution for the individual subsystems guaranteeing a certain overall system accuracy and which, in turn, allows for an overall reduction of model complexity.

2 Problem statement

In this work, we study systems of k interconnected linear time-invariant (LTI) subsystems $G = \mathrm{diag}(G_1, \ldots, G_k)$ with input $v = \begin{bmatrix} v_1^T & \cdots & v_k^T \end{bmatrix}^T$ and output $z = \begin{bmatrix} z_1^T & \cdots & z_k^T \end{bmatrix}^T$. The subsystems are interconnected via matrix K. The external inputs u and outputs y are connected to the subsystems via external input and output matrix L and M, respectively. The complete interconnected system G_c is then given by

$$G_c = MG(I - KG)^{-1}L \tag{1}$$

and represented as block-diagram in Figure 1. Structure-preserving MOR computes a reduced-order model (ROM) $\hat{G}_c$ while preserving the interconnection topology of the system G_c. This can be achieved by computing ROMs for the individual subsystems $\hat{G} = \mathrm{diag}(\hat{G}_1, \ldots, \hat{G}_k)$ [1]. These reduced-order subsystems can be interconnected to find a structure-preserved, reduced-order interconnected system $\hat{G}_c$ given by

$$\hat{G}_c = M\hat{G}(I - K\hat{G})^{-1}L \tag{2}$$

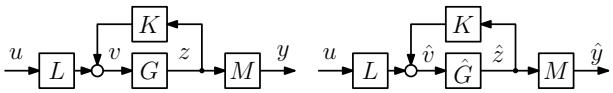

Figure 1: Block-diagram representation of the system G_c (left) and structure-preserved ROM $\hat{G}_c$ (right).

and also represented as block-diagram in Figure 1. In order to determine the contribution of approximation errors of individual subsystems to the complete interconnected system, we seek to find the relation between the error dynamics $E_j := G_j - \hat{G}_j$ and the error dynamics $E_c := G_c - \hat{G}_c$ of the interconnected system. For the given class of interconnected systems, this relation is far from trivial.

3 Proposed approach

Robust control is a field of study that has been dealing with system uncertainties. We can model our subsystem error dynamics E_j as an additive uncertainty to our subsystem G_j. By modeling the error dynamics as $\mathcal{H}_\infty$-norm bounded uncertain systems, we can use a powerful tool, μ-analysis, to compute the L_2-gain bounds on uncertain systems [2]. We then aim to find the relation between such bounds w_j on the subsystem error dynamics

$$\|E_j\|_\infty \leq w_j, \; j = 1, \ldots, k, \tag{3}$$

and a bound w_c on the interconnected system error dynamics

$$\|E_c\|_\infty \leq w_c. \tag{4}$$

Efficient methods to find this relation could lead to the ability to evaluate the propagation of subsystem accuracy to overall model accuracy (a bottom-up approach). Applying this evaluation could then lead to methods to determine accuracy specifications for subsystems that leads to the best overall model accuracy (a top-down approach).

References

[1] Sandberg, H., & Murray, R. M. (2009). Model reduction of interconnected linear systems. Optimal Control Applications and Methods, 30(3), 225-245.

[2] Packard, A., & Doyle, J. (1993). The complex structured singular value. Automatica, 29(1), 71-109.

*Dynamics and Control, Mechanical Engineering, Eindhoven University of Technology, P.O. Box 513, 5600 MB Eindhoven, The Netherlands

†Bernoulli Institute for Mathematics, Computer Science and Artificial Intelligence, University of Groningen, P.O. Box 407, 9700 AK Groningen, The Netherlands

Transfer-based Model Reduction in Structural Dynamics

Luuk Poort
Eindhoven University of Technology*
l.poort@tue.nl

Rob Fey
Eindhoven University of Technology*
r.h.b.fey@tue.nl

Bart Besselink
University of Groningen†
b.besselink@rug.nl

Nathan van de Wouw
Eindhoven University of Technology*
n.v.d.wouw@tue.nl

1 Introduction

To evaluate the dynamics of mechanical systems of interconnected substructures, often large Finite Element models are constructed. To make these models computationally tractable, model reduction (MR) is used to reduce the order of the model, while remaining as accurate as possible. MR for structural systems is usually performed using component mode synthesis (CMS) methods, which give no quantification on the response reduction error. To make sure the approximation is accurate enough, industry typically under-reduces, thus resulting in an unnecessarily large reduced model.

2 Problem statement

This work treats the reduction of k interconnected structural models Σ_j, of the form

$$\Sigma_j : \begin{cases} M_j\ddot{q}_j(t) + L_j\dot{q}_j(t) + K_j q_j(t) = B_j v_j(t), \\ z_j(t) = C_{2,j}\dot{q}_j(t) + C_{1,j} q_j(t) + D_j v_j(t), \end{cases} \tag{1}$$

where q_j, v_j and z_j indicate the degrees of freedom, the input and the output vectors of substructure j, and M_j, L_j and K_j indicate its mass, damping and stiffness matrices, respectively. Input, output and direct feedthrough are described by matrices B_j, $C_{1,j}$, $C_{2,j}$ and D_j.

These substructure models Σ_j are subsequently coupled using connection matrices H, S and R, according to Figure 1. To allow coupling, let us define the system $\Sigma = \mathrm{diag}(\Sigma_1, \ldots, \Sigma_k)$, with inputs $v = [v_1^T, \ldots, v_k^T]^T$ and outputs $z = [z_1^T, \ldots, z_k^T]^T$. The coupled system Σ_c can then be defined, with inputs u and outputs y. We denote the transfer function (TF) representation of system Σ as $G(s)$, of the coupled system Σ_c as $G_c(s)$ and of the subsystems as $G_j(s)$.

Model reduction aims to reduce the coupled system Σ_c of order n to the reduced system $\hat{\Sigma}_c$ of order r, with $r << n$ and without significant loss of accuracy. For computationally efficient reduction, one first reduces the subsystems Σ_j to $\hat{\Sigma}_j$, before coupling the reduced subsystems to form $\hat{\Sigma}_c$. This also results in approximate TF, indicated with a hat operator.

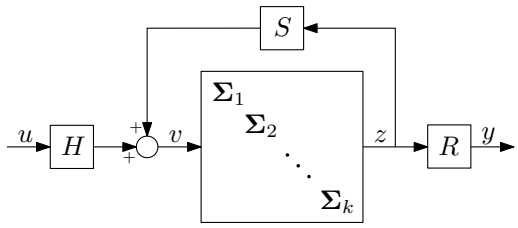

Figure 1: Block-diagram of the interconnected system

The goal of this research is to produce a reduction method that

- provides a measure of the reduction error $\mathscr{M}(G, \hat{G})$ in terms of the TF,
- allows physical interpretation of modes,
- results in accurately reduced substructure and coupled TF, s.t. $\mathscr{M}_i(G_i, \hat{G}_i) \leq \varepsilon_i \; \forall \, i = 1, \ldots, k, c$.

Conventional methods can be roughly divided into CMS, Krylov and Gramian based methods. For CMS methods, the link to a transfer-based accuracy measure is not easily made, whereas Krylov and Gramian based methods usually do not allow the evaluation of deformation shapes, as the second-order structure of (1) is not retained. A new approach is therefore required.

3 Preliminary results and outlook

Applicability of various error measures is discussed with industrial partner ASML. Additionally, literature and numerical study has been performed to evaluate availability and relevance of error measures and reduction methods. Without going into detail, let us mention several optional approaches:

- A CMS method with mode selection based on frequency response approximation.
- Frequency-weighted balanced truncation, based on Power Spectral Density (PSD) information of input and error signals.
- Structure preserving Krylov methods, with additional weighting to improve the accuracy in assembly.

*Dynamics and Control, Mechanical Engineering, Eindhoven University of Technology, P.O. Box 513, 5600 MB Eindhoven, The Netherlands
†Bernoulli Institute for Mathematics, Computer Science and Artificial-Intelligence, University of Groningen, P.O. Box 407, 9700 AK Groningen, The Netherlands

Modeling and Identification of Multirotor Drone Dynamics for Onboard MPC Motion Planning

Mathias Bos, Jan Swevers, Goele Pipeleers
MECO Research Team, Dept. of Mechanical Engineering, KU Leuven, BE-3001 Heverlee
DMMS-M core lab, Flanders Make, BE-3001 Heverlee
Email: firstname.lastname@kuleuven.be

1 Introduction and motivation

Even with the current state of computing hardware with a form factor that is convenient for compact drones, real-time motion planning and control remains a challenge because full autonomous operation requires state estimation, motion planning and control all to be executed onboard at a reasonable update rate. One of the promising techniques for advanced motion planning and control, is Model Prective Control (MPC). Literature shows this technique already being applied on drones, most often restricted to position reference tracking over short horizons using linearized dynamics to limit the computational load [1].

Motion planning using MPC asks for a trade-off between model complexity, and hence the computational load to solve a finite-horizon optimal control problem, and model prediction accuracy. The work presented in this abstract proposes a nonlinear model that is specifically selected to address this trade-off, and suggests simple maneuvers that provide information content ideally suited for parameter estimation solely based on outdoor flight data.

2 Modeling and identification of Quadrotor Dynamics

The proposed model takes roll (ϕ), pitch (θ) and yaw rate (r) references and throttle (T) commands as control inputs. The response of the attitude and thrust control loops is approximated as second (ϕ, θ) and first (r, T) order models. Additionally the model includes following effects:

- Communication delay between the companion computer, where trajectory optimization takes place, and the flight control unit, which executes the low level attitude and thrust control.
- Linear drag and thrust loss on the body axes.
- Battery voltage dependency of the thrust gain.

The results of the fitting of the model components is illustrated in Figures 1 and 2.

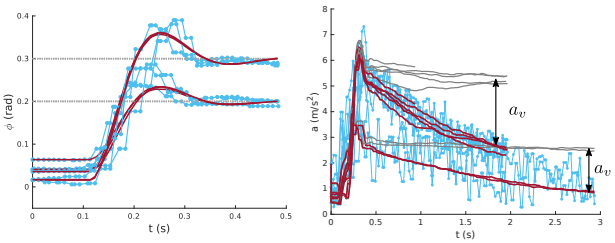

Figure 1: Left: recorded and simulated evolution of the roll angle for a step input reference. Right: recorded and simulated magnitude of the acceleration plotted as a function of time, with a_v the modeled loss of acceleration due to drag and thrust loss.

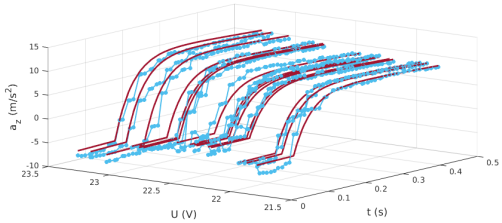

Figure 2: Fitting result for the throttle-thrust relation, displaying vertical acceleration as function of time and battery voltage for throttle steps of varying magnitude.

3 Validation on free flight and conclusion

Figure 3 shows a comparison between the simulation of four models plotted against the recorded data of a free flight. It is clear that linearization, the omission of the battery voltage dependency and the omission of aerodynamic drag all decrement the prediction quality of the simulation. Early tests point out that a control update rate of 20 Hz or more (supported by faster linear feedback control) is realistic, which is to be confirmed during further development stages.

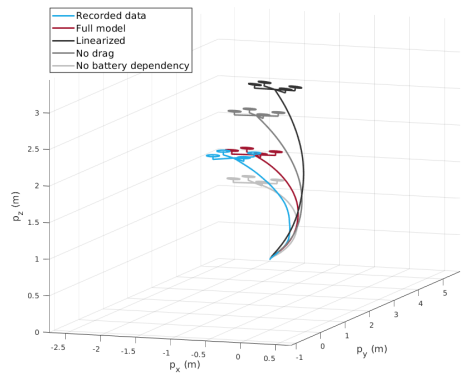

Figure 3: Comparison of simulation of four different model simplifications against recorded data for an outdoor free flight subject to light wind disturbances.

References

[1] H. Nguyen, M. Kamel, K. Alexis and R. Siegwart, "Model Predictive Control for Micro Aerial Vehicles: A Survey," arXiv 2011.11104, 11 2020.

Acknowledgement This work has been carried out within the framework of projects Flanders Make SBO MULTIROB: Rigorous approach for programming and optimal control of multirobot systems and Flanders Make SBO MULTISYSLECO: Multi-System Learning Control. Flanders Make is the Flemish strategic research centre for the manufacturing industry. This work also benefits from project G0C4515N of the Research Foundation - Flanders (FWO - Flanders).

Eigenvalue Assignment for Model Reduction of Networks : Case Studies

Arijit Sarkar[1], Xiaodong Cheng[2], Lanlin Yu[3] and Jacquelien M. A. Scherpen[1]

I. INTRODUCTION

Complex interconnected systems are inevitable in many areas of science and technology. However, the increasing complexity leads to high computational burden to design controllers which motivates us to represent the actual system using a reduced order model which in turn preserves the original network structural properties. In this work we investigate the multi-agent systems with linear subsystems diffusively connected with each other. Synchronization is an important property for the multi-agent systems and it is worthwhile to preserve this property in the reduced order model of the system if the original system is synchronized. It is also preferable that the actual system and reduced order model have similar *Laplacian* spectrum. In this work there is no priori assumption about the stability and passivity of the subsystems like [1]. In [2] similar synchronization preserving model reduction had been investigated but only for undirected network whereas in this work both directed and undirected networks are explored.

II. MODEL REDUCTION

Let us consider a network having N agents and the dynamics of each subsystem is described by

$$\begin{aligned} \dot{x}_i &= Ax_i + Bu_i \\ \eta_i &= Cx_i \end{aligned} \tag{1}$$

where $x_i \in \mathbb{R}^n$, $u_i \in \mathbb{R}^m$, and $\eta_i \in \mathbb{R}^m$ are the states, control inputs and outputs of the individual subsystems and $A \in \mathbb{R}^{n\times n}$, $B \in \mathbb{R}^{n\times m}$ and $C \in \mathbb{R}^{m\times n}$.

The subsystems are connected with each other via diffusive coupling rule

$$u_i = -\sum_{j=1, j\neq i}^{N} w_{ij}(\eta_i - \eta_j) + \sum_{j=1}^{p} f_{ij}\tilde{u}_j \tag{2}$$

where $\tilde{u}_j \in \mathbb{R}^m$ with $j \in \{1, 2, \cdots, p\}$ are the exogenous inputs, $w_{ij} \geq 0$ are the weight of the edge between node i and j of the network structure, $f_{ij} \in \mathbb{R}$. The complete network dynamics can e represented as follows

$$\Sigma : \begin{cases} \dot{x} = (I_N \bigotimes A - L \bigotimes BC)x + (F \bigotimes B)u \\ y = (H \bigotimes C)x \end{cases} \tag{3}$$

where $F \in \mathbb{R}^{N\times p}$, $H \in \mathbb{R}^{q\times N}$, $x := [x_1^\top, \cdots, x_N^\top]^\top \in \mathbb{R}^{nN}$, $u := [u_1^\top, \cdots, u_p^\top]^\top \in \mathbb{R}^{pm}$ and $y := [y_1^\top, \cdots, y_q^\top]^\top \in \mathbb{R}^{qm}$. $L \in \mathbb{N} \times \mathbb{N}$ is the *Laplacian matrix* of the associated strongly connected directed weighted or undirected weighted graph associated with the networked system Σ.

The synchronizing model reduction problem can be formulated as follows.

Problem 1: For the original synchronized network system find a reduced order model

$$\Sigma_r : \begin{cases} \dot{x_r} = (I_r \bigotimes A - L_r \bigotimes BC)x_r + (F_r \bigotimes B)u \\ y_r = (H_r \bigotimes C)x_r \end{cases} \tag{4}$$

such the following hold

i) $L_r \in \mathbb{R}^{r\times r}$ is the *Laplacian matrix* associated with the reduced graph whose topology is similar to the original network topology.

ii) The reduced order network model is also synchronized.

iii) The $\mathcal{H}_2$ approximation error $||\Sigma - \Sigma_r||_2$ between the actual and reduced order system is small enough.

III. EXAMPLES AND APPLICATIONS

The second requirement of the problem can easily be satisfied [2]. For the other two requirements we are investigating multi-agent networks consist of 6 and 10 agents where the individual agents are governed by the satellite dynamics as follows

$$\begin{aligned} \begin{bmatrix} \dot{r}_i \\ \ddot{r}_i \end{bmatrix} &= \begin{bmatrix} 0 & I_3 \\ A_1 & A_2 \end{bmatrix} + \begin{bmatrix} 0 \\ I_3 \end{bmatrix} u_i, \\ \eta_i &= C \begin{bmatrix} r_i \\ \dot{r}_i \end{bmatrix} \end{aligned} \tag{5}$$

where $r_i \in \mathbb{R}^3$ is the position vector of the i-th agent. A novel graph reconstruction approach is being used for this purpose. An optimal choice of eigenvalues is being scrutinized so that the $\mathcal{H}_2$ approximation error between the actual network and the reduced order network is minimum. Moreover, an optimization problem is also being formulated to arrive at a sparse reduced-order network structure.

[1]Jacquelien M. A. Scherpen and Arijit Sarkar are with Jan C. Willems Cemter for Systems and Control, Engineering and Technology Institute Groningen, Faculty of Science and Engineering, University of Groningen, The Netherlands. {{j.m.a.scherpen, a.sarkar}@rug.nl}

[2]Xiaodong Cheng is with Department of Engineering, University of Cambridge, CB2 1PZ, United Kingdom.{xc336@cam.ac.uk}

[3]Lanlin Yu is with the Institute of Advanced Technlogy, Westlake Institute for Advanced study, Westlake University, Hangzhou 310024, China.{yulanlin@westlake.edu.cn}

REFERENCES

[1] X. Cheng, J.M.A. Scherpen and B. Besselink, "Balanced truncation of networked linear passive systems" *Automatica*, vol. 104, pp. 17-25, 2019.

[2] L. Yu, X. Cheng, J.M.A. Scherpen and J. Xiong, "Synchronization preserving model reduction of multi-agent network systems by eigenvalue assignments" *IEEE Conference on Decision and Control*, IEEE pp. 7794-7799, 2019

Uncertainty Propagation for Robust Predictive Modelling of Mechanical Systems

W. van Dijk, W.B.J. Hakvoort, B. Rosic
Department of Mechanics of Solids, Surfaces, and Systems (MS3), University of Twente
P.O. Box 217, 7500 AE Enschede, The Netherlands
{w.vandijk/w.b.j.hakvoort/b.rosic}@utwente.nl

1 Introduction

For model based control of a mechanical system, the equations of motions (EoM) of the system can be used to obtain a model. However, during the derivation of the equations of motion, one is often confronted with incomplete knowledge of the system dynamics. This incomplete knowledge, often expressed in model, parameter, and (initial) state uncertainty, will have a large influence on the quality of the model output, especially when being used for predictive tasks. Therefore, one would like to encapsulate the uncertainties, or at least the 'known' uncertainties, in the model structure.
One approach is to model the uncertainties as (known) distributions and to propagate these distributions through the equations of motion. Monte Carlo methods that rely on the rule of large numbers are often used for the uncertainty propagation task, however, in context of control this is often impractical due to the computationally expensive nature of these methods. Alternatively, polynomial chaos expansion (PCE) can be used [**?**].

2 Polynomial Chaos Expansion

With PCE, the uncertain states of the EoM are expanded using polynomials of the random variables ξ.

$$x(t,\xi) = \sum_i x_i(t)\Phi_i(\xi) \tag{1}$$

In this way, the equations of motion can be cast into an uncertain formulation that is not dependent on the uncertain states $x(t,\xi)$, but on the set of deterministic time-dependent expansion coefficients $x_i(t)$. To obtain the expansion coefficients at each time step, the newly formulated EoM has to be solved only once (deterministically). After finding the expansion coefficients, an approximation of the uncertain states $x(t,\xi)$ and its moments can be constructed cheaply (Figure 1). Polynomial chaos can therefore be used to obtain fast approximations of the uncertain states. However, the use of PCE is currently limited due to two effects, as discussed in the next section.

3 Limitations

Firstly, the required number of expansion coefficients scales exponentially with the expansion order d and the number of uncertain parameters/initial states N. This is problematic as the EoM of mechanical systems typically require a high dimensional (uncertain) parameter space. Secondly, the quality of the state approximations decays for long time integration intervals (Figure 1). Increasing the expansion order d would postpone this decay, however, such an increase is restricted by the first limitation.

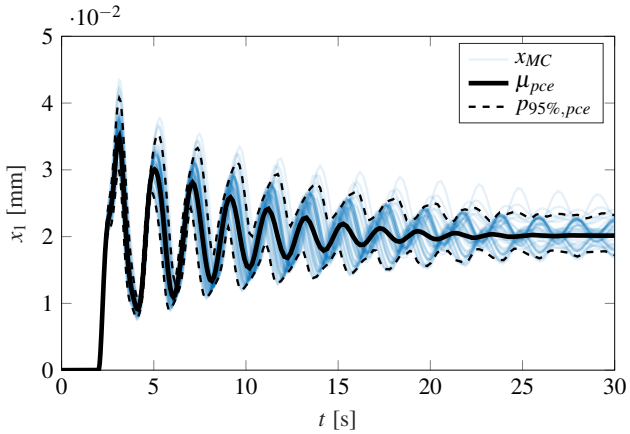

Figure 1: Step response of a double mass spring damper system with parameter uncertainty (damping and stiffness). Only the position of mass 1 is shown. Monte Carlo realisations (▬); Mean from polynomial chaos (▬); 95th percentile from polynomial chaos (- -)

4 Future work

To conclude, work must be done to reduce the above mentioned limitations before using PCE for real-time control of mechanical systems becomes a feasible solution. For this purpose, existing machine learning methods can be used. Furthermore, the effects of certain system properties, such as damping, will be studied and possibly utilized when applying PCE for control purposes.

References

[1] Xiu, D., Karniadakis, G. E. (2002). The Wiener–Askey Polynomial Chaos for Stochastic Differential Equations. SIAM Journal on Scientific Computing, 24(2).

An energy-based approach for viscous damping identification

Carmen Chan-Zheng[1], Pablo Borja, Jacquelien M.A Scherpen
Jan C. Willems Center for Systems and Control
ENgineering and TEchnology institute Groningen (ENTEG)
University of Groningen, The Netherlands
email:{c.chan.zheng, l.p.borja.rosales, j.m.a.scherpen}@rug.nl

1 Introduction

Characterizing the dissipation in mechanical systems is a challenging task due to its complex nonlinear behavior, where the damping elements may depend on the input amplitude, input frequency, joint coordinates, or time-varying coefficients. To simplify the analysis, the damping is commonly described using linear models, e.g., viscous linear damping. Notably, even characterizing these linear damping terms has proven challenging due to the performance of the methods in terms of noise sensitivity, computation cost, among others. However, the damping plays an important role in the performance of controllers, e.g., it partly determines the rate of convergence of a nonlinear system. In this abstract, we extend the methodology proposed in [3] to identify the viscous damping for a larger class of mechanical systems. Furthermore, we explore the synergy of this identification method with PID passivity-based control [1].

2 The damping identification approach

Consider mechanical systems that admit a pH representation of the form

$$\begin{aligned} \begin{bmatrix} \dot{q} \\ \dot{p} \end{bmatrix} &= \begin{bmatrix} 0_{n\times n} & I_n \\ -I_n & -D(q,p) \end{bmatrix} \begin{bmatrix} \nabla_q H(q,p) \\ \nabla_p H(q,p) \end{bmatrix} \\ H(q,p) &= T(q,p) + V(q) \\ T(q,p) &:= \tfrac{1}{2} p^\top M^{-1}(q) p \\ V(q) &:= \tfrac{1}{2}(q-q_\star)^\top K (q-q_\star) \end{aligned} \tag{1}$$

where $q, p \in R^n$ are the generalized positions and momenta vectors, respectively, $H : R^n \times R^n \to R_+$ is the Hamiltonian of the system, $T : R^n \times R^n \to R_+$ is the kinetic energy, $V : R \to R_+$ is the potential energy, $M : R^n \to R^{n\times n}$ is the positive definite mass inertia matrix, $K \in R^{n\times n}$ is the constant positive definite stiffness matrix, $q_\star \in R^n$ is the desired configuration, and $D : R^n \times R^n \to R^{n\times n}$ is positive definite and represents the damping of the system. For simplicity, D is assumed to be diagonal and constant matrix. Furthermore, we assume throughout this abstract, that (1) has an a local isolated minimum at $(q_\star, 0_n)$.

For the upcoming computations, we omit the arguments to simplify the notation. The derivative of the Hamiltonian can be computed as

$$\dot{H} = [\dot{q}^\top \ \dot{p}^\top] \begin{bmatrix} \nabla_q H \\ \nabla_p H \end{bmatrix} = -\dot{q}^\top D \dot{q} \tag{2}$$

Furthermore, note that the derivative of the Hamiltonian can be rewritten as the sum of the partial derivative of the kinetic and potential energy, i.e.,

$$\dot{H} = \dot{T} + \dot{V} = \left(\frac{1}{2} \sum_{i=1}^{n} \dot{q}^\top \frac{\partial M}{\partial q_i} \dot{q} \dot{q}_i \right) + \dot{q}^\top M \ddot{q} + q^\top K \dot{q}. \tag{3}$$

Then, by comparing and integrating (2)-(3), it yields the following energy expresion:

$$\begin{aligned} -\int \dot{q}^\top D \dot{q}\, dt \quad &= \int \left(\tfrac{1}{2} \textstyle\sum_{i=1}^{n} \dot{q}^\top \frac{\partial M}{\partial q_i} \dot{q} \dot{q}_i \right) dt + \dots \\ &\dots + \int \dot{q}^\top M \ddot{q}\, dt + \int (q-q_\star)^\top K \dot{q}\, dt. \end{aligned} \tag{4}$$

Expression (4) can be decoupled into n-equations and rewritten into the matrix form

$$\Psi(\dot{q})\gamma = \Phi(q, \dot{q}, \ddot{q}), \tag{5}$$

where $\Psi(\dot{q})$ and $\Phi(q, \dot{q}, \ddot{q})$ are build by using the measured data (acceleration, velocity, position), and the system parameters (mass and stiffness matrices); while γ contains the unknown viscous damping elements. Therefore, we can compute γ as

$$\gamma = (\Psi(\dot{q})^\top \Psi(\dot{q}))^{-1} \Psi(\dot{q})^\top \Phi(q, \dot{q}, \ddot{q}) \tag{6}$$

We expect to apply the proposed damping identification methodology in combination with the controller and its respective tuning rules described in [1] and [2], respectively, to improve the performance of the transient behavior of nonlinear underactuated mechanical systems (e.g., flexible links planar manipulator).

References

[1] P. Borja, R. Ortega, and J. M. A. Scherpen. New results on stabilization of port-hamiltonian systems via pid passivity-based control. *IEEE Transactions on Automatic Control*, 66(2):625–636, 2021.

[2] C. Chan-Zheng, P. Borja, and J. M. A. Scherpen. Tuning rules for a class of passivity-based controllers for mechanical systems. *IEEE Control Systems Letters*, 5(6):1892–1897, 2021.

[3] Jin-Wei Liang. Damping estimation via energy-dissipation method. *Journal of sound and Vibration*, 307(1-2):349–364, 2007.

[1]The work of Carmen Chan-Zheng is supported by the University of Costa Rica

A scalable multi-step least squares method for network identification with unknown disturbance topology[1]

Stefanie Fonken, Karthik Ramaswamy, Paul Van den Hof
Control Systems Group, Department of Electrical Engineering,
Eindhoven University of Technology, The Netherlands
Email: {s.j.m.fonken, k.r.ramaswamy, p.m.j.vandenhof}@tue.nl

1 Introduction

Dynamic networks are increasing in complexity and size, which gives rise to a demand for accurate and scalable identification methods. For full network identification, direct methods obtain minimal variance results with a lower experimental cost compared to indirect methods. The joint direct method [4] is a direct identification method that exploits a possible reduced rank of the disturbing noise process, but that, due to the required non-convex optimization, is poorly scalable to larger networks. There are multi-step convex identification methods available such as the Sequential Linear Regression (SLR) [1] and extensions of Weighted Null Space Fitting (WNSF) [3] for full network identification. These convex methods are scalable to larger networks, but are limited to parametrizing certain model structures and do not consider reduced-rank noise. All available convex and non-convex methods require prior knowledge on the topology (i.e. rank and structure) of the noise model. Moreover, with a prior structured noise model the variance is reduced compared to full noise models. For situations where this prior information is not readily available, it is attractive to develop methods that include estimating this information from data.

The objective is to obtain a multi-step convex algorithm that estimates the disturbance topology and parametrizes flexible model structures including Box Jenkins (BJ). Moreover, we intend to combine the favorable properties of available methods such as scalability, low experiment cost, and aim for consistency while we additionally obtain a reduced variance. This abstract summarizes the work of [2].

2 Dynamic networks

We consider dynamic networks where the nodes $w_j(t)$ with $j = 1,\dots,L$ are expressed as

$$w_j(t) = \sum_{l\in\mathcal{N}_j} G^0_{jl}(q)w_l(t) + \sum_{k\in\mathcal{R}_j} R^0_{jk}(q)r_k(t) + \sum_{s\in\mathcal{V}_j} H^0_{js}e_s(t),$$

the G^0_{jl} and H^0_{js} are the rational transfer functions to be estimated, with vector $e(t)$ as white noise of which its covariance matrix is allowed to be of reduced rank. The R_{jk} transfer functions and excitation signals $r(t)$ are user manipulated. An example of a network with reduced rank noise is given in Figure 1.

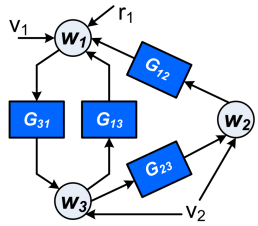

Figure 1: Example of a network with reduced rank noise [4], where $v = He$.

3 Developed method

The main steps of the developed method are described as

1. Estimating the noise rank: *Use high-order ARX models to estimate the innovation signal, from which the noise rank can be estimated,*
2. Estimating the noise correlation structure: *Use the reconstructed innovation signal as measured input to estimate the structure of the noise model,*
3. Parametric identification: *For a BJ network usually a non-convex identification method is needed, we show we can linearly parametrize a BJ network,*

where the first two steps are part of the disturbance topology detection procedure.

References

[1] A. G. Dankers. Optimization method for obtaining estimates in a dynamic network. Technical note, 2019.

[2] S.J.M. Fonken. Multi-step scalable least squares method for network identification with unknown noise topology. Master's thesis, Eindhoven University of Technology, 2020.

[3] M. Galrinho, C. Rojas, and H. Hjalmarsson. Parametric identification using Weighted Null-Space Fitting. *IEEE Transactions on Automatic Control*, 64(7):2798–2813, 2019.

[4] H. H. M. Weerts, P. M. J. Van den Hof, and A. G. Dankers. Prediction error identification of linear dynamic networks with rank-reduced noise. *Automatica*, 98:256 – 268, 2018.

[1] This project has received funding from the European Research Council (ERC), Advanced Research Grant SYSDYNET, under the European Union's Horizon 2020 research and innovation programme (Grant Agreement No. 694504)

Graph-Theoretical Condition for Local Network Identifiability

Antoine Legat and Julien M. Hendrickx*
ICTEAM Institute, UCLouvain, B-1348 Louvain-la-Neuve, Belgium.
Email: { antoine.legat, julien.hendrickx } @uclouvain.be

1 Introduction

The goal of this work is to recover the local dynamics from the global input-output behavior of a networked system and the knowledge of the network topology.

We consider the identification of a network matrix $G(z)$, where the network is made up of n nodes, with node signals $\{w_1(t),\dots,w_n(t)\}$, and external excitation signals $\{r_1(t),\dots,r_n(t)\}$, related to each other by:

$$\begin{aligned} w(t) &= G(z)w(t) + Br(t) + v_1(t) \\ y(t) &= Cw(t) + v_2(t), \end{aligned} \tag{1}$$

where matrices B and C are binary selections defining which nodes are excited and measured, forming the sets $\mathscr{B}$ and $\mathscr{C}$ respectively. The vector $y(t)$ contains the measured nodes, while $v_1(t)$ and $v_2(t)$ are uncorrelated noise vectors. The nonzero entries of the network matrix $G(z)$ define the topology of the network, and are assumed proper and rational.

We assume that the global relation between the excitations r and measures y has been identified, and that the structure of $G(z)$ is known. From this knowledge, we aim at recovering the nonzero entries of $G(z)$.

A first line of work extends the classical closed-loop identification techniques to identify a single module, see e.g. [1]. A recent approach employs graph-theoretical tools to derive identifiability conditions on the graph of the network. Using this approach, [2] addresses the particular case where all nodes are excited/measured. In the general case of partial measurement *and* excitation, [3] introduces a local version of identifiability and derives algebraic necessary and sufficient conditions. In this work, we consider local identifiability with partial excitation and measurement. From the conditions of [3], we derive a graph-theoretical condition which generalizes the results of [2] when not all nodes are excited/measured.

2 Problem reformulation

Starting from the definition of a network system in (1), we first define $T(z) \triangleq (I - G(z))^{-1}$, which is assumed to be proper and stable. The input-output model of the network model (1) is then given by

$$y(t) = CT(z)Br(t) + v_3(t),$$

where $v_3(t) \triangleq CT(z)v_1(t) + v_2(t)$. We assume that $r(t)$ is sufficiently rich so that, for any B and C, $CT(z)B$ can be consistently estimated from $\{y(t), r(t)\}$ data. From the knowledge of $CT(z)B$, the aim is to identify $G(z)$. This motivates the following definition, which restricts the usual generic identifiability from [2] to non-discrete sets of solutions.

Definition 1. *The network matrix G is* generically locally identifiable *from excitations $\mathscr{B}$ and measurements $\mathscr{C}$ if there exists $\varepsilon > 0$ such that for any $\tilde{G}$ consistent with the graph satisfying $||\tilde{G} - G|| < \varepsilon$, there holds*

$$C(I - G(z))^{-1}B = C(I - \tilde{G}(z))^{-1}B \Rightarrow G(z) = \tilde{G}(z), \tag{2}$$

for all G except possibly those lying on a zero measure set.

In this definition, a network matrix $G(z)$ is said *consistent with the graph* if $G_{ij}(z)$ is zero when there is no edge (i, j).

3 Results

In [3], a linearization of (2) yields a necessary and sufficient condition for generic local identifiability, based on the generic rank of a matrix K constructed from B, C and T.

In this work, we show how the generic rank of K relies on the generic rank of certain particular transfer matrices. Besides, we know from [2] that the generic rank of a transfer matrix between two sets of nodes is equal to the number of vertex disjoint paths[1] that can be routed between those two sets.

Combining those results allows to derive a necessary condition for generic local identifiability in terms of paths in the network. We believe that such path-based characterization will pave the way for further developments in the subject.

References

[1] Van den Hof, P. M., Dankers, A., Heuberger, P. S., Bombois, X. "Identification of dynamic models in complex networks with prediction error methods—Basic methods for consistent module estimates," in *Automatica*, 2013.

[2] Hendrickx, J. M., Gevers, M., and Bazanella, A. S. "Identifiability of dynamical networks with partial node measurements," in *IEEE Trans. on Automatic Control*, 2018.

[3] Legat, A. and Hendrickx, J.M. "Local network identifiability with partial excitation and measurement," in *Proceedings of the IEEE CDC*, 2020.

* Work supported by the "RevealFlight" ARC at UCLouvain, and by the MIS grant "Learning from Pairwise Data" of the F.R.S.-FNRS.

[1] A group of paths is said vertex disjoint if no two paths of this group contain the same vertex.

Comparison of Path-Complete Stability Criteria via Quantifier Elimination

Virginie DEBAUCHE & Raphaël JUNGERS
ICTEAM Institute, UCLouvain, B-1348 Louvain-la-Neuve, Belgium
Emails: {virginie.debauche, raphael.jungers}@uclouvain.be

1 Introduction

In this work, we are interested in the stability analysis of discrete-time switching dynamical systems, i.e.

$$x(k+1) \;=\; f_{\sigma(k)}(x(k)), \tag{1}$$

where $x(k) \in \mathbb{R}^n$ is the state and $\sigma(k) \in \{1,\dots,M\} := \langle M \rangle$ for an integer M is the mode of the system. We study especially the *multiple path-complete Lyapunov function* framework introduced in [1] that provides sufficient stability criteria for switching systems by solving Lyapunov inequalities encoded by a directed and labeled graph. Path-complete Lyapunov functions are defined by two components: a *template*, namely a set $\mathscr{V}$ in which the candidate Lyapunov functions are selected, and a *path-complete* graph $\mathscr{G} = (S,E)$ with $E \;\subseteq\; S \times S \times \langle M \rangle$. That is, for every finite sequence of modes, there exists a path in the graph whose sequence of labels is exactly the same. The stability criterion consists in finding a pair $(\mathscr{G} = (S,E), V = \{V_a \mid a \in S\})$ with $V \subseteq \mathscr{V}$ such that the following *Lyapunov inequalities* are satisfied:

$$\forall (a,b,i) \in E,\ \forall x \in \mathbb{R}^n :\ V_b(f_i(x)) \;\leq\; V_a(x). \tag{2}$$

We refer to this notion as a *path-complete Lyapunov function* and we denote it by $V \in PCLF(F,\mathscr{G})$ where $F = \{f_i \mid i \in \langle M \rangle\}$. It turns out that in general, several PCLF, with different templates and different graphs, may be found to establish the stability of system (1) and therefore this brings up the question: are there path-complete graphs "better" than other ones? This has led to the introduction [2] of order relations between graphs. In our case, we will say that a graph $\mathscr{G}_2$ is better than a graph $\mathscr{G}_1$ with respect to a given template $\mathscr{V}$ and a family of switching systems $\mathscr{F}$ if

$$\begin{aligned} &\forall F \in \mathscr{F},\ [\exists V_1 \subseteq \mathscr{V}\ s.t.\ V_1 \in PCLF(F,\mathscr{G}_1) \\ &\quad \Rightarrow\ \exists V_2 \subseteq \mathscr{V}\ s.t.\ V_2 \in PCLF(F,\mathscr{G}_2)] \end{aligned} \tag{3}$$

If (3) holds, we note $\mathscr{G}_1 \;\leq_{\mathscr{V},\mathscr{F}}\; \mathscr{G}_2$.

2 Results

In this work, we consider positive linear discrete-time switching systems, that are systems (1) where $f_i \in \mathbb{R}^{n\times n}_{\geq 0}$, and the template $\mathscr{C}$ of *linear copositive norms*. In this context, the Lyapunov inequalities (2) described by a path-complete graph $\mathscr{G} = (S,E)$ are given by

$$\forall (a,b,i) \in E, \forall x \in \mathbb{R}^n :\ {A_i}^{\top} v_b \;\leq\; v_a, \tag{4}$$

componentwise. It follows that the comparison of two path-complete graphs can be achieved using quantifier elimination on the logical formula (3). By using the *Cylindrical Algebraic Decompositon* (CAD) algorithm, we can establish whether property (3) holds or not for a given pair of graphs. Let us apply this method on a trivial case to underline the output of the algorithm.

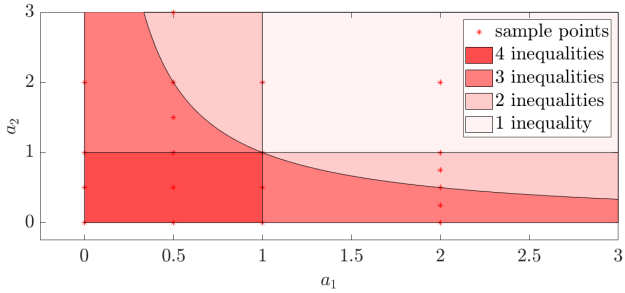

Figure 1: Visualisation of the output of our algorithm on the simplest case of a pair of 1-dimensional matrices $\{a_1, a_2\}$.

Example 1. Consider a positive linear switching system of dimension one with two modes a_1 and $a_2 \in \mathbb{R}_{\geq 0}$. Assume that we use the path-complete graph $\mathscr{G} = (\{a,b\}, \{e_1 = (a,a,1), e_2 = (a,b,1), e_3 = (b,b,2), e_4 = (b,a,2)\})$ to establish the stability of the system. We denote by $\mathscr{G}_{e_i}$ the graph (which is no longer path-complete) that we obtain when we remove the edge e_i of $\mathscr{G}$. It is easy to see that for any $i \in \langle 4 \rangle$, $\mathscr{G} \;\leq_{\mathscr{C},\mathscr{F}}\; \mathscr{G}_{e_i}$ and that there exists at least one system $F = \{a_1, a_2\}$ for which there is a solution $V \in \mathscr{C}$ such that $V \in PCLF(\mathscr{G}_{e_i})$ and none for $\mathscr{G}$. This result can be found by applying the CAD algorithm on the set (4) of four inequalities encoded by the graph $\mathscr{G}$. Indeed, we find the partition of the positive orthant in Figure 1 where the colour depicts the maximal number of inequalities that can be satisfied.

One can see on this trivial example that this algorithm can be used to compare any pair of path-complete graphs for the template of copositive norms and linear switching systems.

Acknowledgements

RJ is a FNRS honorary Research Associate. This project has received funding from the Innoviris Foundation, the FNRS (Chist-Era Druid-net) and ERC (grant 864017-L2C).

References

[1] Ahmadi, A.A., Jungers, R.M., Parrilo, P.A. and Roozbehani M. (2014). Joint spectral radius and path-complete graph Lyapunov functions. *SIAM Journal on Control and Optimization*, 52(1), pp. 687-717.

[2] Philippe, M. and Jungers, R.M. (2019). A complete characterization of the ordering of path-complete methods. *Proceedings of the 22nd ACM International Conference on Hybrid Systems: Computation and Control*, pp. 138-146.

Robustness of the terminal behavior of resistive electrical networks

Anne-Men Huijzer, Arjan van der Schaft, Bart Besselink
Bernoulli Institute for Mathematics, Computer Science and Artificial Intelligence
CogniGron - Groningen Cognitive Systems and Materials Center
University of Groningen
m.a.huijzer@rug.nl, a.j.van.der.schaft@rug.nl, b.besselink@rug.nl

1 Introduction

The study of electrical networks has a long history dating back to Kirchhoff [1] with rich applications ranging from smart grids [2] to computing [3]. Problems of analysing electrical networks are often solved using graph theory, e.g. [4]. Namely, the resistive electrical network can be viewed as a graph; the resistors can be considered as the edges, and the points connecting different resistors as the nodes of the graph. In practice, networks are subject to change or redesign: in this work, we study the robustness of the terminal behaviour of resistive electrical networks with respect to such changes.

2 Main result

Consider a resistive electrical network consisting of m resistors and n nodes connecting them. Assume its network structure is described by the incidence matrix D and that the conductance values of the resistors are collected in a diagonal matrix C. Let $p = \begin{pmatrix} p_1 & p_2 & \dots & p_n \end{pmatrix}^\top$ denote the vector of voltage potentials at the nodes, and $j = \begin{pmatrix} j_1 & j_2 & \dots & j_n \end{pmatrix}^\top$ the vector of nodal currents entering the nodes, e.g., the currents taken from generators or delivered to the loads. By Kirchhoff's voltage law, the vector $v \in \mathbb{R}^m$ of voltages across the edges is related to the voltage potentials as

$$v = D^\top p. \tag{1}$$

Dually, the relation between the vector of nodal currents j and the vector of currents through the edges $i \in \mathbb{R}^m$ is given by Kirchhoff's current law as

$$j = Di. \tag{2}$$

It follows by combining (1) and (2) with Ohm's law $i = Cv$ that the vector of voltage potentials and the vector of nodal currents can be related as

$$j = DCD^\top p = Lp, \tag{3}$$

where $L = DCD^\top$ is the weighted Laplacian corresponding to the resistive electrical network.

Assume that we adapt the conductance values of h resistors in the network by a constant. The updated resistive electrical network is described as

$$j = \tilde{L}\tilde{p} \tag{4}$$

with $\tilde{L}$ given by $\tilde{L} = L + \hat{D}\hat{C}\hat{D}^\top$. Here, $\hat{D}$ is an incidence matrix describing the locations of the adapted resistors and $\hat{C}$ is a diagonal matrix including the size of the adaptations. We are now able to derive the following result, which relates the effective resistance of the perturbed electrical network (4) to that of the original network (3).

Theorem 2.1 *Consider the perturbed electrical network* (4). *Assume that $\tilde{L}$ has only one eigenvalue equal to zero and* $\operatorname{rank}(\hat{D}) = h$. *Then, its effective resistance between nodes k and ℓ, denoted $\tilde{R}_{\text{eff}}(k,\ell)$, equals*

$$\tilde{R}_{\text{eff}}(k,\ell) = R_{\text{eff}}(k,\ell) - p^\top \hat{D}(I + \hat{C}\hat{D}^\top P)^{-1}\hat{C}\hat{D}^\top p,$$

where $P \in \mathbb{R}^{n\times h}$ and $p \in \mathbb{R}^n$ are such that

$$\hat{D} = LP, \qquad e_k - e_\ell = Lp$$

with e_k and e_ℓ the k and ℓ-th column of the identity matrix.

Theorem 2.1 allows us to compute the effective resistance between two nodes in an electrical network based on properties of the *unperturbed* electrical network and the matrices $\hat{C}$ and $\hat{D}$ representing the perturbations. Stated differently, there is no need to explicitly study properties such as the distribution of voltage potentials for the (possibly large-scale) perturbed network, significantly simplifying the computation of effective resistance. The result of Theorem 2.1 can be generalized for the case that $\operatorname{rank}(\hat{D}) < h$.

References

[1] G. Kirchhoff, "Ueber die Auflösung der Gleichungen, auf welche man bei der Untersuchung der linearen Vertheilung galvanischer Ströme geführt wird," *Annalen der Physik und Chemie*, vol. 148, no. 12, pp. 497–508, 1847.

[2] F. Dörfler and F. Bullo, "Kron reduction of graphs with applications to electrical networks," *IEEE Transactions on Circuits and Systems I: Regular Papers*, vol. 60, no. 1, pp. 150–163, 2013.

[3] E. Chicca, F. Stefanini, C. Bartolozzi, and G. Indiveri, "Neuromorphic electronic circuits for building autonomous cognitive systems," *Proceedings of the IEEE*, vol. 102, no. 9, pp. 1367–1388, 2014.

[4] F. Dörfler, J. W. Simpson-Porco, and F. Bullo, "Electrical networks and algebraic graph theory: models, properties, and applications," *Proceedings of the IEEE*, vol. 106, no. 5, pp. 977–1005, 2018.

Behavioural assume-guarantee contracts for linear systems

B. M. Shali, b.m.shali@rug.nl
A. J. van der Schaft, a.j.van.der.schaft@rug.nl
B. Besselink, b.besselink@rug.nl

Bernoulli Institute, University of Groningen, The Netherlands

1 Introduction

Modern engineering systems often comprise a large number of interconnected components. The components of such systems can be very complex themselves, thus making the analysis and design of the overall system prohibitively difficult. One way to circumvent this problem is by adopting a theory for analysis and design that allows components to be considered independently. Contract theories, which find their origins in the field of software engineering, are developed with precisely this in mind. As the name suggest, contract theories revolve around the use of contracts as specifications for system behaviour. The particular way in which this is done varies from one theory to another. Nevertheless, contract theories share a common philosophy, which is captured very elegantly in the mathematical meta-theory of contracts introduced in [1].

Motivated by this, we present contracts as specifications for linear systems. Following the meta-theory in [1], we also define and characterize contract implementation and contract composition.

2 Contracts for linear systems

Consider the linear system

$$\Sigma : \begin{cases} \dot{x} = Ax + Bu, \\ y = Cx + Du, \end{cases} \tag{1}$$

with input u, state x, and output y. In the context of an interconnected system, we are interested in the interaction of Σ with other components, hence we define the *external behaviour* of Σ as

$$\mathfrak{B}(\Sigma) = \{(u,y) \mid \exists x \text{ s.t. (1) holds}\}.$$

The component Σ receives inputs from its environment, which is composed of other components. Therefore, we define an *environment* to be a linear system of the form

$$\mathrm{E} : 0 = E\left(\tfrac{\mathrm{d}}{\mathrm{d}t}\right)u, \tag{2}$$

where $E(s)$ is a polynomial matrix. The environment E represents the *input behaviour*

$$\mathfrak{B}_{\mathrm{i}}(\mathrm{E}) = \{u \in \mathscr{C}_m^\infty \mid \text{(2) holds}\}.$$

The interconnection $\mathrm{E} \wedge \Sigma$ is obtained by setting the input generated by E as input of Σ. As a specification for the external behaviour of Σ, we are interested in guaranteeing properties of the *output behaviour*

$$\mathfrak{B}_{\mathrm{o}}(\mathrm{E} \wedge \Sigma) = \{y \mid \exists u \in \mathfrak{B}_{\mathrm{i}}(\mathrm{E}) \text{ s.t. } (u,y) \in \mathfrak{B}(\Sigma)\}$$

for all relevant environments E. This is formalized via the notion of a contract, defined below.

Definition 1. *A* contract $\mathscr{C} = (\mathrm{A}, \Gamma)$ *is a pair of* assumptions A *and* guarantees Γ *given by*

$$\mathrm{A} : 0 = A\left(\tfrac{\mathrm{d}}{\mathrm{d}t}\right)u \quad \textit{and} \quad \Gamma : G\left(\tfrac{\mathrm{d}}{\mathrm{d}t}\right)y = 0,$$

where $A(s)$ and $G(s)$ are polynomial matrices.

Note that the assumptions A represent the input behaviour $\mathfrak{B}_{\mathrm{i}}(\mathrm{A})$, while the guarantees Γ represent the output behaviour $\mathfrak{B}_{\mathrm{o}}(\Gamma)$. A contract can be used to specify the external behaviour of Σ as follows.

Definition 2. *An environment* E *is* compatible *with* $\mathscr{C} = (\mathrm{A}, \Gamma)$ *if* $\mathfrak{B}_{\mathrm{i}}(\mathrm{E}) \subset \mathfrak{B}_{\mathrm{i}}(\mathrm{A})$. *A system* Σ *of the form* (1) implements $\mathscr{C}$ *if* $\mathfrak{B}_{\mathrm{o}}(\mathrm{E} \wedge \Sigma) \subset \mathfrak{B}_{\mathrm{o}}(\Gamma)$ *for all environments* E *compatible with* $\mathscr{C}$.

The following theorem shows that contract implementation can be verified without the explicit construction of all compatible environments.

Theorem 1. *A system* Σ *of the form* (1) *implements* $\mathscr{C} = (\mathrm{A}, \Gamma)$ *if and only if* $\mathfrak{B}_{\mathrm{o}}(\mathrm{A} \wedge \Sigma) \subset \mathfrak{B}_{\mathrm{o}}(\Gamma)$.

Contracts themselves can be composed in order to analyse and design interconnections. We illustrate this for the series interconnection. Suppose that Σ_1 implements $\mathscr{C}_1$ and Σ_2 implements $\mathscr{C}_2$, and consider their series interconnection $\Sigma_1 \to \Sigma_2$. The *series composition* $\mathscr{C}_1 \to \mathscr{C}_2$ is the tightest contract that $\Sigma_1 \to \Sigma_2$ is guaranteed to implement. The following theorem gives an explicit expression for $\mathscr{C}_1 \to \mathscr{C}_2$ based on $\mathscr{C}_1$ and $\mathscr{C}_2$.

Theorem 2. *The series composition of* $\mathscr{C}_1 = (\mathrm{A}_1, \Gamma_1)$ *to* $\mathscr{C}_2 = (\mathrm{A}_2, \Gamma_2)$ *exists if and only if* $\mathfrak{B}_{\mathrm{o}}(\Gamma_1) \subset \mathfrak{B}_{\mathrm{i}}(\mathrm{A}_2)$, *in which case it is given by* $\mathscr{C}_1 \to \mathscr{C}_2 = (\mathrm{A}_1, \Gamma_2)$.

References

[1] A. Benveniste, B. Caillaud, D. Nickovic, R. Passerone, J.-B. Raclet, P. Reinkemeier, A. Sangiovanni-Vincentelli, W. Damm, T. A. Henzinger, and K. G. Larsen, *Contracts for System Design*. Foundations and trends in electronic design automation, Now Publishers, 2018.

Observability and Determinability of Discrete Time Switched Linear Singular Systems: Multiple Switches Case

Sutrisno and Stephan Trenn
Bernoulli Institute, University of Groningen,
Nijenborgh 9, 9747 AG, Groningen, The Netherlands
Email: s.sutrisno@rug.nl, s.trenn@rug.nl

1 Introduction

We consider the homogeneous discrete-time switched linear singular systems (SwLSS) of the form

$$E_{\sigma(k)}x(k+1) = A_{\sigma(k)}x(k), \tag{1a}$$

$$y(k) = C_{\sigma(k)}x(k), \quad k \in \mathbb{N} \tag{1b}$$

where $k \in \mathbb{N}$ is the time instant, $x(k) \in \mathbb{R}^n$ is the state, $y(k) \in \mathbb{R}^p, p \in \mathbb{N}$, is the output, $\sigma : \mathbb{N} \to \{0,1,2,...,\mathrm{p}\}$ is the switching signal determining which mode $\sigma(k)$ is active at time instant k, $E_i, A_i \in \mathbb{R}^{n\times n}$, $B_i \in \mathbb{R}^{n\times m}$, $C_i \in \mathbb{R}^{p\times n}$, and $D_i \in \mathbb{R}^{p\times m}$ and E_i may be singular. We define the switching signal as follows

$$(\sigma_k), \quad \sigma(k) = \sigma_j \text{ if } k \in [k_j^s, k_{j+1}^s),\ j = \{0,1,2,...\} \tag{2}$$

where $k_j^s \in \mathbb{N}$ denote the switching times with $k_0^s = 0$, $k_{J+1}^s = K+1$, and $\sigma_j \in \{0,1,...,\mathrm{p}\}$. We assume here the switching signal is strictly increasing i.e. $k_{j+1}^s > k_j^s\ \forall j$. We study this system under index-1 assumption w.r.t. the given switching signal (2), see [1, 2] for the solution and the corresponding notations used in this study. The SwLSS (1) is called **observable** on $[0,K]$ w.r.t. the fixed switching signal (2) iff for all solutions on $[0,K]$ the following implication holds:

$$y^1 \equiv y^2 \Rightarrow x^1 \equiv x^2;$$

and the SwLSS (1) is called **determinable** on $[0,K]$ w.r.t. the fixed switching signal (2) iff the following implication holds:

$$y^1_{[0,K]} \equiv y^2_{[0,K]} \Rightarrow x^1(K) = x^2(K).$$

By $\mathbb{S}^{[\tau_D]}_{[0,K]}$ we define the set of all switching signals with each mode is active at least $\tau_D \in \mathbb{N}$ time steps.

2 Main Results

2.1 Observability

The main result for the observability characterization is presented in the following theorem.

Theorem 2.1 *Assume SwLSS* (1) *is of index-1 w.r.t. the fixed switching signal* (2)*. It is observable on* $[0,K]$ *if, and only if,*

$$\mathscr{S}_{\sigma_0} \cap \bigcap_{j=0}^{J} [\Psi_\sigma(j,0)]^{-1}(\mathscr{O}_{\sigma_j}^{k_{j+1}^s - k_j^s - 1}) = \{0\} \tag{3}$$

where for every j,k $\mathscr{S}_0 = [A_0]^{-1}(\operatorname{im} E_0)$,

$$\Psi_\sigma(j,0) = \Phi_{\sigma_j,\sigma_{j-1}}\Phi_{\sigma_{j-1}}^{k_j^s - k_{j-1}^s - 1} \cdots \Phi_{\sigma_1,\sigma_0}\Phi_{\sigma_0}^{k_1^s - k_0^s - 1} I.$$

$$\mathscr{O}_{\sigma_j}^k = \ker[C_{\sigma_j}^\top, (C_{\sigma_j}\Phi_{\sigma_j})^\top, \ldots, (C_{\sigma_j}\Phi_{\sigma_j}^k)^\top]^\top. \tag{4}$$

Note that $[*]^{-1}$ denotes the preimage and not the inverse. In general, the observability depends on the switching times as the switching times appear explicitly in the observability condition (3). We provide some situations in the following where the observability does not depend on the switching times i.e. **constant**.

Proposition 2.2 *Consider the two-dimensional SwLSS* (1) *of index-1 w.r.t. the switching signal* (2)*. Then its observability is constant for every* $\sigma \in \mathbb{S}^{[2]}_{[0,K]}\ \forall K \geq 4$.

Proposition 2.3 *Consider the SwLSS* (1) *of index w.r.t. the switching signal* (2)*. If the unobservable subspace of the initial mode is invariant under* $\Phi_{\sigma(k),\sigma(k-1)}\ \forall k \in \mathbb{N}$ *then its observability is constant for every* $\sigma \in \mathbb{S}^{[2]}_{[0,K]}\ \forall K \geq 2n$.

2.2 Determinability

We define the following sequence for $j = 1,2,\ldots,J$ and for $k \in (k_j^s, k_{j+1}^s - 1)$

$$\mathscr{Q}^0 = \mathscr{S}_0 \cap \ker C_0$$

$$\mathscr{Q}^k = \ker C_{\sigma_j} \cap A_{\sigma_j}\mathscr{Q}^{k-1}, k = k_j^s + 1, k_j^s + 2, \ldots, k_{j+1}^s$$

$$\mathscr{Q}^{k_j^s} = \ker C_{\sigma_j} \cap A_{\sigma_{j-1}}\mathscr{Q}^{k_j^s - 1}.$$

Theorem 2.4 *The SwLSS* (1) *is determinable on* $[0,K], K \in [k_J^s, k_{J+1}^s)$ *w.r.t. the fixed switching signal* (2) *if, and only if* $\mathscr{Q}^K = \{0\}$.

References

[1] Pham Ky Anh, et al. "The one-step-map for switched singular systems in discrete-time." *Proc. 58th IEEE Conf. Decision Control (CDC) 2019.*

[2] Sutrisno, Stephan Trenn. "Observability of Switched Linear Singular Systems in Discrete Time: Single Switch Case." *Proc. of European Control Conference (ECC). to appear.*

Part 4

List of Participants

Leontine Aarnoudse
Dept. of Mechanical Engineering
Eindhoven University of Technology
P.O. Box 513
5600 MB Eindhoven
Netherlands
l.i.m.aarnoudse@tue.nl

Flavia Sofia Acerbo
Dept. of Mechanical Engineering
KU Leuven
Celestijnenlaan 300
3001 Heverlee (Leuven)
Belgium
flaviasofia.acerbo@kuleuven.be

Michele Ambrosino
Service d'Automatique et d'Analyse des Syst'emes
Université Libre de Bruxelles
Avenue Franklin Roosevelt,50
1050 Bruxelles
Belgium
Michele.ambrosino@ulb.be

A.G. Aribowo
Dept. of Mechanical Engineering
Eindhoven University of Technology
P.O. Box 513
5600 MB Eindhoven
Netherlands
A.G.Aribowo@tue.nl

Marcus Becker
Delft Center for Systems and Control
Delft University of Technology
Mekelweg 2
2628 CD Delft
Netherlands
marcus.becker@tudelft.nl

Gerben Izaak Beintema
Dept. of Electrical Engineering
Eindhoven University of Technology
P.O. Box 513
5600 MB Eindhoven
Netherlands
g.i.beintema@tue.nl

Alberto Bertipaglia
3mE
Delft University of Technology
Mekelweg 2
2628 CD Delft
Netherlands
A.Bertipaglia@tudelft.nl

Florence Blondiaux
ICTEAM/INMA
UCLouvain
Avenue Georges Lemaître 4-6/L4.05.01
1348 Louvain-la-Neuve
Belgium
florence.blondiaux@uclouvain.be

S Boersma
Farm Technology Group
Wageningen University
Droevendaalsesteeg 1
6708 PB Wageningen
Netherlands
sjoerd.boersma@wur.nl

Max Bolderman
Dept. of Electrical Engineering
Eindhoven University of Technology
P.O. Box 513
5600 MB Eindhoven
Netherlands
m.bolderman@tue.nl

Mathias Bos
Dept. of Mechanical Engineering
KU Leuven
Celestijnenlaan 300
3001 Heverlee (Leuven)
Belgium
mathias.bos@kuleuven.be

Yorick Broens
Dept. of Electrical Engineering
Eindhoven University of Technology
P.O. Box 513
5600 MB Eindhoven
Netherlands
Y.L.C.Broens@tue.nl

Carmen Chan-Zheng
Engineering and Technology institute Groningen
University of Groningen
ENTEG
Nijenborgh 4
9747AG Groningen
Netherlands
c.chan.zheng@rug.nl

Xiupeng Chen
Dept. of Science and Engineering
University of Groningen
Antaresstraat 23 38
9742 LA Groningen
Netherlands
xiupeng.chen@rug.nl

Koen Classens
Dept. of Mechanical Engineering
Eindhoven University of Technology
P.O. Box 513
5600 MB Eindhoven
Netherlands
k.h.j.classens@tue.nl

Sébastien Colla
ICTEAM/INMA
UCLouvain
Avenue Georges Lemaître 4-6/L4.05.01
1348 Louvain-la-Neuve
Belgium
sebastien.colla@uclouvain.be

Virginie Debauche
Dept. of Mathematical Engineering (INMA)
UCLouvain
Avenue Georges Lemaître 4
1348 Louvain-la-Neuve
Belgium
virginie.debauche@uclouvain.be

Gilles Delansnay
System, Estimation, Control and Optimization
Polytechnic Faculty of University of Mons
Boulevard Dolez 31
7000 Mons
Belgium
gilles.delansnay@umons.ac.be

Ousmane Diao
Mathematics Applied
UCLouvain
Rue J. M de Vismes 3/003
1348 Louvain-la-Neuve
Belgium
ousmane.diao@uclouvain.be

Dries Dirckx
Dept. of Mechanical Engineering
KU Leuven
Celestijnenlaan 300
3001 Heverlee (Leuven)
Belgium
dries.dirckx@kuleuven.be

Stefanie Fonken
Dept. of Electrical Engineering
Eindhoven University of Technology
P.O. Box 513
5600 MB Eindhoven
Netherlands
s.j.m.fonken@tue.nl

Karlijn Fransen
Systems Architecture
Vanderlande Industries B.V.
Vanderlandelaan 2
5466RB Veghel
Netherlands
karlijn.fransen@vanderlande.com

Kathinka Frieswijk
Discrete Technology and Production Automation (DTPA)
University of Groningen
Nijenborgh 4
NL-9747 AG Groningen
Netherlands
k.frieswijk@rug.nl

Prasoon Garg
Dept. of Mechanical Engineering
Eindhoven University of Technology
P.O. Box 513
5600 MB Eindhoven
Netherlands
p.garg.1@tue.nl

Farhad Ghanipoor
Dept. of Mechanical Engineering
Eindhoven University of Technology
P.O. Box 513
5600 MB Eindhoven
Netherlands
farhadghanipoor95@gmail.com

Leila Gharavi
Delft Center for Systems and Control
Delft University of Technology
Mekelweg 2
2628 CD Delft
Netherlands
L.Gharavi@tudelft.nl

Noel" Hallemans
ELEC
Vrije Universiteit Brussel
Rue des Epicéas
25
1170 Brussels
Belgium
noel.hallemans@vub.be

Haleh Hayati
Dept. of Mechanical Engineering
Eindhoven University of Technology
P.O. Box 513
5600 MB Eindhoven
Netherlands
h.hayati@tue.nl

Julien M. Hendrickx
ICTEAM
UCLouvain
Avenue Georges Lemaître 4-6/L4.05.01
1348 Louvain-la-Neuve
Belgium
julien.hendrickx@uclouvain.be

M.A. Huijzer
SCAA
University of Groningen
Spaanse Aakstraat 81
9741CV Groningen
Netherlands
m.a.huijzer@rug.nl

Coen Hutters
Delft Center for Systems and Control
Delft University of Technology
Mekelweg 2
2628 CD Delft
Netherlands
coenhutters@gmail.com

L.C. Iacob
Dept. of Electrical Engineering
Eindhoven University of Technology
P.O. Box 513
5600 MB Eindhoven
Netherlands
l.c.iacob@tue.nl

Aykut Isleyen
Dept. of Mechanical Engineering
Eindhoven University of Technology
P.O. Box 513
5600 MB Eindhoven
Netherlands
a.isleyen@tue.nl

Lars Janssen
Dept. of Mechanical Engineering
Eindhoven University of Technology
P.O. Box 513
5600 MB Eindhoven
Netherlands
l.a.l.janssen@tue.nl

Xavier Jordens
Department of Control Engineering and System Analysis
Université Libre de Bruxelles
Clos de Rambouillet, 14A
1410 Waterloo
Belgium
xavier.jordens@ulb.be

A.Y KAMRI
ICTM
UCLouvain
ICTM Place du Levant 3/L5.03.02
1348 Louvain-la-Neuve
Belgium
yassine.kamri@uclouvain.be

David Kiessling
Dept. of Mechanical Engineering
KU Leuven
Celestijnenlaan 300
3001 Heverlee (Leuven)
Belgium
david.kiessling@kuleuven.be

Jesse Koenders
Energy Systems and Control
DIFFER
P.O. Box 6336
5612 AJ Eindhoven
Netherlands
j.t.w.koenders@differ.nl

J.J. Kon
Dept. of Mechanical Engineering
Eindhoven University of Technology
P.O. Box 513
5600 MB Eindhoven
Netherlands
johankon@live.nl

Erjen Lefeber
Dept. of Mechanical Engineering
Eindhoven University of Technology
P.O. Box 513
5600 MB Eindhoven
Netherlands
A.A.J.Lefeber@tue.nl

Antoine Legat
Dept. of Applied Mathematics
UCLouvain
Allée de la Chêneraie 10
1300 Wavre
Belgium
antoine.legat@uclouvain.be

Ming Li
Dept. of Electrical Engineering
Eindhoven University of Technology
P.O. Box 513
5600 MB Eindhoven
Netherlands
mingliuestc@outlook.com

Tinghua Li
Discrete Technology and Production Automation (DTPA)
University of Groningen
Nijenborgh 4
9747 AG Groningen Groningen
Netherlands
t.li@rug.nl

Ningbo Li
Discrete Technology and Production Automation
University of Groningen
107 KMR 11
Duindoornstraat
9741 PR Groningen
Netherlands
ningbo.li@rug.nl

Maolong Lyu
Delft Center for Systems and Control
Delft University of Technology
Mekelweg 2
2628 CD Delft
Netherlands
M.Lyu@tudelft.nl

Maxime Maton
SECO department
University of Mons
Boulevard Dolez 31
7000 Mons
Belgium
Maxime.MATON@umons.ac.be

Clara Menzen
Delft Center for Systems and Control
Delft University of Technology
Mekelweg 2
2628 CD Delft
Netherlands
c.m.menzen@tudelft.nl

Charles Monnoyer de Galland
ICTEAM/INMA
UCLouvain
Avenue Georges Lemaître 4-6/L4.05.01
1348 Louvain-la-Neuve
Belgium
charles.monnoyer@uclouvain.be

Martin Moriamé
Mathematics (sciences)
UNamur
Rue du pavé
31
6500 Barbencon
Belgium
martin.moriame@unamur.be

Carlos Murguia Rendon
Dept. of Mechanical Engineering
Eindhoven University of Technology
P.O. Box 513
5600 MB Eindhoven
Netherlands
C.G.Murguia@tue.nl

Ilham Naharudinsyah
Dept. of Process and Energy
Delft University of Technology
Hendrik Marsmanlaan 98
2624 TL Delft
Netherlands
i.naharudinsyah@tudelft.nl

Henk Nijmeijer
Dept. of Mechanical Engineering
Eindhoven University of Technology
P.O. Box 513
5600 MB Eindhoven
Netherlands
H.Nijmeijer@tue.nl

Younes Oudich
Department of Control Engineering and System Analysis
Université Libre de Bruxelles
50, av. F.D. Roosevelt
CP 165/55
1050 Brussels
Belgium
younes.oudich@ulb.be

Tijmen Pollack
Dept. of Aerospace Engineering
Delft University of Technology
Haarlemmerstraat 301a
2312DV Leiden
Netherlands
T.S.C.Pollack@tudelft.nl

Luuk Poort
Dept. of Mechanical Engineering
Eindhoven University of Technology
P.O. Box 513
5600 MB Eindhoven
Netherlands
l.poort@tue.nl

Maurice Poot
Dept. of Mechanical Engineering
Eindhoven University of Technology
P.O. Box 513
5600 MB Eindhoven
Netherlands
m.m.poot@tue.nl

Andr´as Retzler
Dept. of Mechanical Engineering
KU Leuven
Celestijnenlaan 300
3001 Heverlee (Leuven)
Belgium
andras.retzler@kuleuven.be

V.D. Reyes Dreke
Dept. of Electrical Engineering
Eindhoven University of Technology
P.O. Box 513
5600 MB Eindhoven
Netherlands
v.d.reyes.dreke@tue.nl

Arijit Sarkar
Discrete Technology and Production Automation, ENTEG
University of Groningen
Nijenborgh 4
9747 AG Groningen
Netherlands
a.sarkar@rug.nl

Bram Seinhorst
Dept. of Mechanics of Solids, Surfaces and Systems
University of Twente
De Horst 2
7522 NB Enschede
Netherlands
b.seinhorst@utwente.nl

Brayan Shali
Bernoulli Institute for Mathematics, Computer Science and Artificial Intelligence
University of Groningen
P.O. Box 407
9700 AK Groningen
Netherlands
b.m.shali@rug.nl

Sil Spanjer
Engineering Technology
University of Twente
De Horst 20
P.O. Box 217
7500 AE Enschede
Netherlands
s.t.spanjer@utwente.nl

Maximilian Stölzle
Cognitive Robotics
Delft University of Technology
Mekelweg 2
2628 CD Delft
Netherlands
M.W.Stolzle@tudelft.nl

Congcong Sun
Plant Science Department
Farm Technology Group, Wageningen University
Van der Waalsstraat
6II
6706 JM Wageningen
Netherlands
sccyycg@gmail.com

Sutrisno Sutrisno
Bernoulli Institute for Mathematics, Computer Science and Artificial Intelligence
University of Groningen
Nijenborgh 9
Room No. 380
9747 AG Groningen
Netherlands
s.sutrisno@rug.nl

Paul Tacx
Dept. of Mechanical Engineering
Eindhoven University of Technology
P.O. Box 513
5600 MB Eindhoven
Netherlands
p.j.m.m.tacx@tue.nl

Laurane Thielemans
Dept. of Mechanical Engineering
Siemens, KU Leuven, LRD
Waaistraat 6 – bus 5105
3000 Leuven
Belgium
laurane.thielemans@siemens.com

Sander Thuijsman
Dept. of Mechanical Engineering
Eindhoven University of Technology
P.O. Box 513
5600 MB Eindhoven
Netherlands
s.b.thuijsman@tue.nl

Anastasios Tsolakis
Cognitive Robotics
Delft University of Technology
Mekelweg 2
2628 CD Delft
Netherlands
tas.tsolakis@gmail.com

Wouter van Dijk
Engineering Technology
University of Twente
De Horst 20
P.O. Box 217
7500 AE Enschede
Netherlands
w.vandijk@utwente.nl

Ricky van Kampen
Energy Systems and Control
DIFFER
P.O. Box 6336
5600 HH Eindhoven
Netherlands
r.j.r.vankampen@differ.nl

Bastiaan Vandewal
Dept. of Mechanical Engineering
KU Leuven
Celestijnenlaan 300
3001 Heverlee (Leuven)
Belgium
bastiaan.vandewal@kuleuven.be

JJ Verbakel
Dept. of Mechanical Engineering
Eindhoven University of Technology
P.O. Box 513
5600 MB Eindhoven
Netherlands
j.j.verbakel@tue.nl

Chris Verhoek
Dept. of Electrical Engineering
Eindhoven University of Technology
P.O. Box 513
5600 MB Eindhoven
Netherlands
c.verhoek@tue.nl

F.M. Viset
Delft Center for Systems and Control
Delft University of Technology
Mekelweg 2
2628 CD Delft
Netherlands
frida.viset@gmail.com

Maarten Vlaswinkel
Dept. of Mechanical Engineering
Eindhoven University of Technology
P.O. Box 513
5600 MB Eindhoven
Netherlands
m.g.vlaswinkel@tue.nl

Benjamin Wauthion
Service d'Automatique et d'Analyse des Syst'emes
Université Libre de Bruxelles
CP 165/55
50, av. F.D. Roosevelt
1050 Bruxelles
Belgium
benjamin.wauthion@ulb.be

Duo Xu
Dept. of Electrical Engineering
Eindhoven University of Technology
P.O. Box 513
5600 MB Eindhoven
Netherlands
d.xu@tue.nl

H. Yin
Engineering and Technology Institute Groningen
University of Groningen
Hoogeweg 3, 3-0
9746TN Groningen
Netherlands
hao.yin@rug.nl